Trabajo de Fin de Máster
Máster en Ingeniería Aeronáutica

Analysis of Dynamical Models and Design of Feedback Control Laws for E-sail Deployment Operations

Autor: Sergio Linares Márquez

Tutores: Guillermo Pacheco Ramos

Rafael Vázquez Valuenzuela

Dpto. Ingeniería Aeroespacial y Mecánica de Fluidos
Escuela Técnica Superior de Ingeniería
Universidad de Sevilla

Sevilla, 2023

Trabajo de Fin de Máster
Máster en Ingeniería Aeronáutica

Analysis of Dynamical Models and Design of Feedback Control Laws for E-sail Deployment Operations

Autor:

Sergio Linares Márquez

Tutores:

Guillermo Pacheco Ramos
Rafael Vázquez Valuenzuela

Dpto. Ingeniería Aeroespacial y Mecánica de Fluidos
Escuela Técnica Superior de Ingeniería
Universidad de Sevilla

Sevilla, 2023

Trabajo de Fin de Máster: Analysis of Dynamical Models and Design of Feedback Control Laws for E-sail Deployment Operations

Autor: Sergio Linares Márquez
Tutores: Guillermo Pacheco Ramos
Rafael Vázquez Valuenzuela

El tribunal nombrado para juzgar el trabajo arriba indicado, compuesto por los siguientes profesores:

Presidente:

Vocal/es:

Secretario:

acuerdan otorgarle la calificación de:

El Secretario del Tribunal

Fecha:

Agradecimientos

Final del principio, principio del comienzo

Sobre el corazón un ancla
y sobre el ancla una estrella

Sergio Linares Márquez
Sevilla, 2023

Resumen

Título

Análisis de modelos dinámicos y diseño de controladores para la fase de despliegue de E-sails

Resumen del trabajo

Las Velas Eléctricas Solares son un sistema de propulsión continua basado en la interacción electrostática entre el viento solar y el campo eléctrico creado por un conjunto de cables muy esbeltos cargados eléctricamente. Con aplicaciones en misiones interplanetarias para vehículos de pequeño y mediano tamaño, el despliegue de este conjunto de cables es uno de los principales problemas a resolver para la adecuada implementación de este tipo de dispositivos. De esta manera, el objetivo del proyecto es analizar de manera extensa el modelo dinámico y el diseño de algoritmos de control tanto lineales como no lineales para maniobras de despliegue de Velas Eléctricas Solares, analizando el rendimiento de las leyes de control desarrolladas a través de la implementación de un Filtro de Kalman Extendido.

Palabras clave

Despliegue, Velas Eléctricas Solares, Modelado Dinámico, Leyes de Control de Bucle Cerrado, Filtro de Kalman Extendido

Conclusiones

A lo largo del proyecto se han derivado las ecuaciones del movimiento bidimensionales de las estrategias de despliegue tangencial y radial utilizando la aproximación de Lagrange. Tomando estos modelos como punto de partida, se han desarrollado leyes de control lineales y no lineales, así como un Filtro de Kalman Extendido (EKF), considerando los actuadores y sensores disponibles, respectivamente. Así, el rendimiento de las leyes de control de bucle cerrado (es decir, los algoritmos de control calculados utilizando el vector de estado estimado por el EKF) se ha evaluado finalmente considerando niveles realistas de ruido en las medidas de los sensores. De este modo, los algoritmos de control implementados demostraron la controlabilidad de ambas estrategias de despliegue, mientras que los órdenes de magnitud de los errores obtenidos eran razonables dado el valor de las perturbaciones introducidas. Además, la estrategia de despliegue radial presentaba unos requerimientos de control significativamente inferiores con respecto a la estrategia tangencial en términos del momento a aplicar en el eje de giro del vehículo espacial, a pesar de su mayor complejidad mecánica y número de variables de control.

Abstract

In this master's thesis, an assessment of the dynamic modelling and control of E-sail deployment operations has been performed. In particular, the two-dimensional equations of motion of both tangential and radial symmetrical deployment strategies have been derived using a Lagrangian-based approximation.

For these dynamical models, both linear and non-linear control full state laws have been developed, as well as an Extended Kalman Filter (EKF), using the available actuators and sensors, respectively. The performance of the output feedback control laws (this is, the feedback control laws computed using the state estimated by the EKF) has been finally assessed taking into account a realistic level of noise within the measurements.

Thus, the implemented control algorithms proved the controllability of both deployment strategies, whereas the order of magnitude of the obtained errors were reasonable given the significance of the introduced perturbations. Additionally, the radial deployment strategy presented significantly lower control requirements with respect to the tangential deployment strategy in terms of the torque to be applied into the hub spin axis, despite its higher mechanical complexity and number of control variables.

Table of Contents

Resumen III
Abstract V

List of Figures IX
List of Tables XI
Notation XIII

1 Introduction **1**
1.1 Aim of the project 3
1.2 Structure 3

2 Introduction to E-sail deployment **5**

3 E-sail deployment model derivation **9**
3.1 Tangential deployment dynamics 9
3.1.1 Unwrap Dynamics 9
3.1.2 Hinging Dynamics 15
3.2 Radial deployment dynamics 21

4 E-sail deployment control assessment **29**
4.1 Tangential deployment 29
4.1.1 Unwrap dynamics 29
Finite horizon LQR control law 31
Non-linear control law 33
4.1.2 Hinging dynamics 36
Finite horizon LQR control law 37
Non-linear control law 39
Infinite horizon LQR control law 39
4.2 Radial deployment 41
Finite horizon LQR control law 43
Infinite horizon LQR control law 45

5 Perturbations assessment **47**

6 Simulation results **51**
6.1 Tangential deployment 51
6.1.1 Unwrap dynamics 51
6.1.2 Hinging dynamics 56
6.2 Radial deployment 61

7 Conclusions and future work **67**
7.1 Future work 68

Bibliography 69

Appendix A Jacobian matrices of the defined dynamical systems **71**

A.1 Tangential deployment 71

A.1.1 Unwrap dynamics 71

A.1.2 Hinging dynamics 74

A.2 Radial deployment 77

Appendix B Non-symmetrical radial deployment model **87**

List of Figures

1.1 E-sail's deflection of solar wind particles. Artist rendering image by A. Szames extracted from *https:// www.electric-sailing.fi/* 1
1.2 E-sail configuration. Adapted from Janhunen et al. [1] 2

2.1 Tangential deployment strategy. Adapted from Fulton and Schaub [2, 3] 5
2.2 Radial deployment strategy. Adapted from Fulton and Schaub [2, 3] 6

3.1 Reference frames and degrees of freedom (unwrap dynamics) 10
3.2 Relationship between the potential energy (associated to the axial flexibility terms) and the kinetic energy of the E-sail system for a range of ω and $m_{E,\,i}$ values (unwrap dynamics). Results evaluated for $m_H = 300$ kg, $R = 1$ m, $l = 4$ km, $N = 8$, $E = 70$ GPa, $D = 0.74$ mm 14
3.3 Reference frames and degrees of freedom (hinging dynamics) 15
3.4 Relationship between the potential energy (associated to the axial flexibility terms) and the kinetic energy of the E-sail system for a range of ω and $m_{E,\,i}$ values (hinging dynamics). Assessment evaluated for $m_H = 300$ kg, $R = 1$ m, $l = 4$ km, $N = 8$, $E = 70$ GPa, $D = 0.74$ mm 20
3.5 Reference frames and degrees of freedom (radial deployment dynamics) 21
3.6 Relationship between the potential energy (associated to the axial flexibility terms) and the kinetic energy of the E-sail system for a range of ω and $m_{E,\,i}$ values (radial deployment dynamics). Assessment evaluated for $m_H = 300$ kg, $R = 1$ m, $l = 4$ km, $N = 8$, $E = 70$ GPa, $D = 0.74$ mm 28

4.1 Linear stability region of the proposed non-linear control law (unwrap dynamics) as a function of k_{u1} and k_{u2}. Assessment evaluated for $m_H = 300$ kg, $R = 1$ m, $l = 10$ m, $N = 8$ 35

5.1 System architecture - perturbations assessment 47

6.1 Relative errors of the hub angular velocity and deployment rate (unwrap dynamics, non-perturbed case) 52
6.2 Evolution of the tension of each tether and the applied torque (unwrap dynamics, non-perturbed case) 53
6.3 Relative errors of the angular hub velocity (ω) within the usage of the proposed linear and non-linear control laws in perturbed and non-perturbed cases (unwrap dynamics) 53
6.4 Relative errors within the deployment rate ($\dot{l}$) within the usage of the proposed linear and non-linear control laws in perturbed and non-perturbed cases (unwrap dynamics) 54
6.5 Evolution of the applied torque (u_s) within the usage of the proposed linear and non-linear control laws in perturbed and non-perturbed cases (unwrap dynamics) 54
6.6 Evolution of the tether tension (T) within the usage of the proposed linear and non-linear control laws in perturbed and non-perturbed cases (unwrap dynamics) 55
6.7 Evolution of the hub angular velocity and the angle of the tethers with respect to the tangential direction (hinging dynamics, non-perturbed case) 56
6.8 Evolution of the tension of each tether and the applied torque (hinging dynamics, non-perturbed case) 57
6.9 Relative errors within the angular hub velocity (ω) within the usage of the proposed linear and non-linear control laws in perturbed and non-perturbed cases (hinging dynamics) 57
6.10 Evolution of the angle of the tethers with respect to the tangential direction (β) within the usage of the proposed linear and non-linear control laws in perturbed and non-perturbed cases (hinging dynamics) 58

6.11 Evolution of the applied torque (u_s) within the usage of the proposed linear and non-linear control laws in perturbed and non-perturbed cases (hinging dynamics) 58
6.12 Evolution of the tether tension (T) within the usage of the proposed linear and non-linear control laws in perturbed and non-perturbed cases (hinging dynamics) 59
6.13 Evolution of the hub angular velocity and the angle of the tethers with respect to the tangential direction within the usage of the proposed infinite horizon LQR (stabilization, hinging dynamics) 60
6.14 Evolution of the tether tension and the applied torque within the usage of the proposed infinite horizon LQR (stabilization, hinging dynamics) 60
6.15 Evolution of the hub angular velocity and the angle of the tethers with respect to the radial direction within the usage of the proposed finite horizon LQR control law in perturbed and non-perturbed cases (radial deployment) 61
6.16 Evolution of the deployment rate and the tension of each tether within the usage of the proposed finite horizon LQR control law in perturbed and non-perturbed cases (radial deployment) 62
6.17 Evolution of the control variables within the usage of the proposed finite horizon LQR control law in perturbed and non-perturbed cases (radial deployment) 63
6.18 Evolution of the hub angular velocity and the angle of the tethers with respect to the radial direction within the usage of the proposed infinite horizon LQR control law in perturbed and non-perturbed cases (stabilization, radial deployment) 64
6.19 Evolution of the tether length and the tension of each tether within the usage of the proposed infinite horizon LQR control law in perturbed and non-perturbed cases (stabilization, radial deployment) 64
6.20 Evolution of the control variables within the usage of the proposed infinite horizon LQR control law in perturbed and non-perturbed cases (stabilization, radial deployment) 65

B.1 Reference frames and degrees of freedom (non-symmetrical radial deployment dynamics) 87

List of Tables

5.1 Specifications of the considered sensors 49

6.1 E-sail parameters to be used within the simulations [4, 5, 6] 51
6.2 Initial conditions (unwrap phase) 52
6.3 Initial conditions (hinging phase) 56
6.4 Initial conditions (stabilization, hinging phase) 59
6.5 Initial conditions (radial deployment) 61
6.6 Initial conditions (stabilization, radial deployment) 63

7.1 Integral of the applied torque (U_1), the axial force applied to the tethers by their individual spooling drives (U_2) and the tangential force applied by the remote units (U_3) within both considered tangential and radial deployment manoeuvres 67

Notation

$\dot{(\cdot)}$	Time derivatives
$(')$	τ derivatives
A	Cross-section area of the tethers
A_h	System matrix associated to the linearization of the derived dynamics (hinging dynamics)
A_r	System matrix associated to the linearization of the derived dynamics (radial deployment dynamics)
A_u	System matrix associated to the linearization of the derived dynamics (unwrap dynamics)
a_{uj}	j auxiliary function for the sake of simplifying the notation of the dynamical system (unwrap dynamics)
a_{hj}	j auxiliary function for the sake of simplifying the notation of the dynamical system (hinging dynamics)
a_{rj}	j auxiliary function for the sake of simplifying the notation of the dynamical system (radial deployment dynamics)
a_s	Slope associated to the bias of each of the considered sensors
B_h	Control matrix associated to the linearization of the derived dynamics (hinging dynamics)
B_r	Control matrix associated to the linearization of the derived dynamics (radial deployment dynamics)
B_u	Control matrix associated to the linearization of the derived dynamics (unwrap dynamics)
b_k	Bias associated to the measurements received at a given k instant
b_{uj}	j auxiliary function for the sake of simplifying the notation of the dynamical system (unwrap dynamics)
b_{hj}	j auxiliary function for the sake of simplifying the notation of the dynamical system (hinging dynamics)
b_{rj}	j auxiliary function for the sake of simplifying the notation of the dynamical system (radial deployment dynamics)
c_{rj}	j auxiliary function for the sake of simplifying the notation of the dynamical system (radial deployment dynamics)
c_{uj}	j auxiliary function for the sake of simplifying the notation of the non-linear control law (unwrap dynamics)
D	Diameter of the tethers
d_u	Persistent perturbation term associated to the non-linear control law (unwrap dynamics)
E	Elastic modulus of the tethers
E_c	Kinetic energy of the E-sail system
$E_{c,\,E}$	Kinetic energy of the ensemble of the tether's end-masses
$E_{c,\,H}$	Kinetic energy of the hub

$E_{c,\,T}$	Kinetic energy of the ensemble of the tethers
E_p	Potential energy of the E-sail system
F	Jacobian matrix of a generic dynamical system
f	Generic system of differential equations comprising the dynamics of the system aimed to be analysed
f_h	Generic form of the system differential equations of motion (hinging dynamics)
f_{hj}	j component of the generic form of the system differential equations of motion (hinging dynamics)
f_r	Generic form of the system differential equations of motion (radial deployment dynamics)
f_{rj}	j component of the generic form of the system differential equations of motion (radial deployment dynamics)
f_u	Generic form of the system differential equations of motion (unwrap dynamics)
f_{uj}	j component of the generic form of the system differential equations of motion (unwrap dynamics)
f_{us}	Generic form of the simplified system differential equations of motion (unwrap dynamics)
f_{usj}	j component of the generic form of the simplified system differential equations of motion (unwrap dynamics)
g_{rj}	j auxiliary function for the sake of simplifying the notation of the dynamical system (radial deployment dynamics)
g_u	Auxiliary function associated to the non-linear control law (unwrap dynamics)
h	Expressions of the received measurements as a function of the state variables
H_k	Jacobian matrix of the system of equations associated to the characterization of the received measurements at a given k instant
I_H	Hub inertia
I_T	Inertia of the ensemble of the tethers
$I_{T,\,i}$	Inertia of the i tether (non-symmetrical radial deployment)
$\overline{k}$	Non-dimensional tether rigidity
J_h	LQR cost function (hinging dynamics)
$J_{h,\,\infty}$	Infinite horizon LQR cost function (hinging dynamics)
J_r	LQR cost function (radial deployment dynamics)
$J_{r,\,\infty}$	Infinite horizon LQR cost function (radial deployment dynamics)
J_u	LQR cost function (unwrap dynamics)
$\overline{k}$	Non-dimensional rigidity of the ensemble of the tethers to be deployed
$K_{f\,k}$	Kalman gain associated to a given k instant
K_h	LQR proportional gain matrix (hinging dynamics)
$K_{h,\,\infty}$	Infinite horizon LQR proportional gain matrix (hinging dynamics)
K_r	LQR proportional gain matrix (radial deployment dynamics)
$K_{r,\,\infty}$	Infinite horizon LQR proportional gain matrix (radial deployment dynamics)
K_u	LQR proportional gain matrix (unwrap dynamics)
k_h	Control gain of the non-linear control law (hinging dynamics)
k_{uj}	j auxiliary function for the sake of simplifying the notation of the non-linear control law (unwrap dynamics)
l	Length of the tethers to be deployed
l_i	Length of the i tether to be deployed (non-symmetrical radial deployment)

l_0	Initial length of the tethers to be deployed
$\overline{l}$	Non-dimensional length of the tethers to be deployed
$\dot{l}$	Deployment velocity of the tethers
$\dot{l}_i$	Deployment velocity of the i tether (non-symmetrical radial deployment)
$\dot{l}_0$	Initial deployment velocity of the tethers
$\ddot{l}$	Deployment acceleration of the tethers
$\ddot{l}_i$	Deployment acceleration of the i tether (non-symmetrical radial deployment)
$\dddot{l}$	Third time derivative of the length of tethers to be deployed
$\mathcal{L}$	Lagrangian of the E-sail system
m_E	End-mass of the ensemble of the tethers to be deployed
$\overline{m_E}$	Non-dimensional end-mass of the ensemble of the tethers to be deployed
$m_{E,\,i}$	End-mass of each of the individual tethers
m_H	Hub mass
$\overline{m_H}$	Non-dimensional hub mass
m_T	Mass of the ensemble of the tethers to be deployed
$\overline{m_T}$	Non-dimensional mass of the ensemble of the tethers to be deployed
$m_{T,\,i}$	Deployed mass of each of the individual tethers
N	Numbers of tethers to be deployed
$\mathcal{N}^h$	Inertial reference frame (hinging dynamics)
$\mathcal{N}^r$	Inertial reference frame (radial dynamics)
$\mathcal{N}^u$	Inertial reference frame (unwrap dynamics)
P	Covariance matrix associated to a given state vector
P_0	Initial value of the covariance matrix associated to a given state vector
P_h	Auxiliary matrix used for the definition of the LQR control algorithm (hinging dynamics)
$P_{h,\,\infty}$	Auxiliary matrix used for the definition of the infinite horizon LQR control algorithm (hinging dynamics)
P_r	Auxiliary matrix used for the definition of the LQR control algorithm (radial deployment dynamics)
$P_{r,\,\infty}$	Auxiliary matrix used for the definition of the infinite horizon LQR control algorithm (radial deployment dynamics)
P_u	Auxiliary matrix used for the definition of the LQR control algorithm (unwrap dynamics)
p_{uj}	j control gain of the non-linear control law (unwrap dynamics)
Q_h	LQR weight matrix associated to the state vector (hinging dynamics)
$Q_{h,\,\infty}$	Infinite horizon LQR weight matrix associated to the state vector (hinging dynamics)
$Q_{h,\,end}$	LQR weight matrix associated to the state vector at the end of the control procedure (hinging dynamics)
Q_j	Generalized force term associated to each j Lagrangian equation
Q_r	LQR weight matrix associated to the state vector (radial deployment dynamics)
$Q_{r,\,\infty}$	Infinite horizon LQR weight matrix associated to the state vector (radial deployment dynamics)
$Q_{r,\,end}$	LQR weight matrix associated to the state vector at the end of the control procedure (radial deployment dynamics)
Q_u	LQR weight matrix associated to the state vector (unwrap dynamics)

$Q_{u,\,end}$	LQR weight matrix associated to the state vector at the end of the control procedure (unwrap dynamics)
q_j	Degree of freedom associated to each j Lagrangian equation
R	Hub radius
R_E	Position vector of the tether tip
$R_{E,\,i}$	Position vector of the i tether tip
$\dot{R}_E$	Velocity vector of the tether tip
$\dot{R}_{E,\,i}$	Velocity vector of the i tether tip
$\ddot{R}_E$	Acceleration vector of the tether tip
$\ddot{R}_{E,\,i}$	Acceleration vector of the i tether tip
R_{f_k}	Covariance matrix of the measurements associated to a given k instant
R_h	LQR weight matrix associated to the control vector (hinging dynamics)
$R_{h,\,\infty}$	Infinite horizon LQR weight matrix associated to the control vector (hinging dynamics)
R_r	LQR weight matrix associated to the control vector (radial deployment dynamics)
$R_{r,\,\infty}$	Infinite horizon LQR weight matrix associated to the control vector (radial deployment dynamics)
$R_{T,\,C}$	Position vector of the tether mid point
$R_{T,\,C_i}$	Position vector of the i tether mid point
$\dot{R}_{T,\,C}$	Velocity vector of the tether mid point
$\dot{R}_{T,\,C_i}$	Velocity vector of the i tether mid point
R_u	LQR weight matrix associated to the control vector (unwrap dynamics)
r	Distance
$\mathcal{S}^h$	Non inertial reference frame (hinging dynamics)
$\mathcal{S}^r$	Non inertial reference frame (radial dynamics)
$\mathcal{S}^u$	Non inertial reference frame (unwrap dynamics)
T	Tension force applied to the ensemble of the tethers
T_{adm}	Admissible tension force of each tether
U_1	Integral of the applied torque within the deployment manoeuvre
U_2	Integral of the reaction applied to the tethers by each of the individual reeling mechanisms within the deployment manoeuvre
U_3	Integral of the tangential force applied by the remote units within the deployment manoeuvre
u	Generic control vector
u_h	Control vector (hinging dynamics)
$u_{h,\,ref}$	Control vector reference value (hinging dynamics)
u_r	Control vector (radial deployment dynamics)
$u_{r,\,ref}$	Control vector reference value (radial deployment dynamics)
$u_{r,\,ref\infty}$	Control vector reference value associated to the infinite horizon LQR (radial deployment dynamics)
u_{rj}	j component of the control vector associated to the radial deployment dynamics
u_s	Torque applied to the hub of the spacecraft
$\overline{u_s}$	Non-dimensional torque applied to the hub of the spacecraft
u_u	Control vector (unwrap dynamics)
$u_{u,\,ref}$	Control vector reference value (unwrap dynamics)
u_1	Torque applied to the hub of the spacecraft (radial deployment)
$\overline{u_1}$	Non-dimensional torque applied to the hub of the spacecraft (radial deployment)

u_2	Reaction applied to the tethers by each of the individual reeling mechanisms (radial deployment)
$u_{2,\,i}$	Reaction applied to the i tether by its individual reeling mechanisms (non-symmetrical radial deployment)
$\overline{u_2}$	Non-dimensional reaction applied to the tethers by each of the individual reeling mechanisms (radial deployment)
$\overline{u_{2,\,i}}$	Non-dimensional reaction applied to the i tether by its individual reeling mechanisms (non-symmetrical radial deployment)
u_3	Tangential force applied by the remote units (radial deployment)
$u_{3,\,i}$	Tangential force applied by the remote unit associated to the i tether (non-symmetrical radial deployment)
$\overline{u_3}$	Non-dimensional tangential force applied by the remote units (radial deployment)
$\overline{u_{3,\,i}}$	Non-dimensional tangential force applied by the remote unit associated to the i tether (non-symmetrical radial deployment)
x	Generic state vector
$\hat{x}$	Mean value of the normal distribution associated to a state vector x
$\hat{x}_0$	Initial value of the mean associated to the normal distribution associated to a state vector x
x_h	State vector (hinging dynamics)
$x_{h,\,ref}$	State vector reference value (hinging dynamics)
x_{hj}	j component of the state vector associated to the hinging dynamics
x_r	State vector (radial deployment dynamics)
$x_{r,\,ref}$	State vector reference value (radial deployment dynamics)
$x_{r,\,ref\infty}$	State vector reference value associated to the infinite horizon LQR (radial deployment dynamics)
x_{rj}	j component of the state vector associated to the radial deployment dynamics
x_u	State vector (unwrap dynamics)
$x_{u,\,ref}$	State vector reference value (unwrap dynamics)
x_{uj}	j component of the state vector associated to the unwrap dynamics
z_k	Measurements received at a given k instant
β	Angle between the tethers and a given direction within the rotational plane, corresponding to the local horizon (hinging dynamics) or the radial direction (radial deployment)
β_i	Angle between the i tether and the radial direction (non symmetrical radial deployment)
β_0	Initial angle between the tethers and a given direction within the rotational plane, corresponding to the local horizon (hinging dynamics) or the radial direction (radial deployment)
$\dot{\beta}$	Rotational velocity of the tethers with respect to the hub
$\dot{\beta}_i$	Rotational velocity of the i tether with respect to the hub
$\dot{\beta}_0$	Initial rotational velocity of the tethers with respect to the hub
$\ddot{\beta}$	Rotational acceleration of the tethers with respect to the hub
$\ddot{\beta}_i$	Rotational acceleration of the i tether with respect to the hub
$\Delta_{h,\,j}$	Flexibility contributions to the j equation of the equations of motion (hinging dynamics)
$\overline{\Delta}_{h,\,j}$	Non-dimensional flexibility contributions to the j equation of the equations of motion (hinging dynamics)
$\Delta_{r,\,j}$	Flexibility contributions to the j equation of the equations of motion (radial deployment dynamics)

$\overline{\Delta}_{r,\,j}$	Non-dimensional flexibility contributions to the j equation of the equations of motion (radial deployment dynamics)
$\Delta_{u,\,j}$	Flexibility contributions to the j equation of the equations of motion (unwrap dynamics)
$\overline{\Delta}_{u,\,j}$	Non-dimensional flexibility contributions to the j equation of the equations of motion (unwrap dynamics)
Δu_h	Disturbance control vector (hinging dynamics)
Δu_r	Disturbance control vector (radial deployment dynamics)
Δu_u	Disturbance control vector (unwrap dynamics)
Δx_h	Disturbance state vector (hinging dynamics)
Δx_r	Disturbance state vector (radial deployment dynamics)
Δx_u	Disturbance state vector (unwrap dynamics)
$\Delta\dot{l}$	Errors within the tether deployment rate
$\Delta\omega$	Errors within the hub rotational velocity
λ	Mass per unit length of each of the tethers
ρ	Mass per unit length of the ensemble of the tethers
$\nu(\tau_k)$	Variance associated to the measurements received at a given k instant
τ	Non-dimensional time variable
$\tau_{man,\,h}$	Non-dimensional time used for the completion of the LQR control procedure (hinging dynamics)
$\tau_{man,\,r}$	Non-dimensional time used for the completion of the LQR control procedure (radial deployment dynamics)
$\tau_{man,\,u}$	Non-dimensional time used for the completion of the LQR control procedure (unwrap dynamics)
θ	Hub rotational angle
θ_0	Initial hub rotational angle
ω	Hub rotational velocity
ω_0	Reference hub rotational velocity
$\overline{\omega}$	Non-dimensional hub rotational velocity
$\dot{\omega}$	Hub rotational acceleration
$\ddot{\omega}$	Second time derivative of the hub rotation velocity

1 Introduction

The Electric Solar Wind Sail (shortened as E-sail) concept is a propellantless mean of continuous propulsion, with applications for interplanetary missions for small and medium-size spacecraft. In spite of the limitations of propellant-based low-thrust continuous propulsion systems (e.g., ion thrusters) for interplanetary applications as a result of the amount of propellant that needs to be consumed, the E-sail concept represents a feasible mean for reaching far away objects without depending on gravity assist manoeuvres.

Additionally, its usage can potentially extend the operational time span of missions that require periodic manoeuvres (e.g., maintenance of HALO orbits around a given Lagrange point). Proposed by Pekka Janhunen in 2004 [7], this propulsion system is based on the interaction between the electrostatic field created by a set of thin and long charged tethers (maintained at a high positive voltage by an electron emitter), and solar wind particles (see Figure 1.1).

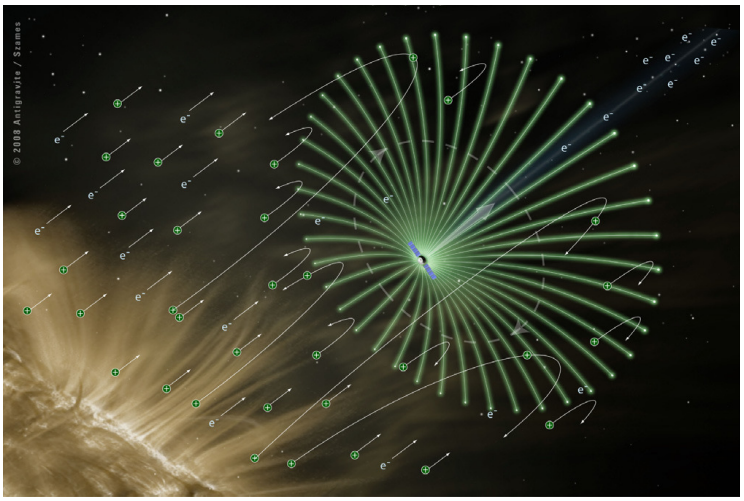

Figure 1.1 E-sail's deflection of solar wind particles. Artist rendering image by A. Szames extracted from *https://www.electric-sailing.fi/*.

Therefore, the thrust is generated by the momentum that the electrostatic field surrounding the E-sail extracts from the incoming solar wind ions. Despite the greater technological maturity of other propellantless propulsion systems (e.g., solar sails), both its lightness and the possibility to orient the subsequent thrust vector make the E-sail concept an alternative propulsion system worth to be considered.

In particular, the mentioned solar sail concept relies on the reflection of the solar wind particles from a large size surface displayed around the vehicle. Thus, momentum is extracted from the incoming ions in order to generate a resultant force on the spacecraft [8]. For instance, the Lightsail 2 mission, currently orbiting the Earth, represents a major success of the implementation of such a device [9].

Nonetheless, the key difference between solar sails and the introduced E-sail concept is that the thrust produced by solar sails is proportional to the inverse of the distance from the Sun squared (that is, r^2), whereas the thrust produced by an E-sail decays inversely with the distance (r) [10, 11]. That makes the E-sail concept feasible for missions with the aim of reaching the outer solar system without the need of gravity assist manoeuvres, in comparison with the limitations that solar sails present on this sense.

Indeed, from its proposal, both their potential applications and the issues regarding its implementation (including among other topics its thrust characterization and the control of its rotational plane) have been assessed by multiple research groups and space agencies [12, 13, 14]. On this matter, ESAIL-EU-FP7, NASA HERTS-1 and NASA HERTS-2 projects have notably contributed to the understanding of E-sail technology [15, 16], providing a solid foundation for its future development.

In spite of the original squared grid E-sail prototype, the currently proposed E-sail configuration relies on an array of radially-oriented long conductive tethers, which are stabilized by the centrifugal force associated to the spacecraft spin (see Figure 1.2); whereas the payload remains in the centre.

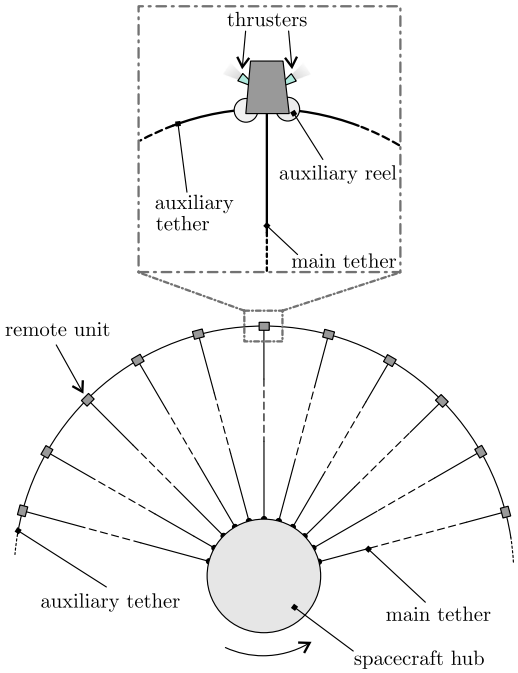

Figure 1.2 E-sail configuration. Adapted from Janhunen et al. [1].

Additionally, each tether holds at his tip a so-called remote unit, equipped with a small thruster to perform adjustments of the E-sail spin rate, and two reels for the deployment of auxiliary tethers. Thus, these units are connected to each other by these auxiliary tethers, which contribute to the stabilization of the fully-deployed E-sail configuration [1].

In the geocentric context, plasma breaks, proposed by Janhunen in 2010, represent another application that arises from the E-sail concept, which in this case relies on the usage of a reduced number of negatively charged tethers with the aim of reducing the decay time of Low Earth Orbit (LEO) satellites after their operational lives [17]. Thus, these latter tethers are unreeled by the satellite in order to produce a drag force as a result of the electrostatic interactions between the tethers and the charged particles in the ionosphere plasma.

1.1 Aim of the project

Given the presented E-sail configuration and taking into account the typical volume restrictions within the launch phase of space vehicles, the deployment of these devices represents a non-trivial problem yet to be resolved for their effective implementation. In fact, at the time of writing this document, no missions have demonstrated a successful deployment of tethers of this nature (i.e., either E-sails, or the simpler plasma break concept).

Thus, the aim of this project is to deeply explore the dynamic modelling and control of E-sail deployment strategies. For this purpose, Lagrangian-based equations of motion have been derived for each of the considered deployment strategies in order to model the physics within the manoeuvre, where the following hypothesis have been taken into account:

- Bidimensional deployment, where the out of plane dynamics are ignored
- Symmetrical deployment of all the tethers
- Gravity effects are not considered, since the spacecraft is assumed to have reached deep space conditions before initiating the deployment
- The E-sail is assumed not to be producing any thrust nor torque within the deployment manoeuvre (i.e., the tethers are assumed to be not charged)

Therefore, these models have been used to explore the control within the manoeuvre, whereas both linear and non-linear control schemes have been proposed for the considered deployment strategies to compare their performance.

Finally, both an Extended Kalman Filter (EKF) and a performance-based algorithm have been developed for the sake of generating the measurements involved within the different deployment strategies. Hence, this architecture aims to evaluate the performance of the output feedback control laws (this is, the feedback control laws computed using the state estimated by the EKF) considering a realistic level of noise within the measurements.

1.2 Structure

The structure of the project is defined as follows:

- **Chapter 2.** Introduction to E-sail deployment. An overview of the literature regarding E-sail deployment operations is presented in order to introduce the different deployment strategies.
- **Chapter 3.** E-sail deployment model derivation. This Chapter comprises the derivation of Lagrangian-based non-dimensional dynamical models used for the characterization of the deployment procedure, which are subsequently used for the exploration of the control within the manoeuvre.
- **Chapter 4.** E-sail deployment control assessment. In this Chapter, the topology of the control laws implemented for each of the derived dynamical models is described.
- **Chapter 5.** Perturbations assessment. In this Chapter, the algorithm used for the consideration of perturbations regarding the sensor modelling through the deployment is presented, in order to assess their effect given the proposed control laws.
- **Chapter 6.** Simulation results. In this Chapter, the results associated to each of the derived dynamical models are presented in order to evaluate the performance of the derived feedback control schemes in both perturbed and non-perturbed cases.
- **Chapter 7.** Conclusions and future lines of research. In this Chapter, both the conclusions from the performed analysis and its associated future lines of research are presented.

2 Introduction to E-sail deployment

In this chapter, an overview of E-sail deployment is given, as well as an introduction to the different deployment strategies in order to derivate their associated dynamical models in Section 3. Thus, as presented in Section 1, the deployment phase is one of the major issues yet to be resolved for the implementation of E-sails (or either the simpler plasma break concept).

On this matter, the ESTCube-1 nanosatellite intended to be the pioneering demonstrator of the deployment of a plasma brake tether [18]. Unfortunately, the unreeling mechanism did not survive to the launch phase due to vibrational loads [19]. Based on the former experience, Aalto-1 mission was equipped with an evolution of the ESTCube-1 deployment mechanism in order to test another plasma brake experiment [20]. In this case, its four tethers were meant to be deployed through centrifugal force. Again, the deployment of the plasma brake did not take place, due to a failure of the unreeling mechanism motor [21].

Consequently, no missions have proved the performance of the E-sail/plasma brake deployment, which justifies the low technological maturity of the current developments of deployment mechanisms [22]. Nonetheless, efforts on this sense made on the frame of ground facilities should be outlined, such as the single-tether deployment system developed by Tinker et al. [23]. This prototype, which was based on the mathematical E-sail deployment model conceived by Hargis et al. [24], was successfully tested on the Marshall Space Flight Center, demonstrating the applicability of such a technology within a controlled environment.

Since E-sail deployment strategies are yet to be proved within a real-life environment, future missions have been proposed to deal with this issue, none of which has succeeded at the time of writing this document: ESTCube-2 (ESTCube-1 descendant) is intended to be a 3U-CubeSat capable of providing in-orbit measurements of Coulomb drag [25]; whereas 3U-CubeSat FORESAIL-1 is designed to deploy a 40- metres-long tether for end-of-life deorbiting purposes [25, 26].

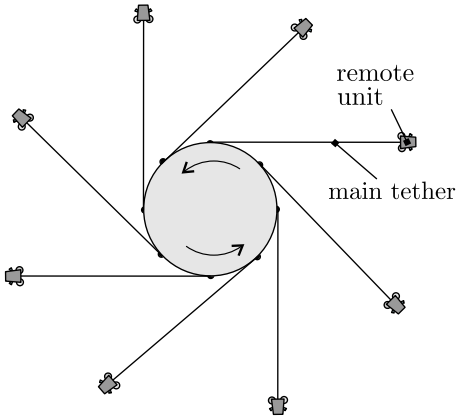

Figure 2.1 Tangential deployment strategy. Adapted from Fulton and Schaub [2, 3].

Moreover, the deployment phase of E-sail is currently been addressed by multiple authors in order to obtain dynamical models of the physics within the process. In particular, some researchers, such as Fulton and Schaub [2, 3], have developed in the past years studies on this matter. In the latter study, the tethers of the considered E-sail, which were assumed to be rotating in their working configuration, were modelled as slender rods assuming the flexibility to be neglected. Given that a tip mass was assumed to be placed at the end of each tether, two deployment strategies were considered: the so-called radial, and tangential deployment.

On one hand, the tangential strategy, similar to a yo-yo de-spinner mechanism (see Figure 2.1), relies on the tangentially aligned deployment of the tethers using the centrifugal acceleration of the end masses. Therefore, the tethers are initially wrapped around a central hub, and they are then unreeled from the hub simultaneously.

In spite of its simplicity, the design of such a deployment system requires further research with regard to the methods for stacking each tether at the initial configuration. Nonetheless, the deployment only relies on the spacecraft spin rate, comprising a free deployment scheme. However, in this strategy, a transition should be made from the purely tangential to the radial operating configuration of the tethers.

Thus, the deployment can be divided in two phases, an unwrap phase that releases the tether, and a hinging phase that performs the transition of the tethers between the tangential and the radial configurations. Nonetheless, given that the overall deployment manoeuvre is controlled through a single hub-mounted actuator, issues regarding the lack of independent control of the individual tethers and the coupling between deployment failure risks should be pointed out.

For this reason, the radially oriented deployment strategy was proposed, relying on the usage of a spooling module (i.e., its own reeling and drive mechanism) for each of the tethers of the E-sail (see Figure 2.2). Therefore, this alternative allows the individual control of each tether, consequently improving the performance of the system in terms of risk of general deployment failure.

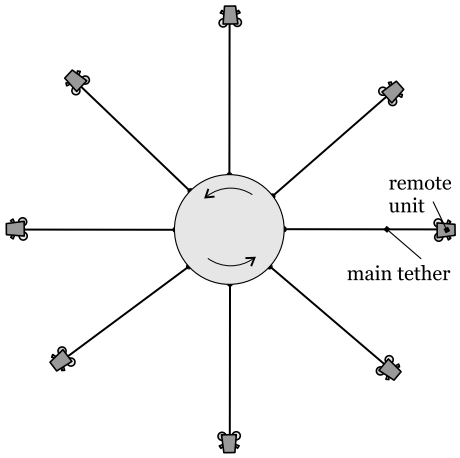

Figure 2.2 Radial deployment strategy. Adapted from Fulton and Schaub [2, 3].

Nonetheless, it should be noted that, in spite of the redundancy improvement that this approach allows, its mechanical complexity (i.e., number of required actuators) increases the total mass and power consumption of the system, as well as synchronization challenges. With respect to the previously presented tangential deployment, this alternative has been further assessed in the literature [4, 27].

For instance, Li et al. [4] studied the radial deployment of a given E-sail through a finite-element method including tether flexibility, whose associated results showed that tangential thrust component provided by the remote units was needed to adequately perform a radial deployment.

For the implementation of such a tangential thrust component, Janhunen et al. [1] proposed two thruster alternatives:

- A cold gas thruster, which can be assumed to have a dry mass of 0.563 kg, with a propellant capability of 0.05 kg, resulting in a total impulse capability of 40 N s.
- An ionic liquid FEEP (Field Emission Electric Propulsion) thruster, which can be assumed to have a dry mass of 0.880 kg, with a propellant capability of 0.07 kg, resulting in a total impulse capability of 2000 N s.

For both cases, the remote units are assumed to have an auxiliary reel system (i.e., for the secondary non-conductive tethers aimed to contribute to the E-sail configuration's stability). In further analysis, thrust requirements for the completion of a radial deployment of this nature will be compared with these specifications in order to assess its feasibility.

Given the performed introduction of the characteristics, advantages and drawbacks of the two considered deployment strategies, Chapter 3 will focus on the modelling of the physics within the two deployment manoeuvres, whereas Chapter 4 will explore their control.

3 E-sail deployment model derivation

In this Chapter, non-dimensional models of both tangential and radial deployment strategies presented in Chapter 2 are aimed to me developed using a Lagrangian-based approximation. Afterwards, in Chapter 4, these models are aimed to be used as a baseline for the exploration of the control requirements within their associated deployment manoeuvres.

Thus, the equations of motion for both approaches have been derived making use of the Lagrangian dynamics formulation, which allows to understand the coupled behaviour between the magnitudes of the problem of concern. The major assumptions to be made for the development of these models are:

- Bidimensional deployment, where the out of plane dynamics are ignored
- Symmetrical deployment of all the N tethers
- The tethers are modelled as length-varying slender rods with mass equal to the current tether mass
- End masses are assumed to be placed at the end of each tether (modelling the remote units to be mounted in a real configuration)
- The spacecraft has reached deep space conditions before initiating deployment (i.e., the gravity effects are not considered as a result of their minor relevance in comparison with the kinetic energy terms governing the system's dynamics) and the sail is not charged during the deployment

Additionally, the tether flexibility is in general not considered throughout the derivation of the models. However, the flexibility terms associated to the axial deformation of the tethers are assessed once each model is derived in order to evaluate its importance at the different deployment phases[1].

3.1 Tangential deployment dynamics

As introduced in Chapter 2, the tangential deployment strategy can be divided in two phases: the so-called unwrap phase, and the hinging phase. For the sake of simplicity, the derivation of the Lagrangian model of this approach has been divided into the same parts. Thus, the unwrap dynamical model is first assessed in Section 3.1.1, whereas the development of the dynamical model of the hinging phase can be found in Section 3.1.2.

3.1.1 Unwrap Dynamics

In order to develop a dynamical model for the unwrap phase of the presented tangential deployment strategy, the definition of both the reference frames and degrees of freedom of Figure 3.1 can be used. Thus, $\mathcal{S}^u$ represents the "moving" reference frame, so that the $\mathcal{S}_1^u$ direction is always parallel to the tether deployment direction, whereas $\mathcal{S}_2^u$ points at the hub-tether junction, outwards the central hub.

[1] Nonetheless, given their minor contribution, these terms will not be considered for the exploration of the control requirements within the deployment in Chapter 4.

On the other hand, the $\mathcal{N}^u$ reference frame represents the inertial reference frame. In Figure 3.1, the degrees of freedom to be used have been defined as well, where l represents the deployed length of the tethers, $\dot{l}$ the deployment velocity, and θ and ω the rotation angle and rotation velocity of the central hub, respectively.

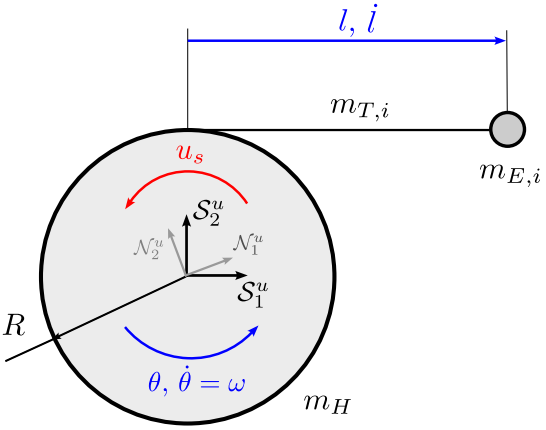

Figure 3.1 Reference frames and degrees of freedom (unwrap dynamics).

Finally, Figure 3.1 also introduces the control parameter to be used for this phase, which in this case represents the torque applied into the hub spin axis (u_s). With these definitions and for the sake of developing a dynamic model for capturing the physics involved in the manoeuvre, the position vector of the tether tip is expressed in the $\mathcal{S}^u$ reference frame as:

$$R_E = l\,\hat{s}_{u,\,1} + R\,\hat{s}_{u,\,2} \tag{3.1}$$

whereas the mid point of the tether is located at:

$$R_{T,\,C} = \frac{l}{2}\,\hat{s}_{u,\,1} + R\,\hat{s}_{u,\,2} \tag{3.2}$$

Given that the $\mathcal{S}^u$ reference frame is not an inertial reference frame, the tether's tip velocity is obtained as:

$$\dot{R}_E = \left.\frac{d(R_E)}{dt}\right|_{\mathcal{S}^u} + \omega_{\mathcal{S}^u/\mathcal{N}^u} \times R_E \tag{3.3}$$

where:

$$\omega_{\mathcal{S}^u/\mathcal{N}^u} = (\omega + \dot{l}/R)\,\hat{s}_{u,\,3} \tag{3.4}$$

Operating with (3.3) and (3.4), the tether-tip velocity is expressed as:

$$\dot{R}_E = -R\,\omega\,\hat{s}_{u,\,1} + l\,(\omega + \dot{l}/R)\,\hat{s}_{u,\,2} \tag{3.5}$$

Analogously, for the obtention of the mid-point velocity of the tethers:

$$\dot{R}_{T,\,C} = \left.\frac{d(R_{T,\,C})}{dt}\right|_{\mathcal{S}^u} + \omega_{\mathcal{S}^u/\mathcal{N}^u} \times R_{T,\,C} \tag{3.6}$$

and following the same presented procedure, (3.6) is expressed as:

$$\dot{R}_{T,\,C} = \left[\dot{l}/2 - R\,(\omega + \dot{l}/R)\right]\,\hat{s}_{u,\,1} + l/2\,(\omega + \dot{l}/R)\,\hat{s}_{u,\,2} \tag{3.7}$$

With (3.5) and (3.7), and assuming the deployment to be symmetrical, the kinetic energy of the system is obtained as:

$$E_c = E_{c,\,H} + E_{c,\,T} + E_{c,\,E} \tag{3.8}$$

where the introduced terms represent:

- The kinetic energy associated to the hub ($E_{c,\,H}$), which experiences a rotational movement, that is:

$$E_{c,\,H} = \frac{1}{2}\,\omega_{\mathcal{N}^u}{}^T\, I_H\, \omega_{\mathcal{N}^u} \tag{3.9}$$

  where $\omega_{\mathcal{N}^u} = \omega\, \hat{s}_{u,\,3}$ is the hub rotational velocity, and I_H represents the hub inertia:

$$I_H = \frac{1}{2}\, m_H\, R^2 + R^2\, (m_T - \rho l) \tag{3.10}$$

  where m_H is the hub mass, m_T is the mass associated to the full-length tethers, R is the hub radius, and $\rho = N\,\lambda$ represents the mass per unit length of the N tethers (given that λ is the mass per unit length of each of the individual tethers).

- The kinetic energy associated to the tethers ($E_{c,\,T}$), which experiences a combination of rotational and translational movements, that is:

$$E_{c,\,T} = \frac{1}{2}\,\omega_{\mathcal{S}^u/\mathcal{N}^u}{}^T\, I_T\, \omega_{\mathcal{S}^u/\mathcal{N}^u} + \frac{1}{2}\,\rho l\, \dot{R}_{T,\,C} \cdot \dot{R}_{T,\,C} \tag{3.11}$$

  where I_T is the inertia associated to the deployed portion of tethers:

$$I_T = \frac{1}{12}\,\rho l^3 + \rho l \left(R^2 + \frac{1}{4}\, l^2\right) \tag{3.12}$$

- The kinetic energy associated to the remote units ($E_{c,\,E}$), which in this case experience a translational movement, that is:

$$E_{c,\,E} = \frac{1}{2}\, m_E\, \dot{R}_E \cdot \dot{R}_E \tag{3.13}$$

  where $m_E = m_{E,\,i}\, N$ represents the mass of the ensemble of the end masses, and $m_{E,\,i}$ is the end-mass of each of the individual tethers.

Therefore, inserting (3.9), (3.11) and (3.13) into (3.8), the kinetic energy of the complete system can be expressed as:

$$\begin{aligned} E_c = &\frac{1}{2}\,\omega^2 \left[\frac{1}{2}\, m_H\, R^2 + R^2\, (m_T - \rho l)\right] + \frac{1}{2}\,(\omega + \dot{l}/R)^2 \left[\frac{1}{12}\,\rho l^3 + \rho l \left(R^2 + \frac{1}{4}\, l^2\right)\right] \\ &+ \frac{1}{8}\,\rho l\, \left[R^2\,(2\omega + \dot{l}/R)^2 + l^2\,(\omega + \dot{l}/R)^2\right] + \frac{1}{2}\, m_E\, \left[R^2\omega^2 + l^2\,(\omega + \dot{l}/R)^2\right] \end{aligned} \tag{3.14}$$

With (3.14), the equations of motion given by Lagrange's approximation are:

$$\frac{d}{dt}\left(\frac{\partial \mathcal{L}}{\partial \dot{q}_j}\right) - \left(\frac{\partial \mathcal{L}}{\partial q_j}\right) = Q_j \tag{3.15}$$

where $\mathcal{L} = E_c - E_p$, and Q_j is the generalized force term associated to each j Lagrangian equation. Since there are no potential energy sources, Lagrange's equations are simplified into:

$$\frac{d}{dt}\left(\frac{\partial E_c}{\partial \dot{q}_j}\right) - \left(\frac{\partial E_c}{\partial q_j}\right) = Q_j \tag{3.16}$$

Therefore, defining $q_1 = l$, the first equation of motion is consequently given by:

$$\begin{aligned} 0 = &\frac{1}{12R^2}\,\dot{\omega}\left(18\rho R^3 l + 7\rho R l^3 + 12 m_E R l^2\right) + \frac{1}{12R^2}\,\ddot{l}\left(15\rho R^2 l + 7\rho l^3 + 12 m_E l^2\right) \\ &+ \frac{1}{24R^2}\,(\dot{l})^2\left(15\rho R^2 + 21\rho l^2 + 24 m_E l\right) - \frac{1}{24R^2}\,\omega^2\left(21\rho R^2 l^2 + 24 m_E R^2 l + 12\rho R^4\right) \end{aligned} \tag{3.17}$$

Defining the following non-dimensional variables:

$$\bar{l} = \frac{l}{R}, \qquad \overline{m_E} = \frac{m_E}{\rho R}, \qquad \overline{\omega} = \frac{\omega}{\omega_0}, \qquad \tau = \frac{t\omega_0}{2\pi} \tag{3.18}$$

where ω_0 represents a reference hub rotation velocity (that can be equalled to the initial spacecraft spin rate for the sake of simplicity). By the introduction of (3.18) into (3.17), the expression is simplified into:

$$\boxed{\begin{aligned} 0 = &\overline{\omega}'\left(72\pi\bar{l} + 28\pi\bar{l}^3 + 48\pi\overline{m_E}\bar{l}^2\right) + \bar{l}''\left(30\bar{l} + 14\bar{l}^3 + 24\overline{m_E}\bar{l}^2\right) \\ &+ \left(\bar{l}'\right)^2\left(15 + 21\bar{l}^2 + 24\overline{m_E}\bar{l}\right) - \overline{\omega}^2\left(48\pi^2 + 84\pi^2\bar{l}^2 + 96\pi^2\overline{m_E}\bar{l}\right) \end{aligned}} \tag{3.19}$$

Analogously, completing the definition of the dynamics of this unwrap phase, the equation associated to $q_2 = \theta$ is given by:

$$\begin{aligned} u_s = &\dot{\omega}\left[\frac{7}{12}\,\rho l^3 + \rho l R^2 + m_E l^2 + \frac{1}{2}\,m_H R^2 + m_T R^2 + m_E R^2\right] + \ddot{l}\left[\frac{7}{12}\,\rho\frac{l^3}{R} + \frac{3}{2}\,\rho l R + m_E\frac{l^2}{R}\right] \\ &+ \omega\dot{l}\left[\rho R^2 + \frac{7}{4}\,\rho l^2 + 2 m_E l\right] + (\dot{l})^2\left[\frac{3}{2}\,\rho R + \frac{7}{4}\rho\frac{l^2}{R} + 2 m_E\frac{l}{R}\right] \end{aligned} \tag{3.20}$$

where u_s represents the torque applied to the hub of the spacecraft, as in Figure 3.1. Simplifying the expression and defining the same non-dimensional variables, including:

$$\overline{m_T} = \frac{m_T}{\rho R}, \qquad \overline{m_H} = \frac{m_H}{\rho R} \tag{3.21}$$

thus, the subsequent differential equation is given by:

$$\boxed{\begin{aligned} \overline{u_s} = &\overline{\omega}'\left[14\pi\bar{l}^3 + 24\pi\bar{l} + 24\pi\overline{m_E}\left(1 + \bar{l}^2\right) + 24\pi\overline{m_T} + 12\pi\overline{m_H}\right] + \bar{l}''\left[7\bar{l}^3 + 18\bar{l} + 12\overline{m_E}\bar{l}^2\right] \\ &+ \overline{\omega}\,\bar{l}'\left[24\pi + 42\pi\bar{l}^2 + 48\pi\overline{m_E}\bar{l}\right] + \left(\bar{l}'\right)^2\left[18 + 21\bar{l}^2 + 24\overline{m_E}\bar{l}\right] \\ = &\frac{48\pi^2 u_s}{\rho R^3 {\omega_0}^2} \end{aligned}} \tag{3.22}$$

where $\overline{u_s}$ is be the control parameter to be used in the sequel. Therefore, to compute the "dimensional" torque u_s to be applied in the real system, $\overline{u_s}$ needs to be postprocessed applying (3.22). As an evolution of the system of differential equations given by (3.19) and (3.22), the elasticity terms associated to the axial forces applied to the tethers can be modelled assuming the tethers to be slender rods with a "beam" modelling of the elastic energy stored within the system. Thus, the potential energy associated to these contributions could be expressed as:

$$-E_p = -\frac{T^2\, l}{2EA} \tag{3.23}$$

where E represents the elastic modulus of the tethers, A stands for the cross-section area of the tethers and T represents the tension force applied to the ensemble of the tethers. In particular, this latter magnitude can be obtained as:

$$T = -m_E\,\ddot{R}_E \cdot \hat{s}_{u,\,1} \tag{3.24}$$

where, as previously derived:

$$\ddot{R}_E = \left.\frac{d(\dot{R}_E)}{dt}\right|_{\mathcal{S}^u} + \omega_{\mathcal{S}^u/\mathcal{N}^u} \times \dot{R}_E \tag{3.25}$$

Simplifying the latter expression given the defined degrees of freedom and reference frames:

$$\ddot{R}_E = -\left(R\dot{\omega} + l\,(\omega + \dot{l}/R)^2\right)\,\hat{s}_{u,\,1} + \left(l\,(\dot{\omega} + \ddot{l}/R) + (\omega + \dot{l}/R)\,(\dot{l} - R\omega)\right)\,\hat{s}_{u,\,2} \tag{3.26}$$

On the other hand, since the only component of the derived acceleration that contributes to the tether tension is the associated to the tangential direction:

$$T = m_E\,\left(R\dot{\omega} + l\,(\omega + \dot{l}/R)^2\right) \tag{3.27}$$

Thus:

$$-E_p = -\frac{{m_E}^2\,l}{2EA}\,\left[R^2\dot{\omega}^2 + l^2\,(\omega + \dot{l}/R)^4 + 2lR\,(\omega + \dot{l}/R)^2\,\dot{\omega}\right] \tag{3.28}$$

Therefore, the axial force contribution to the equations of motion can be derived from the expression:

$$\frac{d}{dt}\left(\frac{\partial(-E_p)}{\partial \dot{q}_j}\right) - \left(\frac{\partial(-E_p)}{\partial q_j}\right) = Q_j \tag{3.29}$$

Operating with (3.29), the flexibility contributions to (3.17) (which will be subsequently denoted as $\Delta_{u,\,1}$) are given by:

$$\begin{aligned}\Delta_{u,\,1} = \frac{{m_E}^2}{2EA}\,\Bigg[&-12l\frac{l}{R}\dot{l}\,(\omega + \dot{l}/R)^3 - 12\frac{l}{R}l^2\,(\omega + \dot{l}/R)^2\,(\dot{\omega} + \ddot{l}/R) - 8l\dot{l}\,(\omega + \dot{l}/R)\,\dot{\omega} \\ &- 4l^2\,(\dot{\omega} + \ddot{l}/R)\dot{\omega}\ddot{\omega} + R^2\dot{\omega}^2 + 4lR\,(\omega + \dot{l}/R)^2\dot{\omega} + 3l^2\,(\omega + \dot{l}/R)^4\Bigg]\end{aligned} \tag{3.30}$$

Defining the non-dimensional rigidity ($\bar{k}$) as:

$$\bar{k} = \frac{EA}{\rho R^2 {\omega_0}^2} \tag{3.31}$$

and simplifying (3.30) as in (3.19), the non-dimensional flexibility terms associated to (3.19) ($\bar{\Delta}_{u,\,1}$) remain as:

$$\bar{\Delta}_{u,\,1} = \frac{3\overline{m_E}^2}{\pi^2\bar{k}}\,\Bigg[-12\bar{l}^2\,\bar{l}'\,\left(2\pi\overline{\omega} + \bar{l}'\right)^3 - 12\bar{l}^3\,\left(2\pi\overline{\omega} + \bar{l}'\right)^2\,\left(2\pi\overline{\omega}' + \bar{l}''\right) \tag{3.32}$$

$$- 8\bar{l}\,\bar{l}'\,\left(2\pi\overline{\omega} + \bar{l}'\right)\,2\pi\overline{\omega}' - 4\bar{l}^2\,\left(2\pi\overline{\omega}' + \bar{l}''\right)\,2\pi\overline{\omega}' + 3\bar{l}^2\,\left(2\pi\overline{\omega} + \bar{l}'\right)^4 \tag{3.33}$$

$$- 4\bar{l}^2\,\left(2\pi\overline{\omega} + \bar{l}'\right)\,2\pi\overline{\omega}'' + 4\pi^2\left(\overline{\omega}'\right)^2 + 4\bar{l}\,\left(2\pi\overline{\omega} + \bar{l}'\right)^2\,2\pi\overline{\omega}'\Bigg] \tag{3.34}$$

Following the same procedure for (3.20), the flexibility contribution in this case ($\Delta_{u,\,2}$) is given by:

$$\begin{aligned}\Delta_{u,\,2} = -\frac{{m_E}^2}{2EA}\,\Bigg[&12l^2\dot{l}\,(\omega + \dot{l}/R)^3 + 12l^3\,(\omega + \dot{l}/R)^2\,(\dot{\omega} + \ddot{l}/R) \\ &+ 8Rl\dot{l}\,(\omega + \dot{l}/R)\,\dot{\omega} + 4l^2R\,(\dot{\omega} + \ddot{l}/R)\,\dot{\omega} + 4l^2R\,(\omega + \dot{l}/R)\,\ddot{\omega}\Bigg]\end{aligned} \tag{3.35}$$

Simplifying (3.35) as in (3.22), the non-dimensional flexibility contribution ($\overline{\Delta}_{u,\,2}$) to (3.22) remains as:

$$\begin{aligned}\overline{\Delta}_{u,\,2} = -\frac{3\overline{m_E}^2}{2\pi^2\bar{k}}\Big[&12\bar{l}^2\bar{l}'\left(2\pi\overline{\omega}+\bar{l}'\right)^3+12\bar{l}^3\left(2\pi\overline{\omega}+\bar{l}'\right)^2\left(2\pi\overline{\omega}'+\bar{l}''\right)\\&+8\bar{l}\bar{l}'\left(2\pi\overline{\omega}+\bar{l}'\right)2\pi\overline{\omega}'+4\bar{l}^2\left(2\pi\overline{\omega}'+\bar{l}''\right)2\pi\overline{\omega}'+4\bar{l}^2\left(2\pi\overline{\omega}+\bar{l}'\right)2\pi\overline{\omega}''\Big]\end{aligned} \tag{3.36}$$

where the non-dimensional rigidity is defined as in (3.31). As introduced, the derived terms in (3.34) and (3.36) have a minor contribution to the overall system dynamics as a result of the nature of the analyzed system. This fact can be justified attending to the parametric study performed within Figure 3.2, where the relationship between the potential energy (Equation (3.28)) and the kinetic energy (Equation (3.14)) of the system has been represented as a function of ω for different values of $m_{E,\,i}$.

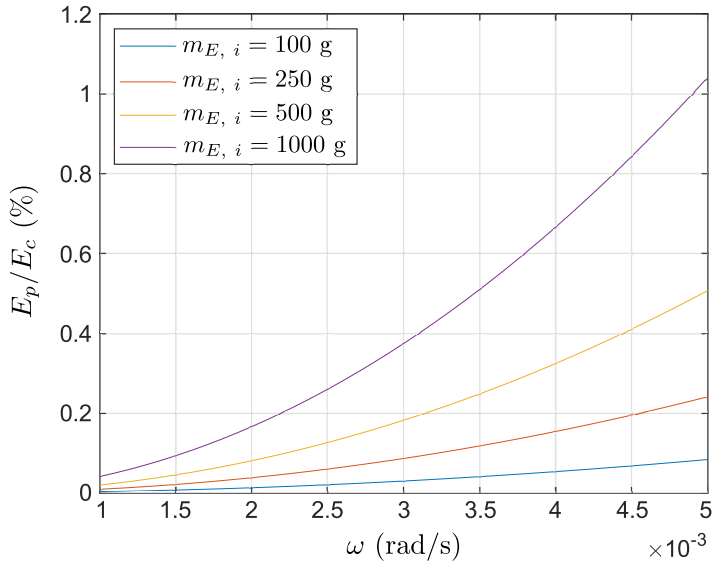

Figure 3.2 Relationship between the potential energy (associated to the axial flexibility terms) and the kinetic energy of the E-sail system for a range of ω and $m_{E,\,i}$ values (unwrap dynamics). Results evaluated for $m_H = 300$ kg, $R = 1$ m, $l = 4$ km, $N = 8$, $E = 70$ GPa, $D = 0.74$ mm.

Thus, for the studied range of both ω and $m_{E,\,i}$ [2], the flexibility terms have a minor relevance with respect to the kinetic energy terms. Therefore, the derived flexibility terms will be disregarded from this point in order to simplify the control assessment of the dynamical system.

[2] Which represent a significant sample of the configurations that could be accounted within real E-sails.

3.1.2 Hinging Dynamics

As in Section 3.1.1, Figure 3.3 defines the reference frames to be used for the development of the hinging dynamical model. Again, $\mathcal{S}^h$ represents the "moving" reference system, whereas in this case $\mathcal{S}_1^h$ always points in the same direction as the tether, and $\mathcal{S}_2^h$ is perpendicular to the latter direction, so that $\mathcal{S}_3^h$ points outwards the rotational plane, in the same direction as $\mathcal{N}_3^h$ (associated to $\mathcal{N}^h$ inertial reference frame).

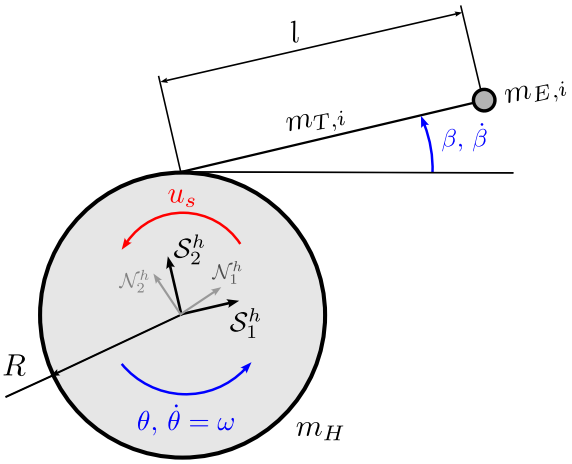

Figure 3.3 Reference frames and degrees of freedom (hinging dynamics).

Additionally, Figure 3.3 defines the degrees of freedom to be used for the dynamic analysis, where β and $\dot{\beta}$ are the angle and angular velocity of the tethers, measured from the purely tangential configuration; and θ and ω are the rotation angle and rotational velocity of the central hub, respectively.

Finally, the torque applied in the hub rotational axis (u_s) is again used as control parameter for the Lagrangian model to be defined. With these definitions and with the aim of deriving a dynamical model for capturing the physics involved in the manoeuvre, the position vector of the tether tip is given in the $\mathcal{S}^h$ reference frame as:

$$R_E = (R\ \sin\beta + l)\ \hat{s}_{h,\,1} + R\ \cos\beta\ \hat{s}_{h,\,2} \tag{3.37}$$

where it should be outlined that, in this case, l is no longer a degree of freedom, and represents the fully-deployed length of the tether. On the other side, the position of the mid point of the tether is obtained as:

$$R_{T,\,C} = (R\ \sin\beta + l/2)\ \hat{s}_{h,\,1} + R\ \cos\beta\ \hat{s}_{h,\,2} \tag{3.38}$$

Since the $\mathcal{S}^h$ reference frame is not an inertial reference system, the velocity of the tether's tip is obtained as:

$$\dot{R}_E = \left.\frac{d(R_E)}{dt}\right|_{\mathcal{S}^h} + \omega_{\mathcal{S}^h/\mathcal{N}^h} \times R_E \tag{3.39}$$

where:

$$\omega_{\mathcal{S}^h/\mathcal{N}^h} = (\omega + \dot{\beta})\ \hat{s}_{h,\,3} \tag{3.40}$$

Operating with (3.39) and (3.40), the tether-tip velocity can be obtained as:

$$\dot{R}_E = -R\ \omega\ \cos\beta\ \hat{s}_{h,\,1} + \Big(R\ \omega\ \sin\beta + l\ (\omega + \dot{\beta})\Big)\ \hat{s}_{h,\,2} \tag{3.41}$$

Similarly, for the derivation of the mid-point velocity of the tethers:

$$\dot{R}_{T,\,C} = \left.\frac{d(R_{T,\,C})}{dt}\right|_{\mathcal{S}^h} + \omega_{\mathcal{S}^h/\mathcal{N}^h} \times R_{T,\,C} \tag{3.42}$$

and using (3.40) and (3.42), this magnitude becomes:

$$\dot{R}_{T,\,C} = -R\,\omega\,\cos\beta\,\hat{s}_{h,\,1} + \left(l/2\,\dot{\beta} + \omega\,(R\,\sin\beta + l/2)\right)\,\hat{s}_{h,\,2} \tag{3.43}$$

With (3.41) and (3.43), and assuming the tethers to be deployed symmetrically, the kinetic energy of the system is obtained as:

$$E_c = E_{c,\,H} + E_{c,\,T} + E_{c,\,E} \tag{3.44}$$

where the terms in (3.44) represent:

- The kinetic energy associated to the hub ($E_{c,\,H}$), which experiences a rotational movement, that is:

$$E_{c,\,H} = \frac{1}{2}\,\omega_{\mathcal{N}^h}{}^T\,I_H\,\omega_{\mathcal{N}^h} \tag{3.45}$$

  where $\omega_{\mathcal{N}^h} = \omega\,\hat{s}_{h,\,3}$ is the hub rotational velocity, and I_H represents the hub inertia:

$$I_H = \frac{1}{2}\,m_H\,R^2 \tag{3.46}$$

  where m_H is the hub mass, and R is the hub radius.

- The kinetic energy associated to the tethers ($E_{c,\,T}$), which experience a combination of rotational and translational movements, that is:

$$E_{c,\,T} = \frac{1}{2}\,\omega_{\mathcal{S}^h/\mathcal{N}^h}{}^T\,I_T\,\omega_{\mathcal{S}^h/\mathcal{N}^h} + \frac{1}{2}\,\rho l\,\dot{R}_{T,\,C}\cdot\dot{R}_{T,\,C} \tag{3.47}$$

  where $\rho = N\,\lambda$ is the mass per unit length of the N tethers (given that λ is the mass per unit length of each of the individual tethers); and I_T the inertia of the ensemble of the tethers, which is given by:

$$I_T = \rho l\left(R^2 + \frac{1}{3}\,l^2 + Rl\sin\beta\right) \tag{3.48}$$

- The kinetic energy associated to the remote units ($E_{c,\,E}$), which in this case experience a purely translational movement:

$$E_{c,\,T} = \frac{1}{2}\,m_E\,\dot{R}_E\cdot\dot{R}_E \tag{3.49}$$

  where $m_E = m_{E,\,i}\,N$ represents the mass of the ensemble of the end masses, and $m_{E,\,i}$ is the end-mass of each of the individual tethers.

Therefore, operating with (3.45), (3.47) and (3.49), the kinetic energy of the complete system remains:

$$\begin{aligned} E_c =& \frac{1}{2}\,\rho l\left[R^2\omega^2 + \frac{1}{4}\,l^2\dot{\beta}^2 + \omega^2\left(\frac{1}{4}\,l^2 + lR\sin\beta\right) + l\omega\dot{\beta}(R\sin\beta + l/2)\right] + \frac{1}{4}\,\omega^2 m_H R^2 \\ &+ \frac{1}{2}\left(\omega+\dot{\beta}\right)^2\rho l\left(R^2 + \frac{1}{3}\,l^2 + Rl\sin\beta\right) + \frac{1}{2}\,m_E\left[\omega^2R^2 + \left(\omega+\dot{\beta}\right)^2 l^2 + 2l\omega R\left(\omega+\dot{\beta}\right)\sin\beta\right] \end{aligned} \tag{3.50}$$

Using Lagrange approximation, the equations of motion of the studied system are given by:

$$\frac{d}{dt}\left(\frac{\partial\mathcal{L}}{\partial\dot{q}_j}\right) - \left(\frac{\partial\mathcal{L}}{\partial q_j}\right) = Q_j \tag{3.51}$$

where $\mathcal{L} = E_c - E_p$, and Q_j represents the generalized force term associated to each j Lagrangian equation. Since there are no potential energy sources, Lagrange's equations are simplified into:

$$\frac{d}{dt}\left(\frac{\partial E_c}{\partial \dot{q}_j}\right) - \left(\frac{\partial E_c}{\partial q_j}\right) = Q_j \tag{3.52}$$

Thus, defining $q_1 = \beta$, the first equation of motion is given by:

$$\begin{aligned} 0 =& \dot{\omega}\left(\rho l R^2 + \frac{7}{12}\rho l^3 + m_E l^2 + m_E l R \sin\beta + \frac{3}{2}\rho R l^2 \sin\beta\right) - \omega^2(\rho l^2 R\cos\beta + m_E l R\cos\beta) \\ &+ \ddot{\beta}\left(\rho l R^2 + \frac{7}{12}\rho l^3 + \rho R l^2 \sin\beta + m_E l^2\right) + \frac{1}{2}\rho R l^2\left(\dot{\beta}\right)^2 \cos\beta \end{aligned} \tag{3.53}$$

Defining the following non-dimensional variables:

$$\bar{l} = \frac{l}{R}, \qquad \overline{m_E} = \frac{m_E}{\rho R}, \qquad \overline{\omega} = \frac{\omega}{\omega_0}, \qquad \tau = \frac{t\omega_0}{2\pi} \tag{3.54}$$

where ω_0 represents a reference hub spin rate (that can be equalled to the initial rotational velocity of the vehicle for the sake of simplicity). By the introduction of (3.54) into (3.53), the expression becomes:

$$\boxed{\begin{aligned} 0 =& \overline{\omega}'\left(24\pi\bar{l} + 36\pi\bar{l}^2\sin\beta + 14\pi\bar{l}^3 + 24\pi\overline{m_E}\left(\bar{l}\sin\beta + \bar{l}^2\right)\right) + 6\left(\beta'\right)^2\bar{l}^2\cos\beta \\ &- 4\pi^2\overline{\omega}^2\left(12\bar{l}^2\cos\beta + 12\overline{m_E}\bar{l}\cos\beta\right) + \beta''\left(12\bar{l} + 12\bar{l}^2\sin\beta + 7\bar{l}^3 + 12\overline{m_E}\bar{l}^2\right) \end{aligned}} \tag{3.55}$$

Analogously, for completing the definition of the dynamical model of this hinging phase, the equation associated to $q_2 = \theta$ is given by:

$$\begin{aligned} u_s =& \dot{\omega}\left(\frac{1}{2}m_H R^2 + 2\rho l R^2 + \frac{7}{12}\rho l^3 + 2\rho R l^2\sin\beta + m_E R^2 + m_E l^2 + 2m_E l R\sin\beta\right) \\ &+ \omega\dot{\beta}\left(2\rho R l^2\cos\beta + 2m_E l R\cos\beta\right) + \left(\dot{\beta}\right)^2\left(\frac{3}{2}\rho R l^2\cos\beta + m_E l R\cos\beta\right) \\ &+ \ddot{\beta}\left(\rho l R^2 + \frac{7}{12}\rho l^3 + \frac{3}{2}\rho R l^2\sin\beta + m_E\, l^2 + m_E\, l R\sin\beta\right) \end{aligned} \tag{3.56}$$

where u_s represents the torque applied to the hub of the spacecraft, as introduced in Figure 3.3. Simplifying 3.56 and using 3.54, including:

$$\overline{m_H} = \frac{m_H}{\rho R} \tag{3.57}$$

the differential equation for $\overline{\omega}$ remains:

$$\boxed{\begin{aligned} \overline{u_s} =& \overline{\omega}'\left(48\pi\bar{l} + 48\pi\bar{l}^2\sin\beta + 14\pi\bar{l}^3 + 12\pi\overline{m_H} + 24\pi\overline{m_E}\left(1 + 2\bar{l}\sin\beta + \bar{l}^2\right)\right) \\ &+ \beta''\left(12\bar{l} + 18\bar{l}^2\sin\beta + 7\bar{l}^3 + 12\overline{m_E}\left(\bar{l}\sin\beta + \bar{l}^2\right)\right) \\ &+ \left(\beta'\right)^2\left(18\bar{l}^2\cos\beta + 12\overline{m_E}\bar{l}\cos\beta\right) + \overline{\omega}\beta'\left(48\pi\bar{l}^2\cos\beta + 48\pi\overline{m_E}\bar{l}\cos\beta\right) \\ =& \frac{48\pi^2 u_s}{\rho R^3{\omega_0}^2} \end{aligned}} \tag{3.58}$$

where $\overline{u_s}$ is be the control parameter to be used for the exploration of the control within the deployment manoeuvre. Hence, to compute the "dimensional" torque u_s to be applied in the real system, $\overline{u_s}$ needs to be postprocessed applying (3.58).

As in Section 3.1.1, the elasticity terms associated to the axial forces applied to the tethers can be derived modelling the potential energy of the system assuming the tethers to be slender beams. Therefore, the elastic energy associated to these contributions can be expressed as:

$$-E_p = -\frac{T^2\, l}{2EA} \tag{3.59}$$

where E represents the elastic modulus of the tethers, A is the cross-section area of the tethers and T stands for the tension force applied to the whole system of the tethers. In particular, this latter magnitude can be obtained as:

$$T = -m_E\, \ddot{R}_E \cdot \hat{s}_{h,\,1} \tag{3.60}$$

where, as in (3.39):

$$\ddot{R}_E = \left.\frac{d(\dot{R}_E)}{dt}\right|_{\mathcal{S}^h} + \omega_{\mathcal{S}^h/\mathcal{N}^h} \times \dot{R}_E \tag{3.61}$$

Given the reference frames and degrees of freedom defined within Figure 3.3, (3.61) remains:

$$\begin{aligned} \ddot{R}_E = &-\left(R\dot{\omega}\cos\beta + l\,(\omega+\dot{\beta})^2 + R\omega^2\sin\beta\right)\hat{s}_{h,\,1} \\ &+\left(l\,(\dot{\omega}+\ddot{\beta}) + R\dot{\omega}\sin\beta + R\omega\dot{\beta}\cos\beta - R\omega\,(\omega+\dot{\beta})\cos\beta\right)\hat{s}_{h,\,2} \end{aligned} \tag{3.62}$$

Thus, given that the only component of the derived acceleration that contributes to the tether tension is the associated to the tangential direction:

$$T = m_E\,\left(R\dot{\omega}\cos\beta + l\,(\omega+\dot{\beta})^2 + R\omega^2\sin\beta\right) \tag{3.63}$$

Hence:

$$\begin{aligned} -E_p = -\frac{{m_E}^2 l}{2EA}\Bigg[&R^2\dot{\omega}^2\cos^2\beta + 2\dot{\omega}Rl\,\left(\omega+\dot{\beta}\right)^2\cos\beta + l^2\,\left(\omega+\dot{\beta}\right)^4 \\ &+2R^2\omega^2\dot{\omega}\cos\beta\sin\beta + 2\omega^2 Rl\,\left(\omega+\dot{\beta}\right)^2\sin\beta + R^2\omega^4\sin^2\beta\Bigg] \end{aligned} \tag{3.64}$$

Using Lagrange's approximation, the axial force contribution to the equations of motion is given by the expression:

$$\frac{d}{dt}\left(\frac{\partial(-E_p)}{\partial\dot{q}_j}\right) - \left(\frac{\partial(-E_p)}{\partial q_j}\right) = Q_j \tag{3.65}$$

Operating with (3.65), the flexibility contributions to (3.53) (which will be subsequently denoted as $\Delta_{h,\,1}$) are given by:

$$\begin{aligned} \Delta_{h,\,1} = -\frac{l{m_E}^2}{2EA}\Bigg[&4Rl\dot{\omega}\,\left(\omega+\dot{\beta}\right)\cos\beta + 4Rl\dot{\omega}\,\left(\dot{\omega}+\ddot{\beta}\right)\cos\beta - 4Rl\dot{\omega}\dot{\beta}\,\left(\omega+\dot{\beta}\right)\sin\beta \\ &+8Rl\omega\dot{\omega}\,\left(\omega+\dot{\beta}\right)\sin\beta + 4Rl\omega^2\,\left(\dot{\omega}+\ddot{\beta}\right)\sin\beta + 4Rl\omega^2\dot{\beta}\,\left(\omega+\dot{\beta}\right)\cos\beta \\ &+12l^2\,\left(\omega+\dot{\beta}\right)^2\left(\dot{\omega}+\ddot{\beta}\right) + 2R^2\dot{\omega}^2\cos\beta\sin\beta + 2Rl\dot{\omega}\,\left(\omega+\dot{\beta}\right)^2\sin\beta \\ &-2R^2\omega^2\dot{\omega}\cos 2\beta - 2Rl\omega^2\,\left(\omega+\dot{\beta}\right)^2\cos\beta - 2R^2\omega^4\cos\beta\sin\beta\Bigg] \end{aligned} \tag{3.66}$$

Defining the non-dimensional rigidity ($\overline{k}$) as in Section 3.1.1:

$$\overline{k} = \frac{EA}{\rho R^2 {\omega_0}^2} \tag{3.67}$$

and simplifying (3.66) as in (3.55), the non-dimensional flexibility term associated to (3.55) ($\overline{\Delta}_{h,\,1}$) is given by:

$$\begin{aligned}\overline{\Delta}_{h,\,1} = &-\frac{3\overline{l}\,\overline{m_E}^2}{2\pi^2\overline{k}}\Big[\Big(8\pi\overline{l}\overline{\omega}''\ (2\pi\overline{\omega}+\beta') + 8\pi\overline{l}\overline{\omega}'\ \left(2\pi\overline{\omega}'+\beta''\right) + 16\pi^2\overline{l}\overline{\omega}^2\beta'\ (2\pi\overline{\omega}+\beta')\\ &- 8\pi^2\overline{l}\overline{\omega}^2\ (2\pi\overline{\omega}+\beta')^2\Big)\cos\beta + \Big(-8\pi\overline{l}\overline{\omega}'\beta'\ (2\pi\overline{\omega}+\beta') + 32\pi^2\overline{l}\overline{\omega}\ \overline{\omega}'\ (2\pi\overline{\omega}+\beta')\\ &+ 16\pi^2\overline{l}\overline{\omega}^2\ \left(2\pi\overline{\omega}'+\beta''\right) + 4\pi\overline{l}\overline{\omega}'\ (2\pi\overline{\omega}+\beta')^2\Big)\sin\beta - 16\pi^3\overline{\omega}^2\overline{\omega}'\cos 2\beta\\ &+ \left(8\pi^2(\overline{\omega}')^2 - 32\pi^4\overline{\omega}^4\right)\cos\beta\sin\beta + 12\overline{l}^2\ (2\pi\overline{\omega}+\beta')^2\ \left(2\pi\overline{\omega}'+\beta''\right)\Big]\end{aligned} \tag{3.68}$$

Analogously, the flexibility contribution to (3.56) ($\Delta_{h,\,2}$) remains:

$$\begin{aligned}\Delta_{h,\,2} = &-\frac{l{m_E}^2}{2EA}\Big[4Rl\ddot{\omega}\ \left(\omega+\dot{\beta}\right)\cos\beta + 4Rl\dot{\omega}\ \left(\dot{\omega}+\ddot{\beta}\right)\cos\beta - 4Rl\dot{\omega}\dot{\beta}\ \left(\omega+\dot{\beta}\right)\sin\beta\\ &+ 12l^2\ \left(\omega+\dot{\beta}\right)^2\ \left(\dot{\omega}+\ddot{\beta}\right) + 2R^2(\dot{\omega})^2\sin 2\beta + 2R^2\omega\ddot{\omega}\sin 2\beta + 4R^2\omega\dot{\omega}\dot{\beta}\cos 2\beta\\ &+ 4Rl\dot{\omega}\ \left(\omega+\dot{\beta}\right)^2\sin\beta + 8Rl\omega\ \left(\omega+\dot{\beta}\right)\ \left(\dot{\omega}+\ddot{\beta}\right)\sin\beta + 4Rl\omega\dot{\beta}\ \left(\omega+\dot{\beta}\right)^2\cos\beta\\ &+ 8Rl\omega\dot{\omega}\ \left(\omega+\dot{\beta}\right)\sin\beta + 4Rl\omega^2\ \left(\dot{\omega}+\ddot{\beta}\right)\sin\beta + 4Rl\omega^2\dot{\beta}\ \left(\omega+\dot{\beta}\right)\cos\beta\\ &+ 12R^2\omega^2\dot{\omega}\sin\beta + 4R^2\omega^3\dot{\beta}\cos\beta\Big]\end{aligned} \tag{3.69}$$

Simplifying (3.69) as in (3.58), the non-dimensional flexibility contribution associated to (3.58) ($\overline{\Delta}_{h,\,2}$) is expressed as:

$$\begin{aligned}\overline{\Delta}_{h,\,2} = &-\frac{6\overline{l}\,\overline{m_E}^2}{\pi^2\overline{k}}\Big[2\pi\overline{l}\overline{\omega}'\ (2\pi\overline{\omega}+\beta')^2 + 4\pi\overline{l}\overline{\omega}\ (2\pi\overline{\omega}+\beta')\ \left(2\pi\overline{\omega}'+\beta''\right) + 8\pi^2\overline{l}\overline{\omega}\ \overline{\omega}'\\ &+ (2\pi\overline{\omega}+\beta')\ \Big(2\pi\overline{l}\overline{\omega}''\ (2\pi\overline{\omega}+\beta') + 2\pi\overline{l}\overline{\omega}'\ \left(2\pi\overline{\omega}'+\beta''\right) + 2\pi\overline{l}\overline{\omega}\beta'\ (2\pi\overline{\omega}+\beta')^2\\ &+ 4\pi^2\overline{l}\overline{\omega}^2\beta'\ (2\pi\overline{\omega}+\beta') + 8\pi^3\overline{\omega}^3\beta'\Big)\cos\beta + \left(2\pi^2\left(\overline{\omega}'\right)^2 + 2\pi^2\overline{\omega}''\overline{\omega}\right)\sin 2\beta\\ &+ 3\overline{l}^2\ (2\pi\overline{\omega}+\beta')^2\ \left(2\pi\overline{\omega}'+\beta''\right) + \Big(-2\pi\overline{l}\overline{\omega}'\beta'\ (2\pi\overline{\omega}+\beta')\\ &+ 4\pi^2\overline{l}\overline{\omega}^2\ \left(2\pi\overline{\omega}'+\beta''\right) + 24\pi^3\overline{\omega}^2\overline{\omega}'\Big)\sin\beta + 4\pi^2\overline{\omega}\ \overline{\omega}'\beta'\cos 2\beta\Big]\end{aligned} \tag{3.70}$$

where the non-dimensional rigidity is defined as in (3.67). As previously mentioned, the derived terms in (3.68) and (3.70) have a minor contribution to the overall system dynamics as a result of the orders of magnitude of the variables involved within the physics of the problem.

This statement can be further justified appealing to the parametric study whose results can be found in Figure 3.4, where the relationship between the potential energy (Equation (3.64)) and the kinetic energy (Equation (3.50)) of the system has been represented as a function of ω for different values of $m_{E,\,i}$.

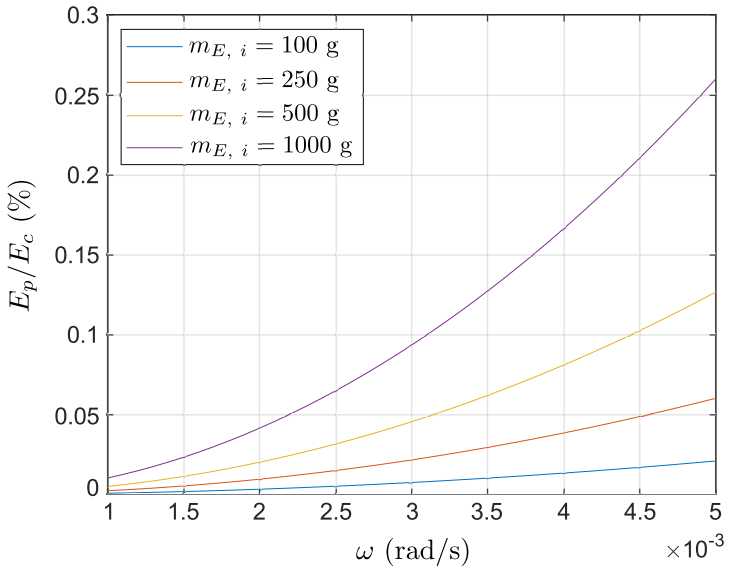

Figure 3.4 Relationship between the potential energy (associated to the axial flexibility terms) and the kinetic energy of the E-sail system for a range of ω and $m_{E,\,i}$ values (hinging dynamics). Assessment evaluated for $m_H = 300$ kg, $R = 1$ m, $l = 4$ km, $N = 8$, $E = 70$ GPa, $D = 0.74$ mm.

Thus, the derived flexibility terms have indeed a minor contribution to the overall dynamics of the E-sail (in comparison with the contributions associated to the kinetic energy of the system) for the studied range of both ω and $m_{E,\,i}$ [3]. For this reason, this terms will be disregarded from this point in order to simplify the control laws intended to be developed within Chapter 4.

[3] Which represent a significant sample of the configurations that can be accounted within real E-sails.

3.2 Radial deployment dynamics

In order to derive a dynamical model for the radial deployment strategy presented within Chapter 2, the reference frames, degrees of freedom and control variables to be used for the description of the manoeuvre are defined within Figure 3.5. Similarly to Section 3.1, $\mathcal{S}^r$ represents the "moving" reference frame, where $\mathcal{S}^r_1$ remains with the same direction as the tether through the deployment, and $\mathcal{S}^r_2$ encloses the reference system by assuring that the subsequent $\mathcal{S}^r_3$ vector points outwards the rotational plane.

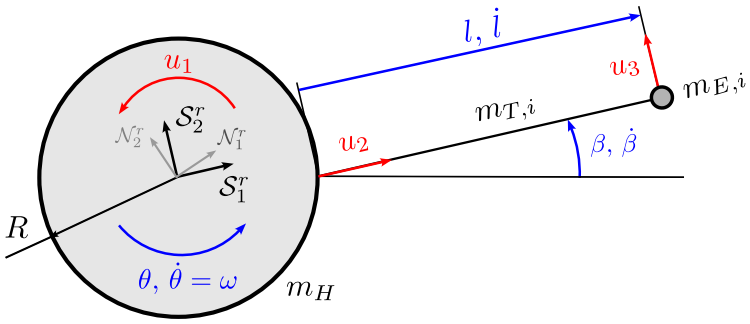

Figure 3.5 Reference frames and degrees of freedom (radial deployment dynamics).

On the other hand, $\mathcal{N}^r$ represents the inertial reference system to be used for the definition of the dynamic model. Continuing with the degrees of freedom to be used for the derivation of the Lagrangian model, three degrees of freedom (in contrast with the two used for each of the phases of the tangential deployment strategy) are considered, including the tether length and deployment rate (l and $\dot{l}$, respectively), the hub rotation angle and spin velocity (θ and ω), and the angle and the angular velocity of the tethers with respect to the purely radial direction (β and $\dot{\beta}$).

With respect of the control variables to be used for the derivation of the dynamical model, again three different magnitudes have been considered, which increases the complexity of the subsequent model with respect to the models derived within Section 3.1. In particular, again the torque applied to the hub spin axis (u_1) is considered, as well as the reaction applied to the tethers by each of their individual reeling mechanisms (u_2).

Additionally, the tangential force applied by the remote units (u_3) is considered as well in order to perform an adequate control of the deployment dynamics. Following with the derivation of the dynamical model of the deployment and given the magnitude definitions presented in Figure 3.5, the position of the tether tip is expressed in the $\mathcal{S}^r$ frame as:

$$R_E = (R\,\cos\beta + l)\,\hat{s}_{r,\,1} - R\,\sin\beta\,\hat{s}_{r,\,2} \tag{3.71}$$

Similarly, the mid point of the tethers is expressed in this reference frame as:

$$R_{T,\,C} = (R\,\cos\beta + l/2)\,\hat{s}_{r,\,1} - R\,\sin\beta\,\hat{s}_{r,\,2} \tag{3.72}$$

Since the $\mathcal{S}^r$ reference frame is not an inertial reference system, the tether's tip velocity is obtained as:

$$\dot{R}_E = \left.\frac{d(R_E)}{dt}\right|_{\mathcal{S}^r} + \omega_{\mathcal{S}^r/\mathcal{N}^r} \times R_E \tag{3.73}$$

where:

$$\omega_{\mathcal{S}^r/\mathcal{N}^r} = (\omega + \dot{\beta})\ \hat{s}_{r,\,3} \tag{3.74}$$

Operating with (3.73) and (3.74), the tether-tip velocity remains:

$$\dot{R}_E = \left(\dot{l} + R\ \omega\ \sin\beta\right)\ \hat{s}_{r,\,1} + \left(R\ \omega\ \cos\beta + l\ \left(\omega + \dot{\beta}\right)\right)\ \hat{s}_{r,\,2} \tag{3.75}$$

Analogously, the obtention of the mid-point velocity of the tethers remains as:

$$\dot{R}_{T,\,C} = \left.\frac{d(R_{T,\,C})}{dt}\right|_{\mathcal{S}^r} + \omega_{\mathcal{S}^r/\mathcal{N}^r} \times R_{T,\,C} \tag{3.76}$$

And operating with (3.74) and (3.76), this magnitude is expressed as:

$$\dot{R}_{T,\,C} = \left(\dot{l}/2 + R\ \omega\ \sin\beta\right)\ \hat{s}_{r,\,1} + \left(R\ \omega\ \cos\beta + l/2\ \left(\omega + \dot{\beta}\right)\right)\ \hat{s}_{r,\,2} \tag{3.77}$$

Using (3.75) and (3.77), and assuming the tethers to be deployed symmetrically, the kinetic energy of the system is expressed as:

$$E_c = E_{c,\,H} + E_{c,\,T} + E_{c,\,E} \tag{3.78}$$

where the terms in (3.78) represent:

- The kinetic energy associated to the hub ($E_{c,\,H}$), which experiences a rotational movement, that is:

$$E_{c,\,H} = \frac{1}{2}\ \omega_{\mathcal{N}^r}{}^T\ I_H\ \omega_{\mathcal{N}^r} \tag{3.79}$$

  where $\omega_{\mathcal{N}^r} = \omega\ \hat{s}_3$ is the hub rotational velocity, and I_H represents the hub inertia:

$$I_H = \frac{1}{2}\ m_H\ R^2 + R^2\ (m_T - \rho l) \tag{3.80}$$

  where m_H is the hub mass, m_T is the mass associated to the full-length tethers, R is the hub radius, and $\rho = N\ \lambda$ represents the mass per unit length of the N tethers (given that λ is the mass per unit length of each of the individual tethers).

- The kinetic energy associated to the tethers ($E_{c,\,T}$), which experience a combination of rotational and translational movements, that is:

$$E_{c,\,T} = \frac{1}{2}\ \omega_{S/N}{}^T\ I_T\ \omega_{S/N} + \frac{1}{2}\ \rho l\ \dot{R}_{T,\,C} \cdot \dot{R}_{T,\,C} \tag{3.81}$$

  where I_T is the inertia associated to the same deployed portion of tethers:

$$I_T = \frac{1}{12}\ \rho l^3 + \rho l\left(R^2 + \frac{1}{4}\ l^2 + Rl\cos\beta\right) \tag{3.82}$$

- The kinetic energy associated to the remote units ($E_{c,\,E}$), which in this case experience a translational movement, that is:

$$E_{c,\,T} = \frac{1}{2}\ m_E\ \dot{R}_E \cdot \dot{R}_E \tag{3.83}$$

  where $m_E = m_{E,\,i}\ N$ is the mass of the ensemble of the end masses, and $m_{E,\,i}$ represents the end-mass of each of the individual tethers.

Therefore, operating with (3.79), (3.81) and (3.83), the kinetic energy of the whole system is expressed as:

$$\begin{aligned} E_c =& \frac{1}{2}\,\omega^2\,\left(\frac{1}{2}\,m_H R^2 + R^2\,(m_T-\rho l)\right) + \frac{1}{2}\,\left(\omega+\dot{\beta}\right)^2\,\left(\frac{1}{3}\,\rho l^3 + \rho l R^2 + \rho R l^2\cos\beta\right) \\ &+ \frac{1}{2}\,\rho l\,\left(\frac{1}{4}\,\left(\dot{l}\right)^2 + \omega^2 R^2 + \omega \dot{l} R\sin\beta + \frac{1}{4}\,l^2\,\left(\omega+\dot{\beta}\right)^2 + \omega R l\,\left(\omega+\dot{\beta}\right)\cos\beta\right) \\ &+ \frac{1}{2}\,m_E\,\left(\left(\dot{l}\right)^2 + R^2\omega^2 + l^2\,\left(\omega+\dot{\beta}\right)^2 + 2\omega\dot{l}R\sin\beta + 2Rl\omega\,\left(\omega+\dot{\beta}\right)\cos\beta\right) \end{aligned} \tag{3.84}$$

Assuming Lagrange's approximation, the equations of motion the system are given by:

$$\frac{d}{dt}\left(\frac{\partial\mathcal{L}}{\partial\dot{q}_j}\right) - \left(\frac{\partial\mathcal{L}}{\partial q_j}\right) = Q_j \tag{3.85}$$

where $\mathcal{L} = E_c - E_p$, and Q_j is the generalized force term associated to each j Lagrangian equation. Since there are no potential energy sources, Lagrange's equations can be simplified into:

$$\frac{d}{dt}\left(\frac{\partial E_c}{\partial\dot{q}_j}\right) - \left(\frac{\partial E_c}{\partial q_j}\right) = Q_j \tag{3.86}$$

Therefore and defining $q_1 = \theta$, the first equation of motion is given by:

$$\begin{aligned} u_1 =& \dot{\omega}\left(\frac{7}{12}\,\rho l^3 + \rho l R^2 + 2\rho R l^2\cos\beta + m_E l^2 + 2m_E R l\cos\beta + \frac{1}{2}\,m_H R^2 + m_T R^2 + m_E R^2\right) \\ &+ \ddot{\beta}\left(\frac{7}{12}\,\rho l^3 + \rho l R^2 + \frac{3}{2}\,\rho R l^2\cos\beta + m_E l^2 + m_E R l\cos\beta\right) + \ddot{l}\,\left(m_E R\sin\beta + \frac{1}{2}\,\rho l R\sin\beta\right) \\ &+ \omega\left(\rho\dot{l}R^2 + 4\rho R l\dot{l}\cos\beta + \frac{7}{4}\rho l^2\dot{l} - 2\rho R l^2\dot{\beta}\sin\beta + 2m_E l\dot{l} + 2m_E R\dot{l}\cos\beta - 2m_E R l\dot{\beta}\sin\beta\right) \\ &+ \dot{\beta}\left(\rho\dot{l}R^2 + \frac{7}{4}\,\rho l^2\dot{l} - \frac{3}{2}\,\rho R l^2\dot{\beta}\sin\beta + 2m_E l\dot{l} + 2m_E R\dot{l}\cos\beta - m_E R l\dot{\beta}\sin\beta + \frac{7}{2}\,\rho l\dot{l}R\cos\beta\right) \\ &+ \frac{1}{2}\,\rho\left(\dot{l}\right)^2 R\sin\beta \end{aligned} \tag{3.87}$$

where, as introduced in Figure 3.5, u_1 represents the torque to be applied in the hub spin axis. Defining the following non-dimensional variables:

$$\bar{l} = \frac{l}{R}, \qquad \overline{m_E} = \frac{m_E}{\rho R}, \qquad \overline{m_H} = \frac{m_H}{\rho R}, \qquad \overline{m_T} = \frac{m_T}{\rho R}, \qquad \overline{\omega} = \frac{\omega}{\omega_0}, \qquad \tau = \frac{t\omega_0}{2\pi} \tag{3.88}$$

where ω_0 represents a reference spacecraft spin rate (that can be equalled to the initial spacecraft angular velocity for the sake of simplicity). Introducing (3.88) into (3.87), the $\overline{\omega}$ differential equation can be simplified

into:

$$\begin{aligned}\overline{u_1} =&\overline{\omega}' \left(14\pi\bar{l}^3+24\pi\bar{l}+48\pi\bar{l}^2\cos\beta+24\pi\overline{m_E}\left(\bar{l}^2+2\bar{l}\cos\beta+1\right)+12\pi\overline{m_H}+24\pi\overline{m_T}\right)\\&+\beta''\left(7\bar{l}^3+12\bar{l}+18\bar{l}^2\cos\beta+12\overline{m_E}\left(\bar{l}^2+\bar{l}\cos\beta\right)\right)+\bar{l}''\left(12\overline{m_E}+6\bar{l}\right)\sin\beta\\&+\overline{\omega}\left(24\pi\bar{l}'+96\pi\bar{l}\bar{l}'\cos\beta+42\pi\bar{l}^2\bar{l}'-48\pi\bar{l}^2\beta'\sin\beta+48\pi\overline{m_E}\left(\bar{l}\bar{l}'+\bar{l}'\cos\beta-\bar{l}\beta'\sin\beta\right)\right)\\&+\beta'\left(12\bar{l}'+21\bar{l}^2\bar{l}'-18\bar{l}^2\beta'\sin\beta+12\overline{m_E}\left(2\bar{l}\bar{l}'+2\bar{l}'\cos\beta-\bar{l}\beta'\sin\beta\right)+42\bar{l}\bar{l}'\cos\beta\right)\\&+6\left(\bar{l}'\right)^2\sin\beta\\=&\frac{48\pi^2u_1}{\rho R^3{\omega_0}^2}\end{aligned}\tag{3.89}$$

where $\overline{u_1}$ is one of the control parameter to be used for the exploration of the control within the deployment procedure. Hence, to compute the "dimensional" torque u_1 to be applied in the real system, $\overline{u_1}$ needs to be postprocessed applying (3.89). Analogously, the equation associated to $q_2 = l$ is given by:

$$\begin{aligned}u_2 =&\ddot{l}\left(\frac{1}{4}\rho l+m_E\right)+\dot{\omega}\left(\frac{1}{2}\rho Rl\sin\beta+m_ER\sin\beta\right)\\&+\omega\left(-\rho R^2\dot{\beta}-\frac{5}{2}\rho Rl\dot{\beta}\cos\beta-\frac{7}{4}\rho l^2\dot{\beta}-2m_El\dot{\beta}\right)\\&+\omega^2\left(-2\rho Rl\cos\beta-\frac{1}{2}\rho R^2-\frac{7}{8}\rho l^2-m_El-m_ER\cos\beta\right)\\&+\left(\dot{\beta}\right)^2\left(-\frac{1}{2}\rho R^2-\rho Rl\cos\beta-\frac{7}{8}\rho l^2-m_El\right)+\frac{1}{8}\rho\left(\dot{l}\right)^2\end{aligned}\tag{3.90}$$

where u_2 represents the reaction applied to the main tethers by their individual spooling drives. Simplifying (3.90) using the variables defined in (3.88), the $\bar{l}^l$ differential equation is given by:

$$\begin{aligned}\overline{u_2} =&\bar{l}''\left(2\bar{l}+8\overline{m_E}\right)+\left(\bar{l}'\right)^2+\overline{\omega}'\left(8\pi\bar{l}\sin\beta+16\pi\overline{m_E}\sin\beta\right)\\&-\overline{\omega}\beta'\left(16\pi+40\pi\bar{l}\cos\beta+28\pi\bar{l}^2+32\pi\overline{m_E}\bar{l}\right)\\&-\overline{\omega}^2\left(64\pi^2\bar{l}\cos\beta+16\pi^2+28\pi^2\bar{l}^2+32\pi^2\overline{m_E}\left(\bar{l}+\cos\beta\right)\right)\\&-\left(\beta'\right)^2\left(4+8\bar{l}\cos\beta+7\bar{l}^2+8\overline{m_E}\bar{l}\right)\\=&\frac{32\pi^2u_2}{\rho R^2{\omega_0}^2}\end{aligned}\tag{3.91}$$

where $\overline{u_2}$ is one of the control parameters to be used for the sake of controlling of the dynamical system. Thus, to compute the "dimensional" force u_2 to be applied in the real system, u_2 needs to be postprocessed applying (3.91). For completing the definition of the dynamics of this deployment strategy, the equation associated to $q_3 = \beta$ is given by:

$$\begin{aligned}u_3\,l =&\dot{\omega}\left(\frac{7}{12}\rho l^3+\rho lR^2+m_El^2+\frac{3}{2}\rho Rl^2\cos\beta+m_ERl\cos\beta\right)\\&+\ddot{\beta}\left(\frac{7}{12}\rho l^3+\rho lR^2+\rho Rl^2\cos\beta+m_El^2\right)+\omega^2\left(\rho Rl^2+m_ERl\right)\sin\beta\\&+\omega\dot{l}\left(\rho R^2+\frac{7}{4}\rho l^2+2m_El+\frac{5}{2}\rho Rl\cos\beta\right)\\&+\dot{\beta}\left(\rho\dot{l}R^2+2\rho Rl\dot{l}\cos\beta+\frac{7}{4}\rho l^2\dot{l}+2m_El\dot{l}-\frac{1}{2}\rho Rl^2\dot{\beta}\sin\beta\right)\end{aligned}\tag{3.92}$$

where u_3 represents the tangential force applied by the remote units. Simplifying (3.92) and using (3.88), the β^I differential equation is given by:

$$\begin{aligned}\overline{u_3}\,\bar{l} =& \overline{\omega}' \left(14\pi\bar{l}^3 + 36\pi\bar{l}^2\cos\beta + 24\pi\bar{l} + 24\pi\overline{m_E}\,\left(\bar{l}^2 + \bar{l}\cos\beta\right)\right) \\ &+ \beta''\,\left(7\bar{l}^3 + 12\bar{l}^2\cos\beta + 12\bar{l} + 12\overline{m_E}\bar{l}^2\right) + \overline{\omega}^2\,\left(48\pi^2\bar{l}^2 + 48\pi^2\overline{m_E}\bar{l}\right)\sin\beta \\ &+ \overline{\omega}\,\bar{l}'\,\left(24\pi + 42\pi\bar{l}^2 + 48\pi\overline{m_E}\bar{l} + 60\pi\bar{l}\cos\beta\right) \\ &+ \beta'\,(12\bar{l}' + 24\bar{l}\bar{l}'\cos\beta + 21\bar{l}^2\bar{l}' + 24\overline{m_E}\bar{l}\bar{l}' - 6\bar{l}^2\beta'\sin\beta) \\ =& \frac{48\pi^2 u_3}{\rho R^2 {\omega_0}^2}\,\bar{l}\end{aligned} \tag{3.93}$$

where $\overline{u_3}$ is one of the control parameters to be used for the control of the dynamics within the deployment. Again, to compute the "dimensional" force u_3 to be applied in the real system, $\overline{u_3}$ needs to be postprocessed applying (3.93). As derived within Section 3.1.1, the elasticity terms associated to the axial forces applied to the tethers can be modelled assuming the tethers to be slender rods or beams. Thus, the potential energy associated to these contributions can be expressed as:

$$-E_p = -\frac{T^2\,l}{2EA} \tag{3.94}$$

where E represents the elastic modulus of the tethers, A is the cross-section area of the tethers and T represents the tension force applied to the system of tethers. In particular, this latter magnitude can be obtained applying:

$$T = -m_E\,\ddot{R}_E \cdot \hat{s}_{r,\,1} \tag{3.95}$$

where, as in (3.73):

$$\ddot{R}_E = \left.\frac{d(\dot{R}_E)}{dt}\right|_{\mathcal{S}^r} + \omega_{\mathcal{S}^r/\mathcal{N}^r} \times \dot{R}_E \tag{3.96}$$

Simplifying (3.96) given the degrees of freedom and reference frames defined in Figure 3.5:

$$\begin{aligned}\ddot{R}_E =& \left(\ddot{l} + R\dot{\omega}\sin\beta - l\,\left(\omega + \dot{\beta}\right)^2 - R\omega^2\cos\beta\right)\hat{s}_{r,\,1} \\ &+ \left(\dot{l}\,\left(\omega + \dot{\beta}\right) + l\,\left(\dot{\omega} + \ddot{\beta}\right) + R\dot{\omega}\cos\beta - R\omega\dot{\beta}\sin\beta + \left(\omega + \dot{\beta}\right)\,\left(\dot{l} + R\omega\sin\beta\right)\right)\hat{s}_{r,\,2}\end{aligned} \tag{3.97}$$

Moreover, since the only component that contributes to the tension is the associated to the tangential direction:

$$T = m_E\,\left(l\,\left(\omega + \dot{\beta}\right)^2 + R\omega^2\cos\beta - \ddot{l} - R\dot{\omega}\sin\beta\right) \tag{3.98}$$

Thus:

$$\begin{aligned}-E_p =& -\frac{l{m_E}^2}{2EA}\,\Big[R^2\omega^4\cos^2\beta + 2Rl\omega^4\cos\beta + Rl\omega^2\left(\dot{\beta}\right)^2\cos\beta \\ &+ 4Rl\omega^3\dot{\beta}\cos\beta - 2R\omega^2\ddot{l}\cos\beta - R^2\omega^2\dot{\omega}\sin 2\beta + l^2\omega^4 + 2l^2\omega^2\left(\dot{\beta}\right)^2 \\ &+ 4l^2\omega^3\dot{\beta} - 2l\omega^2\ddot{l} - 2Rl\omega^2\dot{\omega}\sin\beta + l^2(\dot{\beta})^4 + 4l^2\omega\left(\dot{\beta}\right)^3 - 2l\left(\dot{\beta}\right)^2\ddot{l} \\ &- 2Rl\dot{\omega}\left(\dot{\beta}\right)^2\sin\beta + 4l^2\omega^2\left(\dot{\beta}\right)^2 - 4l\omega\dot{\beta}\ddot{l} - 4Rl\omega\dot{\omega}\dot{\beta}\sin\beta \\ &+ \left(\ddot{l}\right)^2 + 2R\dot{\omega}\ddot{l}\sin\beta + R^2\left(\dot{\omega}\right)^2\sin^2\beta\Big]\end{aligned} \tag{3.99}$$

Given the definition of (3.99), the flexibility contributions to (3.87) (which will be subsequently denoted as $\Delta_{r,\,1}$) are expressed as:

$$\begin{aligned}\Delta_{r,\,1} = \frac{-{m_E}^2}{2EA}\Bigg[&\Big[16Rl\dot{l}\omega^3 + 4Rl\dot{l}\omega\dot{\beta}^2 + 24Rl\dot{l}\omega^2\dot{\beta} - 4R\dot{l}\omega\ddot{l} + 24Rl^2\omega^2\dot{\omega} + 4Rl^2\omega\dot{\beta}\ddot{\beta}\\ &+ 24Rl^2\omega\dot{\omega}\dot{\beta} + 12Rl^2\omega^2\ddot{\beta} - 4Rl\dot{\omega}\ddot{l} - 4Rl\omega\dddot{l} - 4Rl^2\omega\dot{\omega}\dot{\beta} - 2Rl^2\dot{\omega}\dot{\beta}^2\Big]\cos\beta\\ &+\Big[-8Rl\dot{l}\omega\dot{\omega} - 8Rl\dot{l}\omega\dot{\beta} - 8Rl^2\omega^3\dot{\beta} - 2Rl^2\omega\dot{\beta}^3 - 12Rl^2\omega^2\dot{\beta}^2 + 4Rl\omega\ddot{l}\dot{\beta}\\ &- 4Rl^2\dot{\omega}^2 - 4Rl^2\omega\ddot{\omega} - 4Rl^2\ddot{\omega}\dot{\beta} - 4Rl^2\dot{\omega}\ddot{\beta}\Big]\sin\beta - 4l\omega\dot{l}\ddot{l} + 12l^2\dot{l}\omega^3 + 12l^3\omega^2\dot{\omega}\\ &+ 36l^2\dot{l}\omega\dot{\beta}^2 + 12l^3\dot{\omega}\dot{\beta}^2 + 24l^3\omega\dot{\beta}\ddot{\beta} + 36l^2\dot{l}\omega^2\dot{\beta} + 24l^3\omega\dot{\omega}\dot{\beta} + 12l^3\omega^2\ddot{\beta} - 4l\dot{l}\ddot{l}\omega\\ &- 4l^2\dot{\omega}\ddot{l} - 4l^2\omega\dddot{l} + 12l^2\dot{l}\dot{\beta}^3 + 12l^3\dot{\beta}^2\ddot{\beta} - 8l\dot{l}\ddot{l}\dot{\beta} - 4l^2\ddot{l}\dot{\beta} + \Big[4R^2\dot{l}\omega^3 + 12R^2l\omega^2\dot{\omega}\Big]\cos^2\beta\\ &- 4R^2l\omega\dot{\omega}\dot{\beta}\cos 2\beta + \Big[-2R^2\dot{l}\omega\dot{\omega} - 2R^2l\dot{\omega}^2 - 2R^2l\omega\ddot{\omega} - 4R^2l\omega^3\dot{\beta}\Big]\sin 2\beta\Bigg]\end{aligned} \tag{3.100}$$

Defining the non-dimensional rigidity ($\bar{k}$) as:

$$\bar{k} = \frac{EA}{\rho R^2{\omega_0}^2} \tag{3.101}$$

and simplifying (3.100) as in (3.89), the non-dimensional flexibility term associated to (3.89) ($\bar{\Delta}_{r,\,1}$) is given by:

$$\begin{aligned}\bar{\Delta}_{r,\,1} = \frac{-6\,\bar{m_E}^2}{\pi^2\,\bar{k}}\Bigg[&\Big[27\pi^3\bar{l}\bar{l}'\bar{\omega}^3 + 2\pi\bar{\omega}\bar{l}\bar{l}'\beta'^2 + 24\pi^2\bar{l}\bar{l}'\bar{\omega}^2\beta' - 2\pi\bar{l}'\bar{l}'' + 48\pi^3\bar{l}^2\bar{\omega}^2\bar{\omega}' + 2\pi\bar{l}^2\bar{\omega}\beta'\beta''\\ &+ 24\pi^2\bar{l}^2\bar{\omega}\bar{\omega}'\beta' + 12\pi^2\bar{l}^2\bar{\omega}^2\beta'' - 2\pi\bar{l}\bar{\omega}'\bar{l}'' - 2\pi\bar{\omega}\bar{l}\bar{l}''' - 4\pi^2\bar{l}^2\bar{\omega}\bar{\omega}'\beta' - \pi\bar{l}^2\bar{\omega}'\beta'^2\Big]\cos\beta\\ &+\Big[-8\pi^2\bar{l}\bar{l}'\bar{\omega}\bar{\omega}' - 4\pi\bar{l}\bar{l}'\bar{\omega}'\beta' - 16\pi^3\bar{l}^2\bar{\omega}^3\beta' - \pi\bar{l}^2\bar{\omega}\beta'^3 - 12\pi^2\bar{l}^2\bar{\omega}^2\beta'^2 + 2\pi\bar{l}\bar{\omega}\bar{l}''\beta'\\ &- 4\pi^2\bar{l}^2\bar{\omega}'^2 - 4\pi^2\bar{l}^2\bar{\omega}\bar{\omega}'' - 2\pi\bar{l}^2\bar{\omega}''\beta' - 2\pi\bar{l}^2\bar{\omega}'\beta''\Big]\sin\beta - 2\pi\bar{l}\bar{l}'^2\bar{\omega} + 24\pi^3\bar{l}^2\bar{l}'\bar{\omega}^3\\ &+ 24\pi^3\bar{l}^3\bar{\omega}^2\bar{\omega}' + 18\pi\bar{l}\bar{l}'\bar{\omega}\beta'^2 + 6\pi\bar{l}^3\bar{\omega}'\beta'^2 + 12\pi\bar{l}^3\bar{\omega}\beta'\beta'' + 36\pi^2\bar{l}^2\bar{l}'\bar{\omega}^2\beta' + 24\pi^2\bar{l}^3\bar{\omega}\bar{\omega}'\beta'\\ &+ 12\pi^2\bar{l}^3\bar{\omega}^2\beta'' - 2\pi\bar{l}\bar{l}'\bar{l}''\bar{\omega} - 2\pi\bar{l}^2\bar{l}''\bar{\omega}' - 2\pi\bar{l}^2\bar{\omega}\bar{l}''' + 3\bar{l}^2\bar{l}'\beta'^3 + 4\bar{l}^3\beta'^2\beta'' - 2\bar{l}\bar{l}'\bar{l}''\beta'\\ &- \bar{l}^2\bar{l}'''\beta' + \Big[8\pi^3\bar{l}'\bar{\omega}^3 + 24\pi^3\bar{l}\bar{\omega}^2\bar{\omega}'\Big]\cos^2\beta - 4\pi^2\bar{l}\bar{\omega}\bar{\omega}'\beta'\cos 2\beta + \Big[-2\pi^2\bar{l}'\bar{\omega}\bar{\omega}' - 2\pi^2\bar{l}\bar{\omega}'^2\\ &- 2\pi^2\bar{l}\bar{\omega}\bar{\omega}'' - 8\pi^3\bar{l}\bar{\omega}^3\beta'\Big]\sin 2\beta\Bigg]\end{aligned} \tag{3.102}$$

Analogously, the flexibility contribution to (3.90) ($\Delta_{r,\,2}$) remains:

$$\begin{aligned}\Delta_{r,\,2} = \frac{l\,{m_E}^2}{2EA}\Bigg[&2R\omega^4\cos\beta + R\omega^2\dot{\beta}^2\cos\beta + 4R\omega^3\dot{\beta}\cos\beta + 2l\omega^4 + 4l\omega^2\dot{\beta}^2 + 8l\omega^3\dot{\beta}\\ &- 2\omega^2\ddot{l} - 2R\omega^2\dot{\omega}\sin\beta + 2l\dot{\beta}^4 + 8l\omega\dot{\beta}^3 - 2\dot{\beta}^2\ddot{l} - 2R\dot{\omega}\dot{\beta}^2\sin\beta + 8l\omega^2\dot{\beta}^2\\ &- 4\omega\dot{\beta}\ddot{l} - 4R\omega\dot{\omega}\dot{\beta}\sin\beta\Bigg]\end{aligned} \tag{3.103}$$

Simplifying (3.103) and using the non-dimensional rigidity definition in (3.101), the non-dimensional flexibility contribution associated to (3.91) ($\overline{\Delta}_{r,\,2}$) is expressed as:

$$\begin{aligned}\overline{\Delta}_{r,\,2} = &\frac{\overline{m_E}^2}{\pi^2\,\overline{k}}\Big[16\pi^4\overline{\omega}^4\cos^2\beta + 64\pi^4\overline{l}\overline{\omega}^4\cos\beta + 8\pi^2\overline{l}\overline{\omega}^2\beta'^2\cos\beta + 64\pi^3\overline{l}\overline{\omega}^3\beta'\cos\beta\\ &- 8\pi^2\overline{\omega}^2\overline{l}''\cos\beta - 8\pi^3\overline{\omega}^2\overline{\omega}'\sin 2\beta + 48\pi^4\overline{\omega}^4\overline{l}^2 + 24\pi^2\overline{l}^2\overline{\omega}^2\beta'^2 + 3\overline{l}^2\beta'^4\\ &+ 96\pi^3\overline{l}^2\overline{\omega}^3\beta' - 16\pi^2\overline{l}\overline{\omega}^2\overline{l}'' - 32\pi^3\overline{l}\overline{\omega}^2\overline{\omega}'\sin\beta + 24\pi\overline{l}^2\overline{\omega}\beta'^3\\ &- 4\overline{l}\beta'^2\overline{l}'' - 8\pi\overline{l}\overline{\omega}'\beta'^2\sin\beta + 48\pi^2\overline{l}^2\overline{\omega}^2\beta'^2 - 16\pi\overline{l}\overline{\omega}\beta'\overline{l}''\\ &- 32\pi^2\overline{l}\overline{\omega}\overline{\omega}'\beta'\sin\beta + \overline{l}''^2 + 4\pi\overline{\omega}'\overline{l}''\sin\beta + 4\pi^2\overline{\omega}'^2\sin^2\beta\Big]\end{aligned} \tag{3.104}$$

To finish with, the flexibility terms associated to (3.92) ($\Delta_{r,\,3}$) are given by:

$$\begin{aligned}\Delta_{r,\,3} = &-\frac{l\,m_E{}^2}{2EA}\Big[2R\dot{l}\omega^2\dot{\beta}\cos\beta + 4R\dot{l}\omega^3\cos\beta + 20l\dot{l}\omega^2\dot{\beta} + 4l\dot{l}\omega^3 + 12l\dot{l}\dot{\beta}^3 + 36l\dot{l}\omega\dot{\beta}^2 - 8\dot{l}\dot{\beta}\ddot{l}\\ &- 8R\dot{l}\dot{\omega}\dot{\beta}\sin\beta + 8l\dot{l}\omega^2\dot{\beta} - 8\dot{l}\omega\ddot{l} - 8R\dot{l}\omega\dot{\omega}\sin\beta + 2R\dot{l}\omega^2\dot{\beta}\cos\beta + 4Rl\omega\dot{\omega}\dot{\beta}\cos\beta\\ &+ 2Rl\omega^2\ddot{\beta}\cos\beta - 2Rl\omega^2\dot{\beta}^2\sin\beta + 4R\dot{l}\omega^3\cos\beta + 12Rl\dot{\omega}^2\cos\beta - 4Rl\omega^3\dot{\beta}\sin\beta\\ &+ 8l\dot{l}\omega^2\dot{\beta} + 24l^2\omega\dot{\omega}\dot{\beta} + 12l^2\omega^2\ddot{\beta} + 8l\omega^3\dot{l} + 12l^2\omega^2\dot{\omega} + 12l^2\dot{\beta}^2\ddot{\beta} + 12l^2\dot{\omega}\dot{\beta}^2\\ &+ 24l^2\omega\dot{\beta}\ddot{\beta} - 4l\ddot{\beta}\ddot{l} - 4l\dot{\beta}\dddot{l} - 4Rl\dot{\omega}\ddot{\beta}\sin\beta - 4Rl\omega\ddot{\beta}\sin\beta - 4Rl\omega\dot{\beta}^2\cos\beta - 4l\dot{\omega}\ddot{l} - 4l\omega\dddot{l}\\ &- 4Rl\dot{\omega}^2\sin\beta - 4Rl\omega\dot{\omega}\sin\beta - 4Rl\omega\dot{\omega}\dot{\beta}\cos\beta + R^2\omega^4\sin 2\beta + 2Rl\omega^4\sin\beta + Rl\omega^2\dot{\beta}^2\sin\beta\\ &+ 4Rl\omega^3\dot{\beta}\sin\beta - 2R\omega^2\ddot{l}\sin\beta + 2R^2\omega^2\dot{\omega}\cos 2\beta + 2Rl\omega^2\dot{\omega}\cos\beta + 2Rl\omega\dot{\beta}^2\cos\beta\\ &+ 4Rl\omega\dot{\omega}\dot{\beta}\cos\beta - 2R\dot{\omega}\ddot{l}\cos\beta - R^2\dot{\omega}^2\sin 2\beta\Big]\end{aligned} \tag{3.105}$$

Simplifying (3.105) using the defined non-dimensional variables in (3.88) and (3.101), the flexibility contribution associated to (3.93) ($\overline{\Delta}_{r,\,3}$) is expressed as:

$$\begin{aligned}\overline{\Delta}_{r,\,3} = &-\frac{3\,\overline{l}\,\overline{m_E}^2}{2\pi^2\,\overline{k}}\Big[8\pi^2\overline{l}'\overline{\omega}^2\beta'\cos\beta + 32\pi^3\overline{l}'\overline{\omega}^3\cos\beta + 80\pi^2\overline{l}\overline{l}'\overline{\omega}^2\beta' + 32\pi^3\overline{l}\overline{l}'\overline{\omega}^3 + 12\overline{l}\overline{l}'\beta'^3\\ &+ 72\pi\overline{l}\overline{l}'\overline{\omega}\beta'^2 - 8\overline{l}'\beta'\overline{l}'' - 16\pi\overline{l}'\overline{\omega}'\beta'\sin\beta + 32\pi^2\overline{l}\overline{l}'\overline{\omega}^2\beta' - 16\pi\overline{l}'\overline{\omega}\overline{l}'' - 32\pi^2\overline{l}'\overline{\omega}\overline{\omega}'\sin\beta\\ &+ 8\pi^2\overline{l}'\overline{\omega}^2\beta'\cos\beta + 16\pi^2\overline{l}\overline{\omega}\overline{\omega}'\beta'\cos\beta + 8\pi^2\overline{l}\overline{\omega}^2\beta''\cos\beta - 8\pi^2\overline{l}\overline{\omega}^2\beta'^2\sin\beta\\ &+ 32\pi^3\overline{l}'\overline{\omega}^3\cos\beta + 48\pi^2\overline{l}\overline{\omega}'^2\cos\beta - 32\pi^3\overline{l}\overline{\omega}^3\beta'\sin\beta + 32\pi^2\overline{l}\overline{l}'\overline{\omega}^2\beta' + 96\pi^2\overline{l}^2\overline{\omega}\overline{\omega}'\beta'\\ &+ 48\pi^2\overline{l}^2\overline{\omega}^2\beta'' + 64\pi^3\overline{l}\overline{\omega}^3\overline{l}' + 96\pi^3\overline{l}^2\overline{\omega}^2\overline{\omega}' + 12\overline{l}^2\beta'^2\beta'' + 24\pi\overline{l}^2\overline{\omega}'\beta'^2 + 48\pi\overline{l}^2\overline{\omega}\beta'\beta''\\ &- 4\overline{l}\beta''\overline{l}'' - 4\overline{l}\beta'\overline{l}''' - 8\pi\overline{l}\overline{\omega}''\beta'\sin\beta - 8\pi\overline{l}\overline{\omega}'\beta''\sin\beta - 8\pi\overline{l}\overline{\omega}'\beta'^2\cos\beta - 8\pi\overline{l}\overline{\omega}'\overline{l}''\\ &- 8\pi\overline{l}\overline{l}'''\overline{\omega} - 16\pi^2\overline{l}\overline{\omega}'^2\sin\beta - 16\pi\overline{l}\overline{\omega}\overline{\omega}''\sin\beta - 16\pi\overline{l}\overline{\omega}\overline{\omega}'\beta'\cos\beta + 16\pi^4\overline{\omega}^4\sin 2\beta\\ &+ 32\pi^4\overline{l}\overline{\omega}^4\sin\beta + 4\pi^2\overline{l}\overline{\omega}^2\beta'^2\sin\beta + 32\pi^3\overline{l}\overline{\omega}^3\beta'\sin\beta - 8\pi^2\overline{\omega}^2\overline{l}''\sin\beta\\ &+ 16\pi^3\overline{\omega}^2\overline{\omega}'\cos 2\beta + 16\pi^3\overline{l}\overline{\omega}^2\overline{\omega}'\cos\beta + 4\pi\overline{l}\overline{\omega}'\beta'^2\cos\beta + 16\pi^2\overline{l}\overline{\omega}\overline{\omega}'\beta'\cos\beta\\ &- 4\pi\overline{\omega}'\overline{l}''\cos\beta - 4\pi^2\overline{\omega}'^2\sin 2\beta\Big]\end{aligned} \tag{3.106}$$

As in Section 3.1, the terms derived in (3.102), (3.104) and (3.106) have a minor contribution to the overall deployment dynamics as a result of the orders of magnitude of the variables involved within the physics of the problem.

This fact can be further justified by the parametric study of Figure 3.6, where the relationship between the potential energy (Equation (3.99)) and the kinetic energy (Equation (3.84)) of the system has been represented as a function of ω for different values of $m_{E,\,i}$.

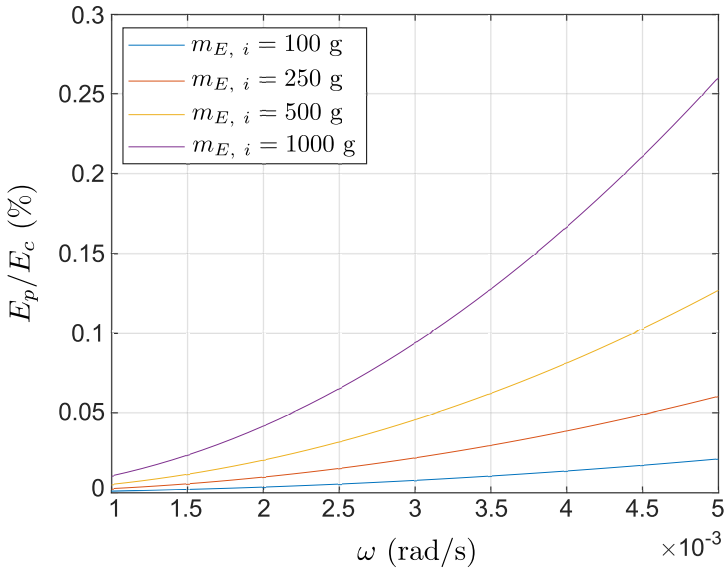

Figure 3.6 Relationship between the potential energy (associated to the axial flexibility terms) and the kinetic energy of the E-sail system for a range of ω and $m_{E,\,i}$ values (radial deployment dynamics). Assessment evaluated for $m_H = 300$ kg, $R = 1$ m, $l = 4$ km, $N = 8$, $E = 70$ GPa, $D = 0.74$ mm.

Hence, for the studied range of both ω and $m_{E,\,i}$ [4], the flexibility terms have a minor relevance with respect to the kinetic energy terms. Therefore, the derived flexibility terms will be disregarded from this point in order to simplify the derivation of the feedback control laws associated to the dynamical system.

[4] Which represent a significant sample of the configurations that could be accounted within real E-sails.

4 E-sail deployment control assessment

In this Chapter, the architecture of the feedback control schemes implemented for the sake of assuring a proper E-sail deployment is assessed. Therefore, Section 4.2 comprises the feedback controls applied to the radial deployment dynamics, whereas Section 4.1 analyses the ones associated to the tangential deployment strategy. For this latter case, the analysis is divided in the two phases introduced within Chapter 3 (unwrap and hinging dynamics).

4.1 Tangential deployment

As previously introduced, the control assessment associated to the tangential deployment strategy has been divided in the two phases introduced within Chapter 3 in order to allow the usage of the previously derived equations of motion. For each of the considered dynamics, both a linear and non-linear control schemes are presented in order to compare their performance.

Moreover, as mentioned in Chapter 3, both dynamical models relies on the torque to be applied to the hub spin axis (u_s, whereas the non-dimensional torque is denoted as $\overline{u_s}$) as the only control parameter for assuring a proper deployment of the E-sail on both phases, in comparison with the higher number of control parameters within the radial deployment strategy.

4.1.1 Unwrap dynamics

To begin with the control assessment associated to this phase of the deployment, the target system behaviour of the unwrap stage is the maintenance of the spacecraft rate throughout the deployment, which is assumed to enforce the deployment rate to be constant as well. In order to study the controllability of the system, the unwrap dynamical model (Equations (3.19) and (3.22)) can be written as:

$$\begin{aligned} a_{u1}\,\dot{x}_{u4} + a_{u2}\,\dot{x}_{u2} + a_{u3}\,{x_{u2}}^2 - a_{u4}\,{x_{u4}}^2 &= 0 \\ b_{u1}\,\dot{x}_{u4} + b_{u2}\,\dot{x}_{u2} + b_{u3}\,x_{u2}\,x_{u4} + b_{u4}\,{x_{u2}}^2 &= u_u \end{aligned} \tag{4.1}$$

where a_{u1}, a_{u2}, a_{u3}, a_{u4}, b_{u1}, b_{u2}, b_{u3} and b_{u4} are positively defined auxiliary functions given by;

$$a_{u1} = 72\pi\,x_{u1} + 28\pi\,(x_{u1})^3 + 48\pi\overline{m_E}\,(x_{u1})^2 \tag{4.2}$$

$$a_{u2} = 30\,x_{u1} + 14\,(x_{u1})^3 + 24\overline{m_E}\,(x_{u1})^2 \tag{4.3}$$

$$a_{u3} = 15 + 21\,(x_{u1})^2 + 24\overline{m_E}\,x_{u1} \tag{4.4}$$

$$a_{u4} = 48\pi^2 + 84\pi^2\,(x_{u1})^2 + 96\pi^2\overline{m_E}\,x_{u1} \tag{4.5}$$

On the other side, for b_{u1}, b_{u2}, b_{u3} and b_{u4}:

$$b_{u1} = 14\pi\,(x_{u1})^3 + 24\pi\,x_{u1} + 24\pi\overline{m_E}\left(1 + (x_{u1})^2\right) + 24\pi\overline{m_T} + 12\pi\overline{m_H} \tag{4.6}$$

$$b_{u2} = 7\,(x_{u1})^3 + 18\,x_{u1} + 12\overline{m_E}\,(x_{u1})^2 \tag{4.7}$$

$$b_{u3} = 24\pi + 42\pi\,(x_{u1})^2 + 48\pi\overline{m_E}\,x_{u1} \tag{4.8}$$

$$b_{u4} = 18 + 21\,(x_{u1})^2 + 24\overline{m_E}\,x_{u1} \tag{4.9}$$

where the state vector of this unwrap phase (x_u) has been defined as:

$$x_u = [\bar{l},\, \bar{l}',\, \theta,\, \overline{\omega}]^T = [x_{u1},\, x_{u2},\, x_{u3},\, x_{u4}]^T \tag{4.10}$$

and, similarly, its associated control vector (u_u) remains:

$$u_u = \overline{u_s} \tag{4.11}$$

The system of differential equations in (4.1) can be expressed as:

$$\dot{x}_u = f_u(x_u,\, u_u,\, \tau) = [f_{u1},\, f_{u2},\, f_{u3},\, f_{u4}]^T \tag{4.12}$$

Therefore, f_u is comprised by four expressions ($f_{u1},\, f_{u2},\, f_{u3}$ and f_{u4}) defined as:

- f_{u1}

$$f_{u1} = \dot{x}_{u1} = x_{u2} \tag{4.13}$$

- f_{u2}

$$f_{u2} = \dot{x}_{u2} = \frac{1}{b_{u2} - b_{u1}\,\dfrac{a_{u2}}{a_{u1}}}\left[\left(b_{u1}\,\frac{a_{u3}}{a_{u1}} - b_{u4}\right)(x_{u2})^2 - b_{u1}\,\frac{a_{u4}}{a_{u1}}\,(x_{u4})^2 - b_{u3}\,x_{u4}\,x_{u2} + u_u\right] \tag{4.14}$$

- f_{u3}

$$f_{u3} = \dot{x}_{u3} = x_{u4} \tag{4.15}$$

- f_{u4}

$$f_{u4} = \dot{x}_{u4} = \frac{-a_{u2}\,f_{u2} - a_{u3}\,(x_{u2})^2 + a_{u4}\,(x_{u4})^2}{a_{u1}} \tag{4.16}$$

With this formulation and as previously introduced, both a linear and non-linear feedback control laws are intended to be developed in order to assure an adequate system behaviour throughout this deployment phase.

Finite horizon LQR control law

On one hand, an LQR (Linear Quadratic Regulator) control law with "finite horizon" has been implemented as the linear control scheme to be applied to this dynamical system. Thus, the architecture of this control law relies on the expression of both the state (Equation (4.10)) and control (Equation (4.11)) vectors as a sum of a reference value and an error or disturbance variable, that is:

$$x_u = x_{u,\,ref} + \Delta x_u \tag{4.17}$$

where $x_{u,\,ref}$ represents the desired E-sail evolution. For the sake of deriving the expression of $x_{u,\,ref}$ and since the main target through this phase is the maintenance of the spacecraft rate (that is, $\overline{\omega}_{ref} = 1$), if the term related to $\bar{l}''$ in (3.19) is assumed to be negligible (that is, $a_{u2}\,\bar{l}'' \simeq 0$), $\bar{l}'_{\,ref}$ remains:

$$\bar{l}'_{\,ref} = \overline{\omega}_{ref}{}^2 \sqrt{\frac{a_{u4}}{a_{u3}}} = \sqrt{\frac{48\pi^2 + 84\pi^2\bar{l}^2 + 96\pi^2\overline{m_E}\bar{l}}{15 + 21\bar{l}^2 + 24\overline{m_E}\bar{l}}} \tag{4.18}$$

Given that, for typical E-sail configurations, the contributions associated to $\overline{m_E}$ are the most relevant terms within the derived expression, (4.18) can be approximated by:

$$\bar{l}'_{\,ref} \simeq \sqrt{\frac{96\pi^2\overline{m_E}\bar{l}}{24\overline{m_E}\bar{l}}} = 2\pi \tag{4.19}$$

Assuming (4.19) and since the time order associated to $\dot{x}_{u2} = \bar{l}''$ is negligible in comparison with $\dot{x}_{u4}$, the dynamical system in (4.1) can be simplified into a single differential equation given by:

$$b_{u1}\,\dot{x}_{u4} + b_{u3}\,x_{u2}\,x_{u4} + b_{u4}\,x_{u2}{}^2 = u_u \tag{4.20}$$

taking into account the previous definition of the state and control vectors. Thus, this simplified dynamical system (f_{us}) can be expressed as:

$$\dot{x}_u = f_{us}(x_u,\, u_u,\, \tau) = [f_{us1},\, f_{us2},\, f_{us3},\, f_{us4}]^T \tag{4.21}$$

where again f_{us} is comprised by four expressions ($f_{us1},\, f_{us2},\, f_{us3}$ and f_{us4}) defined as:

- f_{us1}

$$f_{us1} = \dot{x}_{u1} = x_{u2} \tag{4.22}$$

- f_{us2}

$$f_{us2} = \dot{x}_{u2} = 0 \tag{4.23}$$

- f_{us3}

$$f_{us3} = \dot{x}_{u3} = x_{u4} \tag{4.24}$$

- f_{us4}

$$f_{us4} = \dot{x}_{u4} = \frac{u_u - b_{u3}\,x_{u2}\,x_{u4} - b_{u4}\,x_{u2}{}^2}{b_{u1}} \tag{4.25}$$

where the desired E-sail behaviour (i.e., $x_{u4} = 1$) is indeed an equilibrium of the dynamics. Thus, the reference state ($x_{u,\,ref}$) to be considered for the control law remains:

$$x_{u,\,ref} = [2\pi\tau,\, 2\pi,\, \tau,\, 1]^T \tag{4.26}$$

Analogously, the control to be implemented is comprised as well by two components:

$$u_u = u_{u,\,ref} + \Delta u_u \tag{4.27}$$

where $u_{u,\,ref}$ is obtained by replacing $x_{u,\,ref}$ into (4.20), comprising an open-loop control law, remaining:

$$u_{u,\,ref} = b_{u3}\,\overline{\omega}_{ref}\,\bar{l}'_{ref} + b_{u4}\,\left(\bar{l}'_{ref}\right)^2 \tag{4.28}$$

On the other side, for the determination of the second term of the controller, Δu_u is assumed to have the form of:

$$\Delta u_u = K_u(\tau)\,\Delta x_u \tag{4.29}$$

where $K_u(\tau)$ is a matrix whose value varies with τ, so that a given cost function is minimized. To compute this magnitude, the original set of differential equations governing the E-sail's behaviour should be linearized around the reference state evolution $x_{u,\,ref}$ (i.e., the desired E-sail behaviour), so that a linear system expressed in the disturbance variables is obtained as:

$$\Delta\dot{x}_u = A_u(\tau)\,\Delta x_u + B_u(\tau)\,\Delta u_u \tag{4.30}$$

where $A_u(\tau)$ and $B_u(\tau)$ matrices can be computed as:

$$A_u(\tau) = \left.\frac{\partial f_u(x_u,\,u_u,\,\tau)}{\partial x_u}\right|_{x_{u,\,ref}(\tau),\,u_{u,\,ref}(\tau),\,\tau} \tag{4.31}$$

and analogously:

$$B_u(\tau) = \left.\frac{\partial f_u(x_u,\,u_u,\,\tau)}{\partial u_u}\right|_{x_{u,\,ref}(\tau),\,u_{u,\,ref}(\tau),\,\tau} \tag{4.32}$$

Details regarding the derivation of the terms within A_u and B_u can be found in Appendix A. Therefore, taking into account Equations (4.30), (4.31) and (4.32), and defining the cost function to be minimized as:

$$J_u = \int_0^{\tau_{man,\,u}} \left(\Delta x_u{}^T(\tau)\,Q_u\,\Delta x_u(\tau) + \Delta u_u{}^T(\tau)\,R_u\,\Delta u_u(\tau) + \Delta x_u{}^T(\tau)\,Q_{u,\,end}\,\Delta x_u(\tau)\right) d\tau \tag{4.33}$$

where $\tau_{man,\,u}$ is the time horizon of the control to be performed, which is defined in this case as:

$$\tau_{man,\,u} = \bar{l}_{total} \,/\, \bar{l}'_{ref} \tag{4.34}$$

where $\bar{l}_{total}$ represents the non-dimensional full length of the tethers aimed to be deployed. On the other hand, the matrices Q_u, R_u and $Q_{u,\,end}$ are the weights of the state, the control and the state at the end of the time horizon respectively, which comprise the tuning parameters of the controller determining its behaviour (e.g., more aggressive or more conservative).

These matrices are assumed to be symmetrical, and Q_u and $Q_{u,\,end}$ are defined strictly positive (i.e., all their eigenvalues are positive), whereas $R_u \geq 0$ (i.e., all their eigenvalues are non-negative). Given the cost function defined by 4.33, the optimum value of K_u minimizing J_u is the one obtained by the resolution of the so-called Ricatti differential equation:

$$-\dot{P}_u = A_u{}^T\,P_u + P_u\,A_u - P_u\,B_u\,R_u{}^{-1}\,B_u{}^T\,P_u + Q_u \tag{4.35}$$

verifying the final condition:

$$P_u\,(\tau_{man,\,u}) = Q_{u,\,end} \tag{4.36}$$

whereas $K_u(\tau)$ is then computed as:

$$K_u(\tau) = -{R_u}^{-1}\, {B_u}^T\, P_u\,(\tau) \tag{4.37}$$

Riccati's differential equation is always solvable. Nonetheless, it cannot be solved in real time since the problem is defined through a final condition instead of an initial one (it should be solved in advance for a given reference state evolution, storing the subsequent values of $K_u(\tau)$). Therefore, expressing all the terms as a function of the state variables, the control law to be finally considered is:

$$u_u(x_u,\, \tau) = u_{u,\, ref} + K_u(\tau)\,(x_u - x_{u,\, ref}) \tag{4.38}$$

Non-linear control law

In order to compare the performance of the feedback control scheme given by (4.38), a non-linear feedback control is aimed to be derived. In particular, this feedback control law is intended to partially compensate the non-linear terms of the considered dynamics, whereas their control parameters are defined in order to assure the linear stability of the subsequent dynamical system. Thus, defining $\delta x_{u2} = x_{u2} - 2\pi$ and $\delta x_{u4} = x_{u4} - 1$, the dynamical system given by (4.1) can be expressed in terms of error or disturbance variables as:

$$\begin{aligned}
\delta\dot{x}_{u4} =& -c_{u1}\,(\delta\dot{x}_{u2} + 2\pi)^2 - c_{u2}\,(\delta x_{u4} + 1)^2 - c_{u3}\,(\delta x_{u2} + 2\pi)\,(\delta x_{u4} + 1) + c_{u4}\,u_u \\
\delta\dot{x}_{u2} =& c_{u5}\,(\delta x_{u4} + 1)^2 - c_{u6}\,(\delta x_{u2} + 2\pi)^2 - c_{u7}\,\delta\dot{x}_{u4}
\end{aligned} \tag{4.39}$$

where the τ derivatives of both x_{u1} and x_{u3} have not been taking into account since their associated equilibriums only depend on x_{u2} and x_{u4}. Additionally, a series of auxiliary functions have been defined in order to simplify the control architecture intended to be derived:

$$c_{u1} = \frac{b_{u4} - b_{u2}\,\dfrac{a_{u3}}{a_{u2}}}{b_{u1} - b_{u2}\,\dfrac{a_{u1}}{a_{u2}}}\,, \qquad c_{u2} = \frac{b_{u2}\,\dfrac{a_{u4}}{a_{u2}}}{b_{u1} - b_{u2}\,\dfrac{a_{u1}}{a_{u2}}} \tag{4.40}$$

$$c_{u3} = \frac{b_{u3}}{b_{u1} - b_{u2}\,\dfrac{a_{u1}}{a_{u2}}}\,, \qquad c_{u4} = \frac{1}{b_{u1} - b_{u2}\,\dfrac{a_{u1}}{a_{u2}}} \tag{4.41}$$

$$c_{u5} = \frac{a_{u4}}{a_{u2}}\,, \qquad c_{u6} = \frac{a_{u3}}{a_{u2}}\,, \qquad c_{u7} = \frac{a_{u1}}{a_{u2}} \tag{4.42}$$

Operating with (4.39):

$$\begin{aligned}
\delta\dot{x}_{u4} =& -c_{u1}\,(\delta x_{u2})^2 - c_{u2}\,(\delta x_{u4})^2 - c_{u3}\,\delta x_{u2}\,\delta x_{u4} - (4\pi\,c_{u1} + c_{u3})\,\delta x_{u2} - (2\,c_{u2} + 2\pi\,c_{u3})\,\delta x_{u4} \\
& - 4\pi^2\,c_{u1} - c_{u2} - 2\pi\,c_{u3} + c_{u4}\,\left(u_{u,\, ref} + \delta u_u\right) \\
\delta\dot{x}_{u2} =& c_{u5}\,(\delta x_{u4})^2 - c_{u6}\,(\delta x_{u2})^2 - c_{u7}\,\delta\dot{x}_{u4} + 2c_{u5}\,\delta x_{u4} - 4\pi\,c_{u6}\,\delta x_{u2} + c_{u5} - 4\pi^2\,c_{u6}
\end{aligned} \tag{4.43}$$

Defining:

$$u_{u,\, ref} = \frac{4\pi^2 c_{u1} + c_{u2} + 2\pi c_{u3}}{c_{u4}} = 4\pi^2\left(b_{u4} - b_{u2}\,\frac{a_{u3}}{a_{u2}}\right) + b_{u2}\,\frac{a_{u4}}{a_{u2}} + 2\pi\,b_{u3} \tag{4.44}$$

and equivalently:

$$\delta u_u = \frac{c_{u1}\ (\delta x_{u2})^2 + c_{u2}\ (\delta x_{u4})^2 + c_{u3}\ \delta x_{u2}\ \delta x_{u4} - p_{u1}\ \delta x_{u4} - p_{u2}\ \delta x_{u2}}{c_{u4}} \tag{4.45}$$

where p_{u1} and the p_{u2} are positively defined the control gains. Thus, the system of differential equations in (4.43) remains:

$$\begin{aligned} \delta \dot{x}_{u4} &= -k_{u1}\ \delta x_{u4} - k_{u2}\ \delta x_{u2} \\ \delta \dot{x}_{u2} &= k_{u3}\ \delta x_{u4} - k_{u4}\ \delta x_{u2} + c_{u5}\,(\delta x_{u4})^2 - c_{u6}\,(\delta x_{u2})^2 + d_u \end{aligned} \tag{4.46}$$

where the coefficients k_{ux} are given by:

$$k_{u1} = p_{u1} + 2\ c_{u2} + 2\pi\ c_{u3}\ , \qquad k_{u2} = p_{u2} + 4\pi\ c_{u1} + c_{u3} \tag{4.47}$$

$$k_{u3} = 2\ c_{u5} + c_{u7}\ k_{u1}\ , \qquad k_{u4} = 4\pi\ c_{u6} - c_{u7}\ k_{u2} \tag{4.48}$$

and, on the other hand, the 'persistent perturbation' term (d_u) is defined as:

$$d_u = c_{u5} - 4\pi^2\ c_{u6} \tag{4.49}$$

Therefore, the system can be expressed as:

$$\begin{bmatrix} \delta \dot{x}_{u4} \\ \delta \dot{x}_{u2} \end{bmatrix} = \begin{bmatrix} -k_{u1} & -k_{u2} \\ k_{u3} & -k_{u4} \end{bmatrix} \begin{bmatrix} \delta x_{u4} \\ \delta x_{u2} \end{bmatrix} + \begin{bmatrix} 0 \\ g_u \end{bmatrix} + \begin{bmatrix} 0 \\ d_u \end{bmatrix} \tag{4.50}$$

where:

$$g_u = c_{u5}\,(\delta x_{u4})^2 - c_{u6}\,(\delta x_{u2})^2 \tag{4.51}$$

Applying the so-called Routh-Hurwitz Criterion, the subsequent linear dynamical system (i.e., omitting the g_u and d_u associated terms) would be stable if the following criteria are met:

- First condition. It should be verified that:

$$-k_{u1} - k_{u4} < 0 \tag{4.52}$$

  Expressing (4.52) as a function of k_{u1} and k_{u2}, the Inequality remains:

$$k_{u1} > c_{u7}\ k_{u2} - 4\pi c_{u6} \tag{4.53}$$

- Second condition, which verifies that the determinant of the linear system remains positive:

$$k_{u1}\ k_{u4} + k_{u2}\ k_{u3} > 0 \tag{4.54}$$

  Simplifying (4.54), the expression remains:

$$k_{u1} < \frac{c_{u5}}{2\pi c_{u6}}\ k_{u2} \tag{4.55}$$

Therefore, conditions (4.53) and (4.55) define an interval for k_{u1}:

$$c_{u7}\ k_{u2} - 4\pi c_{u6} < k_{u1} < \frac{c_{u5}}{2\pi c_{u6}}\ k_{u2} \tag{4.56}$$

The region defining the linear stability of the dynamical system has been plotted as a function of k_{u1} and k_{u2} in Figure 4.1 for a typical E-sail configuration, where this interval limits the definition of the control parameters (i.e., p_{u1} and p_{u2}) influencing the performance of the subsequent feedback control law.

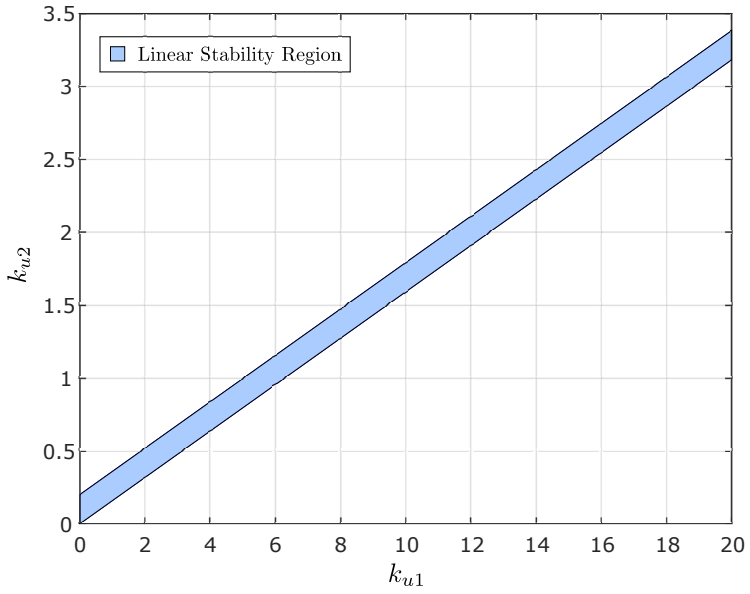

Figure 4.1 Linear stability region of the proposed non-linear control law (unwrap dynamics) as a function of k_{u1} and k_{u2}. Assessment evaluated for $m_H = 300$ kg, $R = 1$ m, $l = 10$ m, $N = 8$.

Assuming the linearized system to be stable, if both the initial conditions and the persistent perturbation term (d_u) are sufficiently small, the system will always remain close to the equilibrium, representing a locally-defined stability criterion that could therefore validate the architecture of the developed control law. Thus, the control law aimed to be implemented remains:

$$\begin{aligned} u_u = &\left(b_{u4} - b_{u2}\,\frac{a_{u3}}{a_{u2}}\right)\,(x_{u2})^2 + b_{u2}\,\frac{a_{u4}}{a_{u2}}\,(x_{u4})^2 + b_{u3}\,x_{u2}\,x_{u4} \\ &- \left(b_{u1} - b_{u2}\,\frac{a_{u1}}{a_{u2}}\right)\,(p_{u1}\,\delta x_{u4} + p_{u2}\,\delta x_{u2}) \end{aligned} \tag{4.57}$$

Given this formulation, the performance of the control law given by (4.57) will be compared with the one given by (4.38) within Chapter 6 for a typical E-sail configuration.

4.1.2 Hinging dynamics

Following with the feedback control schemes to be applied to the hinging dynamical model, again both linear and non-linear control laws are proposed for comparing their control requirements and dynamical features. In particular, the target of this hinging phase is the stabilization of the fully-deployed tether ensemble to the radial position ($\beta = \pi/2$ rad). For the derivation of the control laws to be applied to this hinging phase, it associated dynamical model (Equations (3.55) and (3.58)) could be expressed as:

$$\begin{aligned} a_{h1}\,\dot{x}_{h2} + a_{h2}\,\dot{x}_{h4} + a_{h3}\,{x_{h4}}^2 - a_{h4}\,{x_{h2}}^2 &= 0 \\ b_{h1}\,\dot{x}_{h2} + b_{h2}\,\dot{x}_{h4} + b_{h3}\,x_{h2}\,x_{h4} + b_{h4}\,{x_{h4}}^2 &= u_h \end{aligned} \tag{4.58}$$

where a_{h1}, a_{h2}, b_{h1} and b_{h2} are positively defined auxiliary functions, where the functions a_{h3}, a_{h4}, b_{h3} and b_{h4} can be either positive or negative. On one hand, a_{h1}, a_{h2}, a_{h3} and a_{h4} are given by:

$$a_{h1} = 24\pi\,\bar{l} + 36\pi\bar{l}^2\sin x_{h3} + 14\pi\bar{l}^3 + 24\pi\overline{m_E}\left(\bar{l}\sin x_{h3} + \bar{l}^2\right) \tag{4.59}$$

$$a_{h2} = 12\bar{l} + 12\bar{l}^2\sin x_{h3} + 7\bar{l}^3 + 12\overline{m_E}\bar{l}^2 \tag{4.60}$$

$$a_{h3} = 6\bar{l}^2\cos x_{h3} \tag{4.61}$$

$$a_{h4} = 4\pi^2\left(12\bar{l}^2 + 12\overline{m_E}\bar{l}\right)\cos x_{h3} \tag{4.62}$$

On the other hand, for b_{h1}, b_{h2}, b_{h3} and b_{h4}:

$$b_{h1} = 48\pi\bar{l} + 48\pi\bar{l}^2\sin x_{h3} + 14\pi\bar{l}^3 + 12\pi\overline{m_H} + 24\pi\overline{m_E}\left(1 + 2\bar{l}\sin x_{h3} + \bar{l}^2\right) \tag{4.63}$$

$$b_{h2} = 12\bar{l} + 18\bar{l}^2\sin x_{h3} + 7\bar{l}^3 + 12\overline{m_E}\left(\bar{l}\sin x_{h3} + \bar{l}^2\right) \tag{4.64}$$

$$b_{h3} = 48\pi\left(\bar{l}^2 + \overline{m_E}\bar{l}\right)\cos x_{h3} \tag{4.65}$$

$$b_{h4} = \left(18\bar{l}^2 + 12\overline{m_E}\bar{l}\right)\cos x_{h3} \tag{4.66}$$

where the state vector (x_h) is defined as:

$$x_h = [\theta,\ \overline{\omega},\ \beta,\ \beta']^T = [x_{h1},\ x_{h2},\ x_{h3},\ x_{h4}]^T \tag{4.67}$$

and, equivalently, the control vector (u_h) remains:

$$u_h = \overline{u_s} \tag{4.68}$$

Thus, the dynamical model in (4.58) can be written as:

$$\dot{x}_h = f_h\,(x_h, u_h,\ \tau) = [f_{h1},\ f_{h2},\ f_{h3},\ f_{h4}]^T \tag{4.69}$$

Hence, f_h is comprised by four functions ($f_{h1},\ f_{h2},\ f_{h3}$ and f_{h4}) defined as:

- f_{h1}

$$f_{h1} = x_{h2} \tag{4.70}$$

- f_{h2}

$$f_{h2} = \frac{1}{b_{h1} - b_{h2}\,\dfrac{a_{h1}}{a_{h2}}}\left[\left(b_{h2}\,\frac{a_{h3}}{a_{h2}} - b_{h4}\right)(x_{h4})^2 + u_h - b_{h2}\,\frac{a_{h4}}{a_{h2}}\,(x_{h2})^2 - b_{h3}\,x_{h2}\,x_{h4}\right] \tag{4.71}$$

- f_{h3}

$$f_{h3} = x_{h4} \tag{4.72}$$

- f_{h4}

$$f_{h4} = \frac{1}{a_{h2}}\,\left[a_{h4}\,(x_{h2})^2 - a_{h3}\,(x_{h4})^2 - a_{h1}\,f_{h2}\right] \tag{4.73}$$

Finite horizon LQR control law

As the linear control law to be applied to the hinging dynamical system, an LQR (Linear Quadratic Regulator) control law with "finite horizon" is intended to be implemented. As introduced within Section 4.1.1, this control law is based on the expression of both the state (Equation (4.67)) and control (Equation (4.68)) vectors as a sum of a reference value (corresponding to the desired E-sail evolution for the case of the state vector) and an error or disturbance variable, that is:

$$x_h = x_{h,\,ref} + \Delta x_h \tag{4.74}$$

where $x_{h,\,ref}$ represents the desired system behaviour through this phase. Given that the ensemble of the tethers are aimed to be stabilized at the radial position (that is, $\beta_{ref} = x_{h3} = \pi/2$, $\beta'_{ref} = x_{h4} = 0$):

$$a_{h3}(x_{h3} = \pi/2) = 0, \quad a_{h4}(x_{h3} = \pi/2) = 0, \quad b_{h3}(x_{h3} = \pi/2) = 0, \quad b_{h4}(x_{h3} = \pi/2) = 0 \tag{4.75}$$

Therefore and since β is intended not to be varying with τ, Equations (3.67) and (3.58) yields to:

$$\overline{\omega}' = 0 \tag{4.76}$$

Additionally, since it is desired to maintain the initial spacecraft rate through the deployment:

$$\overline{\omega}_{ref} = 1 = \text{cte.} \tag{4.77}$$

Thus, the reference state ($x_{h,\,ref}$) remains

$$x_{h,\,ref} = [\tau,\ 1,\ \pi/2,\ 0]^T \tag{4.78}$$

where the transition to the purely radial configuration is assumed to be instantaneous. Similarly, the control vector is comprised as well by two components:

$$u_h = u_{h,\,ref} + \Delta u_h \tag{4.79}$$

where $u_{h,\,ref}$ is obtained by replacing $x_{h,\,ref}$ into (3.58), comprising an open-loop control law. As a result of the definition of the reference state in (4.78), the reference control is zero for this hinging phase:

$$u_{h,\,ref} = 0 \tag{4.80}$$

On the other side, for the determination of the second term of the controller, Δu_h is assumed to have the form of:

$$\Delta u_h = K_h(\tau)\ \Delta x_h \tag{4.81}$$

where $K_h(\tau)$ is a τ-dependant matrix which minimizes a given cost function. To compute this magnitude, the original system of differential equations needs to be linearized around the reference state evolution $x_{h,\ ref}$ in order to obtain a linear system function of the disturbance variables as:

$$\Delta \dot{x}_h = A_h(\tau)\ \Delta x_h + B_h(\tau)\ \Delta u_h \tag{4.82}$$

where $A_h(\tau)$ and $B_h(\tau)$ matrices can be obtained from:

$$A_h(\tau) = \left.\frac{\partial f_h(x_h,\ u_h,\ \tau)}{\partial x_h}\right|_{x_{h,\ ref}(\tau),\ u_{h,\ ref}(\tau),\ \tau} \tag{4.83}$$

and analogously:

$$B_h(\tau) = \left.\frac{\partial f_h(x_h,\ u_h,\ \tau)}{\partial u_h}\right|_{x_{h,\ ref}(\tau),\ u_{h,\ ref}(\tau),\ \tau} \tag{4.84}$$

The derivation of the terms comprising the matrices A_h and B_h can be found in Appendix A. Taking into account Equations (4.82), (4.83) and (4.84), and defining the cost function of the controller as:

$$J_h = \int_0^{\tau_{man,\ h}} \left({\Delta x_h}^T(\tau)\ Q_h\ \Delta x_h(\tau) + {\Delta u_h}^T(\tau)\ R_h\ \Delta u_h(\tau) + {\Delta x_h}^T(\tau)\ Q_{h,\ end}\ \Delta x_h(\tau) \right) d\tau \tag{4.85}$$

where $\tau_{man,\ h}$ is the time horizon of the control to be performed, and the matrices Q_h, R_h and $Q_{h,\ end}$ are the weights of the state, the control and the state at the end of the time horizon respectively, which comprise the tuning parameters of the control law.

These matrices are assumed to be symmetrical, and Q_h and $Q_{h,\ end}$ are defined strictly positive (i.e., all their eigenvalues are positive), whereas $R_h \geq 0$ (i.e., all their eigenvalues are non-negative). Given the cost function in 4.85, the optimum value of K_h minimizing J_h is the one obtained by the resolution of the so-called Ricatti differential equation:

$$-\dot{P}_h = {A_h}^T\ P_h + P_h\ A_h - P_h\ B_h\ {R_h}^{-1}\ {B_h}^T\ P_h + Q_h \tag{4.86}$$

verifying the final condition:

$$P_h\ (\tau_{man,\ h}) = Q_{h,\ end} \tag{4.87}$$

whereas $K_h(\tau)$ is then obtained as:

$$K_h(\tau) = -{R_h}^{-1}\ {B_h}^T\ P_h\ (\tau) \tag{4.88}$$

In spite of the fact that the Riccati's differential equation is always solvable, it cannot be solved in real time since the problem is defined through a final condition instead of an initial one (instead it should be solved in advance for a given reference state evolution, storing the subsequent values of $K_h(\tau)$). Thus, expressing all the contributions as a function of the state vector, the feedback control scheme to be finally implemented remains:

$$u_h(x_h,\ \tau) = u_{h,\ ref} + K_h(\tau)\ (x_h - x_{h,\ ref}) \tag{4.89}$$

Non-linear control law

On the other hand, a non-linear control law is intended to be implemented in order to assure a proper system behaviour through this deployment phase. In order to implement such a feedback control law, Equations (3.67) and (3.58) can be simplified considering β to be very close to the purely radial configuration (that is, $\beta \simeq \pi/2$). Therefore, the conditions in (4.75) are met and the dynamical model could be simplified into a single equation function of β^{II} as:

$$\left(b_{h2} - b_{h1}\,\frac{a_{h2}}{a_{h1}}\right)\,\beta^{II} = \overline{u_s} \tag{4.90}$$

Since the reference trajectory aims to stabilize the E-sail in the radial direction ($\beta = \pi/2$, $\beta^I = 0$), the proposed control law is based on equalizing β^{II} to a linear expression function of the error in β^I:

$$\overline{u_s} = -k_h\,\left(b_{h2} - b_{h1}\,\frac{a_{h2}}{a_{h1}}\right)\delta\beta^I \tag{4.91}$$

where $k_h > 0$ represents a positive gain, $\delta\beta^I = \beta^I - {\beta^I}_{ref}$, and ${\beta^I}_{ref} = 0$. As in Section 4.1.1, the performance of the control law given by (4.91) will be compared with the control scheme in (4.89) within Chapter 6 for a typical E-sail configuration.

Infinite horizon LQR control law

Finally, for the radial stabilization of the E-sail once the proposed hinging manoeuvre is completed (i.e., for the mitigation of possible perturbations once the E-sail has transitioned from the tangential aligned position to the purely radial configuration) an LQR (Linear Quadratic Regulator) with "infinite horizon" is implemented. This control law relies on the linearization of the original dynamical system (Equation (4.69)), where the definition of the state and the control vectors can be found in (4.67) and (4.68).

Therefore, the state and the control vectors are expressed as a sum of a reference value and a disturbance term (Equations (4.74) and (4.79)), whereas these references are the ones given by (4.78) and (4.80), as in the "finite horizon" LQR controller previously proposed, but not taking into account the evolution of θ since the reference in this control law is, by definition, not a function of τ. Thus, the second term in (4.79) is similarly obtained as:

$$\Delta u_h = K_{h,\infty}\,\Delta x_h \tag{4.92}$$

where in this case the matrix $K_{h,\infty}$ is not a function of τ as a result of the topology of the controller. For the obtention of this matrix, which is defined so that a given cost function is minimized, the original set of differential equations has to be linearized around the reference state, obtaining the linear system defined by (4.82), whereas in this case A_h and B_h are not a function of τ since the reference does not change with this non-dimensional time. The obtention of these matrices are similarly given by (4.83) and (4.84), whereas, for this control scheme, the definition of the cost function to be minimized is expressed as:

$$J_{h,\infty} = \int_0^\infty \left({\Delta x_h}^T\,Q_{h,\infty}\,\Delta x_h + {\Delta u_h}^T\,R_{h,\infty}\,\Delta u_h\right)\,d\tau \tag{4.93}$$

The matrices $Q_{h,\infty}$ and $R_{h,\infty}$ analogously represent the weights of the state and the control respectively, which comprise the tuning parameters of the controller. These matrices are assumed to be symmetrical, and $Q_{h,\infty}$ is defined strictly positive (i.e., all their eigenvalues are positive), whereas $R_{h,\infty} \geq 0$ (i.e., all their eigenvalues are non-negative). Given the cost function in 4.93, the optimum value of $K_{h,\infty}$ minimizing $J_{h,\infty}$ is the one obtained by the resolution of the so-called Ricatti algebraic equation:

$$Q_{h,\infty} + {A_h}^T\,P_{h,\infty} + P_{h,\infty}\,A_h - P_{h,\infty}\,B_h\,{R_{h,\infty}}^{-1}\,{B_h}^T\,P_{h,\infty} = 0 \tag{4.94}$$

which is only solvable if the system is controllable (i.e., the controllability matrix is full-rank). Thus, $K_{h,\infty}$ can be subsequently obtained from:

$$K_{h,\infty} = -{R_{h,\infty}}^{-1} {B_h}^T P_{h,\infty} \tag{4.95}$$

Therefore, the control law intended to be implemented for this stabilization phase is given by:

$$u_h(x_h) = u_{h,ref} + K_{h,\infty}(x_h - x_{h,ref}) \tag{4.96}$$

4.2 Radial deployment

Once the control schemes associated to the tangential deployment dynamics have been reviewed within Section 4.1, the feedback control schemes to be applied for assuring a proper deployment for the radial strategy are aimed to be analyzed in this Section. In particular, the target of this radial strategy is to achieve a purely radial (i.e., $\beta = 0$) deployment manoeuvre with both constant deployment $\left(\overline{l'} = \text{cte.}\right)$ and spacecraft rates ($\overline{\omega} = \text{cte.}$).

In order to achieve the introduced behaviour, it should be accounted that the main difference between the radial dynamical model (Equations (3.89), (3.91) and (3.93)) and the ones associated to the tangential deployment strategy (Equations (3.19) and (3.22) for the unwrap phase, and Equations (3.55) and (3.58) for the hinging phase) is the amount of control variables that the radial strategy implements. That is, instead of achieving the control of the system only by the torque applied to the hub spin axis (u_1, whereas the non-dimensional torque is denoted as $\overline{u_1}$), two additional control magnitudes are defined.

In particular, these variables comprise the reaction applied to the tethers by their individual spooling drives (u_2, whereas the non-dimensional force is denoted as $\overline{u_2}$), and the tangential force applied by the remote units (u_3, whereas the non-dimensional force is denoted as $\overline{u_3}$), which as an overall allow a higher control capacity with respect to the tangential deployment strategy (nonetheless, the higher complexity of the radial dynamical model should be noted as well). As a result of this latter statement, only a linear control law is intended to be derived for this deployment strategy. Thus, in order to begin with the control analysis of this dynamical model, Equations (3.89), (3.91) and (3.93) can be expressed as:

$$\begin{aligned} a_{r1}\,\dot{x}_{r6} + a_{r2}\,\dot{x}_{r2} + a_{r3}\,\dot{x}_{r4} + a_{r4}\,x_{r6} + a_{r5}\,x_{r2} + a_{r6}\,{x_{r4}}^2 &= u_{r1} \\ b_{r1}\,\dot{x}_{r4} + {x_{r4}}^2 + b_{r2}\,\dot{x}_{r6} - b_{r3}\,x_{r2}\,x_{r6} - b_{r4}\,{x_{r6}}^2 - b_{r5}\,{x_{r2}}^2 &= u_{r2} \\ c_{r1}\,\dot{x}_{r6} + c_{r2}\,\dot{x}_{r2} + c_{r3}\,{x_{r6}}^2 + c_{r4}\,x_{r4}\,x_{r6} + c_{r5}\,x_{r2} &= u_{r3}\,x_{r3} \end{aligned} \tag{4.97}$$

where a series of auxiliary functions (e.g., a_{r1}, b_{r2}, c_{r3}) have been defined in order to simplify the original set of differential equations. In particular, these expressions are given by:

$$\begin{aligned} a_{r1} =& 14\pi\,(x_{r3})^3 + 24\pi\,x_{r3} + 48\pi\,(x_{r3})^2\cos x_{r1} + 24\pi\overline{m_E}\,\left((x_{r3})^2 + 2\,x_{r3}\cos x_{r1} + 1\right) \\ &+ 12\pi\overline{m_H} + 24\pi\overline{m_T} \end{aligned} \tag{4.98}$$

$$a_{r2} = 7\,(x_{r3})^3 + 12\,x_{r3} + 18\,(x_{r3})^2\cos x_{r1} + 12\overline{m_E}\left((x_{r3})^2 + x_{r3}\cos x_{r1}\right) \tag{4.99}$$

$$a_{r3} = (12\overline{m_E} + 6x_{r3})\sin x_{r1} \tag{4.100}$$

$$\begin{aligned} a_{r4} =& 24\pi\,x_{r4} + 96\pi\,x_{r3}\,x_{r4}\cos x_{r1} + 42\pi\,\,(x_{r3})^2\,x_{r4} - 48\pi\,(x_{r3})^2\,x_{r2}\sin x_{r1} \\ &+ 48\pi\overline{m_E}\,(x_{r3}\,x_{r4} + x_{r4}\cos x_{r1} - x_{r3}\,x_{r2}\sin x_{r1}) \end{aligned} \tag{4.101}$$

$$a_{r5} = 12\,x_{r4} + 21\,(x_{r3})^2\,x_{r4} - 18\,(x_{r3})^2\,x_{r2}\sin x_{r1} + 42\,x_{r3}\,x_{r4}\,\cos x_{r1} \tag{4.102}$$

$$+ 12\overline{m_E}\,(2\,x_{r3}\,x_{r4} + 2\,x_{r4}\cos x_{r1} - x_{r3}\,x_{r2}\sin x_{r1}) \tag{4.103}$$

$$a_{r6} = 6\sin x_{r1} \tag{4.104}$$

Analogously, for b_{r1}, b_{r2}, b_{r3}, b_{r4} and b_{r5}:

$$b_{r1} = 2\,x_{r3} + 8\overline{m_E} \tag{4.105}$$

$$b_{r2} = (8\pi\, x_{r3} + 16\pi\overline{m_E})\sin x_{r1} \tag{4.106}$$

$$b_{r3} = 16\pi + 40\pi\, x_{r3}\cos x_{r1} + 28\pi\,(x_{r3})^2 + 32\pi\overline{m_E}x_{r3} \tag{4.107}$$

$$b_{r4} = 64\pi^2\, x_{r3}\cos x_{r1} + 16\pi^2 + 28\pi^2\,(x_{r3})^2 + 32\pi^2\overline{m_E}\,(x_{r3} + \cos x_{r1}) \tag{4.108}$$

$$b_{r5} = 4 + 8\, x_{r3}\cos x_{r1} + 7\,(x_{r3})^2 + 8\overline{m_E}\, x_{r3} \tag{4.109}$$

And finally, for c_{r1}, c_{r2}, c_{r3}, c_{r4} and c_{r5}:

$$c_{r1} = 14\pi\,(x_{r3})^3 + 36\pi\,(x_{r3})^2\cos x_{r1} + 24\pi\, x_{r3} + 24\pi\overline{m_E}\left((x_{r3})^2 + x_{r3}\cos x_{r1}\right) \tag{4.110}$$

$$c_{r2} = 7\,(x_{r3})^3 + 12\,(x_{r3})^2\cos x_{r1} + 12x_{r3} + 12\overline{m_E}\,(x_{r3})^2 \tag{4.111}$$

$$c_{r3} = \left(48\pi^2\,(x_{r3})^2 + 48\pi^2\overline{m_E}\, x_{r3}\right)\sin x_{r1} \tag{4.112}$$

$$c_{r4} = 24\pi + 42\pi\,(x_{r3})^2 + 48\pi\overline{m_E}\, x_{r3} + 60\pi\, x_{r3}\cos x_{r1} \tag{4.113}$$

$$c_{r5} = 12\, x_{r4} + 24\, x_{r3}\, x_{r4}\cos x_{r1} + 21\,(x_{r3})^2 x_{r4} + 24\overline{m_E}\, x_{r3}\, x_{r4} - 6\,(x_{r3})^2 x_{r2}\sin x_{r1} \tag{4.114}$$

where the state vector (x_r) has been defined as:

$$x_r = \left[\beta,\, \beta',\, \bar{l},\, \bar{l}',\, \theta,\, \overline{\omega}\right]^T = [x_{r1},\, x_{r2},\, x_{r3},\, x_{r4},\, x_{r5},\, x_{r6}]^T \tag{4.115}$$

and, equivalently, the control vector (u_r) remains:

$$u_r = [\overline{u_1},\, \overline{u_2},\, \overline{u_3}]^T = [u_{r1},\, u_{r2},\, u_{r3}]^T \tag{4.116}$$

Moreover, the system of differential equations in (4.97) can be expressed as:

$$\dot{x}_r = f_r\,(x_r, u_r,\, \tau) = [f_{r1},\, f_{r2},\, f_{r3},\, f_{r4},\, f_{r5},\, f_{r6}]^T \tag{4.117}$$

Thus, f_r is comprised by six components (f_{r1}, f_{r2}, f_{r3}, f_{r4}, f_{r5} and f_{r6}) defined as:

- f_{r1}

$$f_{r1} = x_{r2} \tag{4.118}$$

- f_{r2}

$$\begin{aligned} f_{r2} = &\frac{1}{a_{r3}\,\dfrac{b_{r2}}{b_{r1}}\,\dfrac{c_{r2}}{c_{r1}} + a_{r2} - a_{r1}\,\dfrac{c_{r2}}{c_{r1}}}\left[u_{r1} - \frac{a_{r3}}{b_{r1}}\, u_{r2} + \left(\frac{a_{r3}\, b_{r2}}{b_{r1}\, c_{r1}} - \frac{a_{r1}}{c_{r1}}\right) u_{r3}\, x_{r3}\right. \\ &+ \left(a_{r1}\,\frac{c_{r3}}{c_{r1}} - a_{r3}\,\frac{b_{r2}}{b_{r1}}\,\frac{c_{r3}}{c_{r1}} - a_{r3}\,\frac{b_{r4}}{b_{r1}}\right)(x_{r6})^2 + \left(a_{r1}\,\frac{c_{r4}}{c_{r1}} - a_{r3}\,\frac{b_{r2}}{b_{r1}}\,\frac{c_{r4}}{c_{r1}}\right) x_{r4}\, x_{r6} \\ &- a_{r3}\,\frac{b_{r3}}{b_{r1}}\, x_{r2}\, x_{r6} + \left(a_{r1}\,\frac{c_{r5}}{c_{r1}} - a_{r5} - a_{r3}\,\frac{b_{r2}}{b_{r1}}\,\frac{c_{r5}}{c_{r1}}\right) x_{r2} + \left(\frac{a_{r3}}{b_{r1}} - a_{r6}\right)(x_{r4})^2 \\ &\left. - a_{r3}\,\frac{b_{r5}}{b_{r1}}\,(x_{r2})^2 - a_{r4}\, x_{r6}\right] \end{aligned} \tag{4.119}$$

- f_{r3}

$$f_{r3} = x_{r4} \tag{4.120}$$

- f_{r4}

$$\begin{aligned} f_{r4} = & \frac{1}{b_{r1}} \left[u_{r2} - \frac{b_{r2}}{c_{r1}} u_{r3}\, x_{r3} + b_{r2} \frac{c_{r2}}{c_{r1}} f_{r2} + \left(b_{r2} \frac{c_{r3}}{c_{r1}} + b_{r4} \right) (x_{r6})^2 + b_{r2} \frac{c_{r4}}{c_{r1}} x_{r4}\, x_{r6} \right. \\ & \left. + b_{r3}\, x_{r2}\, x_{r6} - (x_{r4})^2 + b_{r2} \frac{c_{r5}}{c_{r1}} x_{r2} + b_{r5}\, (x_{r2})^2 \right] \end{aligned} \tag{4.121}$$

- f_{r5}

$$f_{r5} = x_{r6} \tag{4.122}$$

- f_{r6}

$$f_{r6} = \frac{1}{c_{r1}} \left[u_{r3}\, x_{r3} - c_{r2}\, f_{r2} - c_{r3}\, (x_{r6})^2 - c_{r4}\, x_{r4}\, x_{r6} - c_{r5}\, x_{r2} \right] \tag{4.123}$$

With this formulation, the topology of the control laws to be applied to both the deployment and stabilization phases can be derived in order to assure an adequate system behaviour.

Finite horizon LQR control law

In order to control the system dynamics through the deployment, an LQR (Linear Quadratic Regulator) control law with "finite horizon" is intended to be implemented. Thus, the topology of this control law, as introduced within Section 4.1, relies on the expression of both the state (Equation (4.115)) and control (Equation (4.116)) vectors as a sum of a reference value and an error or disturbance variable, that is:

$$x_r = x_{r,\, ref} + \Delta x_r \tag{4.124}$$

where $x_{r,\, ref}$ represents the desired E-sail evolution, which is defined in this case as:

$$x_{r,\, ref} = [0,\ 0,\ \bar{l}_{ref},\ \bar{l}'_{ref},\ \tau,\ 1]^T \tag{4.125}$$

on the basis of the previously introduced target E-sail behaviour, where $\bar{l}'_{ref}$ represents the reference deployment rate aimed to be conserved through the simulation, and $\bar{l}_{ref} = \bar{l}'_{ref}\, \tau$. Analogously, the control to be implemented is comprised as well by two components:

$$u_r = u_{r,\, ref} + \Delta u_r \tag{4.126}$$

where $u_{r,\, ref}$ is obtained by replacing $x_{r,\, ref}$ into (3.89), (3.91) and (3.93), comprising an open-loop control law:

$$u_{r,\, ref} = \left[\overline{u_{1,\, ref}},\ \overline{u_{2,\, ref}},\ \overline{u_{3,\, ref}} \right]^T \tag{4.127}$$

As a result of the definition of the reference state in (4.125), the reference control remains (omitting the terms associated to either β', β'', $\overline{\omega}'$ or $\bar{l}''$ as a result of the proposed E-sail evolution, and simplifying the β

associated terms as a result of its zero reference value):

$$\begin{aligned}
\overline{u_{1,\,ref}} &= \left[24\pi\bar{l}'_{ref} + 96\pi\bar{l}_{ref}\bar{l}'_{ref} + 42\pi\left(\bar{l}_{ref}\right)^2\bar{l}'_{ref} + 48\pi\overline{m_E}\left(\bar{l}_{ref}\bar{l}'_{ref} + \bar{l}'_{ref}\right)\right]\overline{\omega}_{ref} \\
\overline{u_{2,\,ref}} &= \left(\bar{l}'_{ref}\right)^2 - \left[64\pi^2\bar{l}_{ref} + 16\pi^2 + 28\pi^2\left(\bar{l}_{ref}\right)^2 + 32\pi^2\overline{m_E}\left(\bar{l}_{ref} + 1\right)\right]\left(\overline{\omega}_{ref}\right)^2 \\
\overline{u_{3,\,ref}} &= \frac{1}{\bar{l}_{ref}}\left(24\pi + 42\pi\left(\bar{l}_{ref}\right)^2 + 48\pi\overline{m_E}\bar{l}_{ref} + 60\pi\bar{l}_{ref}\right)\overline{\omega}_{ref}\,\bar{l}'_{ref}
\end{aligned} \tag{4.128}$$

On the other side, for the determination of the second contribution to the control law, Δu_r is assumed to have the form of:

$$\Delta u_r = K_r(\tau)\,\Delta x_r \tag{4.129}$$

where $K_r(\tau)$ is a τ-dependant matrix whose values minimize a given cost function. To compute this magnitude, the original set of differential equations governing the physics of the system needs be linearized around the reference state evolution ($x_{r,\,ref}$), so that a linear system expressed in the disturbance variables is obtained as:

$$\Delta\dot{x}_r = A_r(\tau)\,\Delta x_r + B_r(\tau)\,\Delta u_r \tag{4.130}$$

where $A_r(\tau)$ and $B_r(\tau)$ matrices can be obtained from:

$$A_r(\tau) = \left.\frac{\partial f_r(x_r,\,u_r,\,\tau)}{\partial x_r}\right|_{x_{r,\,ref}(\tau),\,u_{r,\,ref}(\tau),\,\tau} \tag{4.131}$$

and similarly:

$$B_r(\tau) = \left.\frac{\partial f_r(x_r,\,u_r,\,\tau)}{\partial u_r}\right|_{x_{r,\,ref}(\tau),\,u_{r,\,ref}(\tau),\,\tau} \tag{4.132}$$

Details regarding the derivation of the terms within A_r and B_r can be found in Appendix A. Taking into account Equations (4.130), (4.131) and (4.132), and defining the cost function to be minimized as:

$$J_r = \int_0^{\tau_{man,\,r}} \left(\Delta x_r{}^T(\tau)\,Q_r\,\Delta x_r(\tau) + \Delta u_r{}^T(\tau)\,R_r\,\Delta u_r(\tau) + \Delta x_r{}^T(\tau)\,Q_{r,\,end}\,\Delta x_r(\tau)\right) d\tau \tag{4.133}$$

where $\tau_{man,\,r}$ is the time horizon of the control to be performed, which can be obtained from:

$$\tau_{man,\,r} = \bar{l}_{total}/\bar{l}'_{ref} \tag{4.134}$$

where $\bar{l}_{total}$ represents the non-dimensional full length of the tethers aimed to be deployed. On the other hand, the matrices Q_r, R_r and $Q_{r,\,end}$ represent the weights of the state, the control and the state at the end of the time horizon respectively, which comprise the tuning parameters of the controller determining its behaviour. These matrices are assumed to be symmetrical, and Q_r and $Q_{r,\,end}$ are defined strictly positive (i.e., all their eigenvalues are positive), whereas $R_r \geq 0$ (i.e., all their eigenvalues are non-negative).

Given the cost function defined by 4.133, the optimum value of K_r minimizing J_r is the one obtained by the resolution of the so-called Ricatti differential equation:

$$-\dot{P}_r = A_r{}^T\,P_r + P_r\,A_r - P_r\,B_r\,R_r{}^{-1}\,B_r{}^T\,P_r + Q_r \tag{4.135}$$

verifying the final condition:

$$P_r\,(\tau_{man,\,r}) = Q_{r,\,end} \tag{4.136}$$

whereas $K_r(\tau)$ is then computed as:

$$K_r(\tau) = -R_r{}^{-1}\,B_r{}^T\,P_r\,(\tau) \tag{4.137}$$

Riccati's differential equation is always solvable. Nonetheless, it cannot be solved in real time since the problem is defined through a final condition instead of an initial one (it should be solved in advance for a given reference state evolution, storing the subsequent values of $K_r(\tau)$). Therefore, expressing all the terms as a function of the state vector, the control law to be implemented has the form of:

$$u_r(x_r,\, \tau) = u_{r,\, ref} + K_r(\tau)\ (x_r - x_{r,\, ref}) \tag{4.138}$$

Infinite horizon LQR control law

Finally, for the stabilization of the E-sail once the proposed deployment procedure is fulfilled (i.e., for the mitigation of possible perturbations once the E-sail has achieved its radial deployment) an LQR (Linear Quadratic Regulator) with "infinite horizon" is implemented.

Similarly to the previously described finite horizon LQR, this control law relies on the linearization of the original dynamics (Equation (4.117)), where the definition of the state and the control vectors can be found in (4.115) and (4.116). Therefore, the state and the control vectors are expressed as a sum of a reference value and a disturbance term (Equations (4.124) and (4.126)), whereas the reference state vector is given in this case by:

$$x_{r,\, ref_\infty} = [\sim,\ 1,\ \pi/2,\ 0,\ \bar{l}_{total},\ 0]^T \tag{4.139}$$

where $\sim$ denotes that the evolution of θ is not taking into account since the reference state and control vector are, by definition, not a function of τ for this control law. On the other side, the reference control vector is obtained by replacing (4.139) into (3.89), (3.91) and (3.93), comprising an open-loop control law:

$$u_{r,\, ref_\infty} = \left[\overline{u_{1,\, ref_\infty}},\ \overline{u_{2,\, ref_\infty}},\ \overline{u_{3,\, ref_\infty}}\right]^T \tag{4.140}$$

Identically to the "finite horizon" LQR controller previously proposed (Equation (4.128)), the components of (4.140) are given by (once the negligible terms from (4.128) have being disregarded as a result of the new reference state):

$$\begin{aligned}
\overline{u_{1,\, ref_\infty}} &= 0 \\
\overline{u_{2,\, ref_\infty}} &= -\left[64\pi^2\bar{l}_{total} + 16\pi^2 + 28\pi^2\left(\bar{l}_{total}\right)^2 + 32\pi^2\overline{m_E}\left(\bar{l}_{total} + 1\right)\right]\left(\overline{\omega}_{ref}\right)^2 \\
\overline{u_{3,\, ref_\infty}} &= 0
\end{aligned} \tag{4.141}$$

Thus, the second contribution to (4.126) is similarly obtained as:

$$\Delta u_r = K_{r,\, \infty}\, \Delta x_r \tag{4.142}$$

where in this case $K_{r,\, \infty}$ is not a function of τ as a result of the topology of the controller. For the obtention of this matrix, which is defined in order to minimize a given cost function, the original set of differential equations has to be linearized around the reference state, obtaining the linear system defined by (4.130), whereas in this case A_r and B_r are not a function of τ since the reference does not change with this non-dimensional time. The obtention of these matrices are similarly given by (4.131) and (4.132), whereas, for this control scheme, the definition of the cost function to be minimized is expressed as:

$$J_{r,\, \infty} = \int_0^\infty \left(\Delta {x_r}^T\ Q_{r,\, \infty}\, \Delta x_r + \Delta {u_r}^T\ R_{r,\, \infty}\, \Delta u_r\right) d\tau \tag{4.143}$$

The matrices $Q_{r,\, \infty}$ and $R_{r,\, \infty}$ analogously represent the weights of the state and the control, which comprise the tuning parameters of the controller. These matrices are assumed to be symmetrical, and $Q_{r,\, \infty}$ is defined strictly positive (i.e., all their eigenvalues are positive), whereas $R_{r,\, \infty} \geq 0$ (i.e., all their eigenvalues are non-negative).

Given the cost function defined by 4.143, the optimum value of $K_{r,\infty}$ minimizing $J_{r,\infty}$ is the one obtained by the resolution of the so-called Ricatti algebraic equation:

$$Q_{r,\infty} + {A_r}^T P_{r,\infty} + P_{r,\infty} A_r - P_{r,\infty} B_r {R_{r,\infty}}^{-1} {B_r}^T P_{r,\infty} = 0 \tag{4.144}$$

which is only solvable if the system is controllable (i.e., the controllability matrix is full-rank). Thus, $K_{r,\infty}$ can be obtained from:

$$K_{r,\infty} = -{R_{r,\infty}}^{-1} {B_r}^T P_{r,\infty} \tag{4.145}$$

Therefore, expressing all the terms as a function of the state variables, the control law to be finally considered for this stabilization phase is:

$$u_r(x_r) = u_{r,\, ref_\infty} + K_{r,\infty} (x_r - x_{r,\, ref_\infty}) \tag{4.146}$$

5 Perturbations assessment

In this Chapter, the algorithm that has been considered in order to assess the effects of perturbations into the proposed control laws is analyzed. In particular, the perturbations that have been introduced into the derived dynamical systems are the ones associated to the dynamics of the sensors involved within the deployment procedure.

Therefore, the measurements that these devices provide contain a certain error, which in this case is characterized by a given white noise and bias. The architecture of the system implemented for the sake of evaluating the behaviour of the derived dynamics with respect to the these perturbations can be found within Figure 5.1.

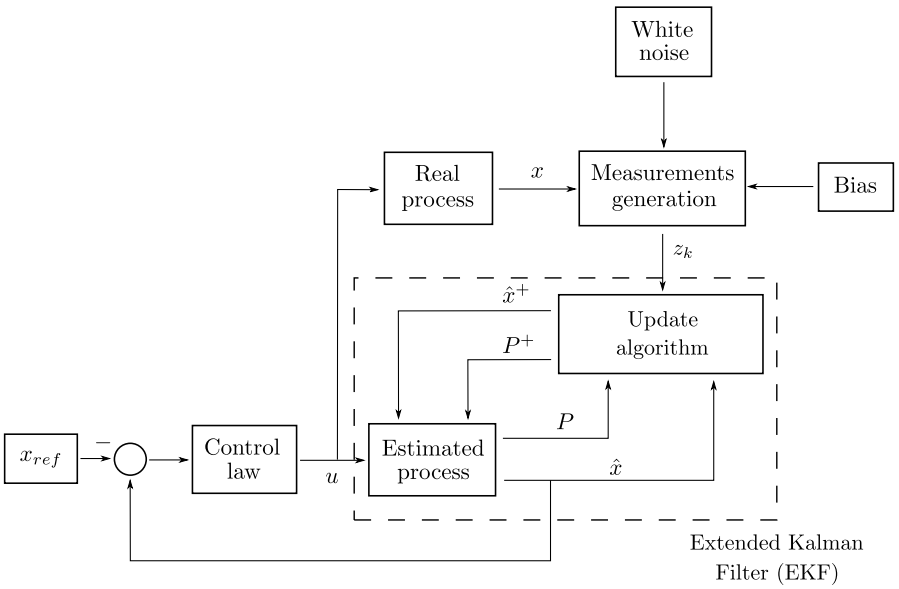

Figure 5.1 System architecture - perturbations assessment.

Thus, the integration of the introduced measurements is accomplished through an Extended Kalman Filter (EKF) in order to compute an estimation of the state vector, which is then used to compute the feedback control. The topology of the former algorithm will be generically introduced, so that it can be either used for the three presented dynamics (i.e., unwrap, hinging and radial deployment dynamical systems).

Thus, the implementation of the Filter is described for a generic state vector (x), a generic control vector (u) and a time variable (τ), so that the subsequent system of differential equations comprising the "process" is given by:

$$\dot{x} = f(x,\, u,\, \tau) \tag{5.1}$$

where all the variables within x are assumed to be following a normal distribution whose mean is $\hat{x}$, with a covariance matrix denoted as P. On the other side, a series of measurements (z_k) following normal distributions are available at each k instant, which are modelled as:

$$z_k = h(x_k,\, \tau_k) + \nu(\tau_k) + b_k \tag{5.2}$$

These measurements are generated at each k instant from the "real" state vector (i.e., through functions $h(x_k,\, \tau_k)$), assuming a certain variance ($\nu(\tau_k)$) and bias (b_k) for each of the considered sensors. Particularly, this bias is computed as:

$$b_k = a_s\, \tau_k \tag{5.3}$$

where a_s stands for the slope associated to the bias of the considered sensor, which is assumed to be constant through the manoeuvre. To implement the filter, at each k instant the Jacobian matrix of the estimated process is evaluated at the estimated state vector and control variables as:

$$F\ (\hat{x}(\tau),\, \tau) = \left.\frac{\partial f(x,\, u,\, \tau)}{\partial x}\right|_{x=\hat{x},\, u} \tag{5.4}$$

Similarly, the Jacobian matrix of the measurements has to be evaluated within the estimated state vector as:

$$H_k\ (\hat{x}_k) = \left.\frac{\partial h(x,\, \tau_k)}{\partial x}\right|_{x=\hat{x}_k} \tag{5.5}$$

Finally, the "error" of the available measurements with respect of the estimated state vector (δz_k) has to be computed equivalently at each k instant, considering the current bias (if applicable) of each of the sensors:

$$\delta z_k = z_k - b_k - h(\hat{x}_k,\, \tau_k) \tag{5.6}$$

With all the defined variables, the Extended Kalman Filter (EKF) algorithm can be divided at each of the update intervals (i.e., the time between the reception of a k measurement (τ_k), and the next one (τ_{k+1})), into the following steps:

1. **Initialization.** In $\tau = \tau_k$, the estimations of both the process and its covariance matrix start from $\hat{x}^+(\tau_k)$ and $P^+(\tau_k)$, respectively (if $k = 0$, $\hat{x}^+(\tau_0) = \hat{x}_0$ and $P^+(\tau_0) = P_0$ are taken).

2. **Propagation.** For $\tau \in [\tau_k, \tau_{k+1}]$, the estimated state is propagated using the non-linear process model:

$$\dot{\hat{x}} = f(\hat{x},\, u,\, \tau) \tag{5.7}$$

with the initial condition:

$$\hat{x}(\tau_k) = \hat{x}^+(\tau_k) \tag{5.8}$$

And equivalently, for the propagation of the covariance matrix:

$$\dot{P} = F(\hat{x},\, \tau)\, P + P\, F^T(\hat{x},\, \tau) \tag{5.9}$$

with the initial condition:

$$P(t_k) = P^+(\tau_k) \tag{5.10}$$

In parallel and as stated in Figure 5.1, the "real" process (i.e., the real dynamical system is known so that the measurements can be computed throughout the simulation) has to be simulated using the originally derived non-linear model of the E-sail behaviour.

3. **Update.** In $\tau_k = \tau_{k+1}$, the system receives a set of measurements $z(\tau_{k+1})$ (computed from a corruption algorithm from the real state vector, as introduced during the description of the analysis). Calling $\hat{x}^-(\tau_{k+1}) = \hat{x}(\tau_{k+1})$, and $P^-(\tau_{k+1}) = P(\tau_{k+1})$, the errors of the measurements can be now computed as:

$$\delta z_{k+1} = z_{k+1} - b_{k+1} - h(\hat{x}_{k+1},\ \tau_{k+1}) \tag{5.11}$$

and equivalently, for the Jacobian matrix of the measurements:

$$H_{k+1} = H(\hat{x}_{k+1},\ \tau_{k+1}) \tag{5.12}$$

With these magnitudes, the Kalman gain at the instant $k+1$ ($K_{f_{k+1}}$) can be now determined as:

$$K_{f_{k+1}} = P^-(\tau_{k+1})\ {H_{k+1}}^T (H_{k+1}\ P^-(\tau_{k+1})\ {H_{k+1}}^T + R_{f_{k+1}})^{-1} \tag{5.13}$$

where $R_{f_{k+1}}$ represents the covariance matrix of the available measurements, which is defined as a purely diagonal matrix containing the variances of each of the sensors assuming each of them to be independent of each other. Thus, the process could be again initialized turning back to step 1 as:

$$\hat{x}^+(\tau_{k+1}) = \hat{x}^-(\tau_{k+1}) + K_{f_{k+1}}\ \delta z_{k+1} \tag{5.14}$$

and equivalently for the covariance matrix of the process:

$${P^+}_{k+1} = (I - K_{f_{k+1}}\ H_{k+1})\ {P^-}_{k+1} \tag{5.15}$$

4. Iteration for the next value of k.

This algorithm allows the estimation of the state vector throughout the simulation, allowing the integration of the sensor measurements within the estimation process. This estimation is consequently used to compute the control variables (see Figure 5.1), producing a degradation of the performance of the designed control system with respect to the reference "ideal" case (i.e., where no perturbations have been taken into account).

To finish with this Chapter, Table 5.1 contains the specifications of the sensors intended to be used for the implementation of the described procedure. Thus, for the unwrap phase of the tangential deployment strategy, only two measurements regarding the hub angular velocity and the tether deployment rate are available, whose characteristics are found within Table 5.1.

Table 5.1 Specifications of the considered sensors.

Parameter	Value	Units
White noise standard deviation of the ω gyroscope	$2{\cdot}10^{-3}$	rad/s
Slope of the bias of the ω gyroscope	$4{\cdot}10^{-10}$	rad/s^2
White noise standard deviation of the $\dot{\beta}$ encoder	$4{\cdot}10^{-2}$	rad/s
Slope of the bias of the $\dot{\beta}$ encoder	$4{\cdot}10^{-8}$	rad/s^2
White noise standard deviation of the deployment rate ($\dot{l}$) sensor	$1{\cdot}10^{-3}$	m/s
Slope of the bias of the sensor of the the deployment rate ($\dot{l}$) sensor	$2{\cdot}10^{-6}$	m/s^2
Update interval	2π	s

Equivalently, for the hinging phase, the characteristics of the sensors regarding the hub angular velocity, and the time variation of the angle with respect to the tangential direction ($\dot{\beta}$, as defined within Figure 3.3) are specified within Table 5.1.

Finally, for the radial deployment strategy, sensors associated to the hub angular velocity, the tether deployment rate and the time derivative of the angle with respect to the purely radial direction (again $\dot{\beta}$, as defined within Figure 3.5) are considered, where again their specifications can be found in Table 5.1.

6 Simulation results

In this Chapter, the results from the performed simulations will be presented for the sake of evaluating the performance of the derived control laws within both perturbed and non-perturbed cases. For this purpose, the assessment is divided again into the two considered deployment strategies (i.e., radial and tangential deployment strategies), whereas in this latter case, the unwrap and hinging deployment phases are treated separately.

Table 6.1 E-sail parameters to be used within the simulations [4, 5, 6].

Magnitude	Value	Units
Hub mass (m_H)	300	kg
Hub radius (R)	1	m
Initial spacecraft angular velocity (ω_0)	$2 \cdot 10^{-3}$	rad/s
Number of tethers (N)	8	-
Total length of the tethers	4	km
Mass per unit length of the tethers (λ)	$1.155 \cdot 10^{-5}$	kg/m
Tether end-mass ($m_{E,i}$)	1	kg
Admissible tension of the tethers (T_{adm})	0.09	N

For the simulation of all the presented cases, a series of E-sails parameters have been commonly defined for all the simulations (Table 6.1), so that a comparison between the different cases can be easily conducted. As a final remark, it should be noted that, in spite of the fact that the derived dynamical models and control laws are non-dimensional, the results are presented in their dimensional form within the Chapter.

6.1 Tangential deployment

To begin with the tangential deployment strategy, as previously mentioned, the analysis has been divided into the introduced unwrap and hinging phases in order to use the derived dynamical models for the completion of the simulations.

6.1.1 Unwrap dynamics

To begin with the unwrap phase of the deployment, the initial conditions given by Table 6.2 are the ones intended to be used for all the simulations to be performed within this Subsection. It should be noted that the initial length of the tethers (l_0) cannot be strictly equalled to zero since a singularity appears within the integration of the system of differential equations otherwise.

Thus, the performance of both feedback control laws (i.e., the finite horizon LQR and the non-linear control law) is intended to be compared for an ideal case where no perturbations are considered, and for a perturbed case where the dynamics of the sensors involved within the process are taken into account.

Table 6.2 Initial conditions (unwrap phase).

Magnitude	Value	Units
Initial spacecraft angular velocity (ω_0)	$2 \cdot 10^{-3}$	rad/s
Initial spacecraft spin angle (θ_0)	0	rad
Initial deployment rate ($\dot{l}_0$)	$2 \cdot 10^{-3}$	m/s
Initial tether length (l_0)	$1 \cdot 10^{-3}$	m

In the first place, the evolution of the hub angular velocity and the deployment rate throughout the manoeuvre for both of the considered control laws in the non-perturbed case can be found in Figure 6.1. The latter Figure represents the relative differences of both magnitudes with respect to their initial conditions, which are intended to be maintained within the manoeuvre.

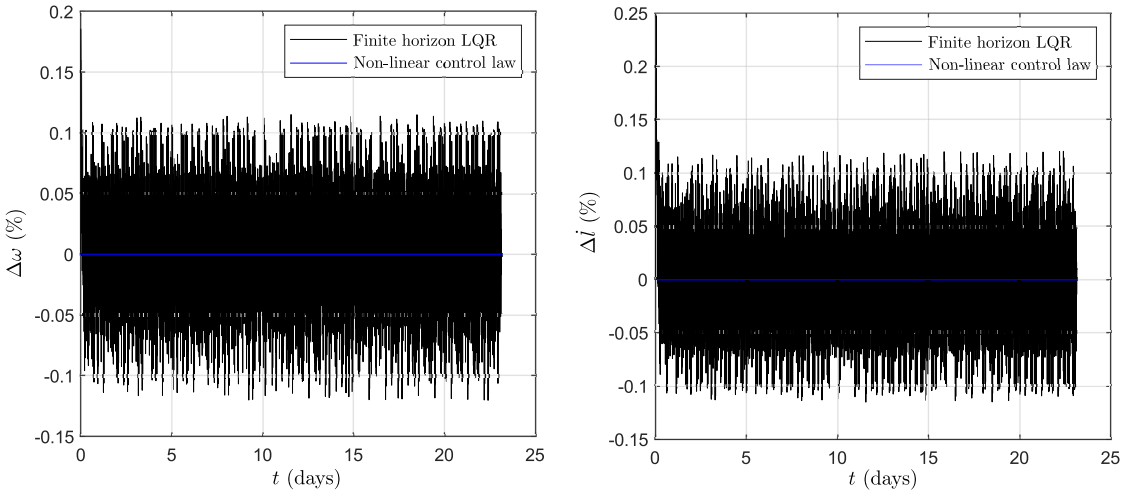

(a) Hub angular velocity errors ($\Delta\omega$)

(b) Deployment rate errors ($\Delta\dot{l}$)

Figure 6.1 Relative errors of the hub angular velocity and deployment rate (unwrap dynamics, non-perturbed case).

Therefore, it can be stated that both of the proposed control laws accomplish a nearly perfect feedback control for this non-perturbed case, where the differences of both magnitudes with respect to their target values are nearly negligible. This similarity in both behaviours can be further justified appealing to the evolution of the tension within the tethers and the applied torque through the deployment for both control algorithms given by Figure 6.2.

On one hand, it should be outlined that tension profile is purely linear for both linear and non-linear control laws, where the maximum tension through the manoeuvre is obtained at the end of the unwrap phase, being on the order of a 70 % of the considered admissible tension, statement that validates the intended deployment to be performed in terms of the structural integrity of the tethers.

Similarly, the applied torque is characterized by a lineal profile for both controllers, where the orders of magnitude required within the manoeuvre are reasonable attending to the ones proposed within the work of authors of the field for similar E-sail configurations [4, 3].

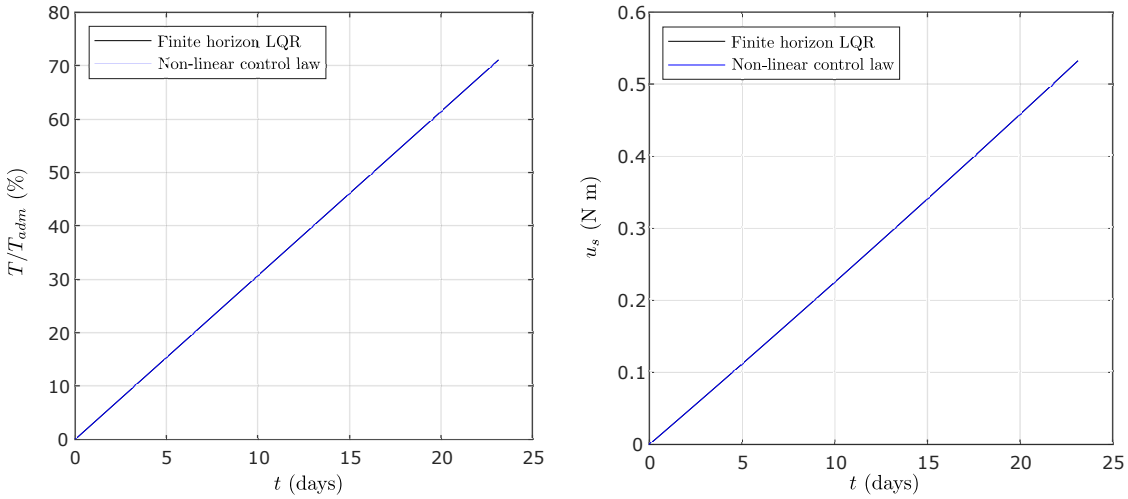

(a) Tether tension (T)

(b) Applied torque (u_s)

Figure 6.2 Evolution of the tension of each tether and the applied torque (unwrap dynamics, non-perturbed case).

In order the compare the performance of the introduced control laws, a perturbed case including the dynamics of the sensors involved within the process has been simulated taking into account the system architecture described within Chapter 5. Thus, the evolution of the relative errors within the angular hub velocity for both the linear and non-linear control law has been obtained as a result of the simulation of the proposed perturbed cases (Figure 6.3).

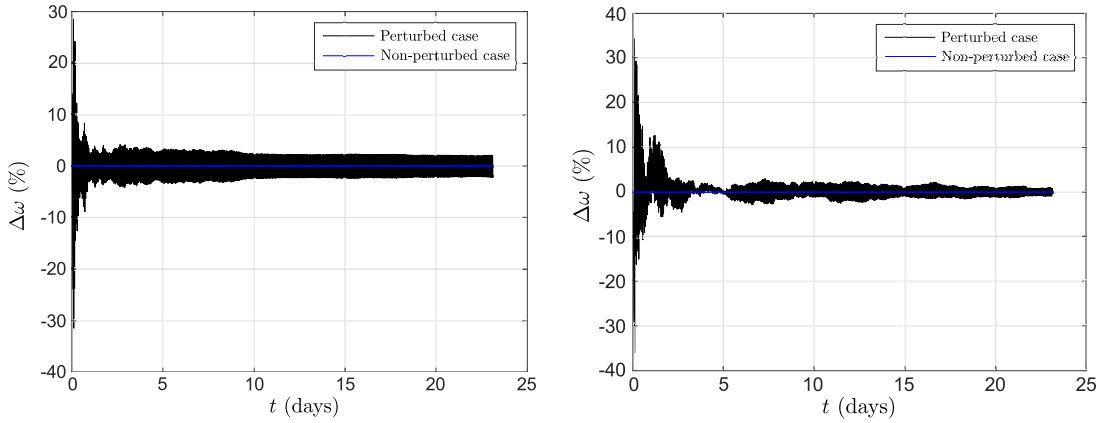

(a) Finite horizon LQR

(b) Non-linear control law

Figure 6.3 Relative errors of the angular hub velocity (ω) within the usage of the proposed linear and non-linear control laws in perturbed and non-perturbed cases (unwrap dynamics).

As it can be observed, the finite horizon control law allows the controllability of the system in terms of ω, mitigating the initial perturbation so that the errors at the steady state phase of the deployment in terms of the spacecraft rate are on the order of a 2 % of its reference value (which represents a reasonable behaviour taking into account the order of magnitude of the perturbations that are introduced into the system).

This behaviour is similarly obtained with the usage of the proposed non-linear control law, where in this case the system experiences a more oscillating behaviour at the early deployment stages. To continue with the analysis, the relative errors of the deployment rate for both the perturbed and non-perturbed cases considering the two proposed control laws can be found in Figure 6.4.

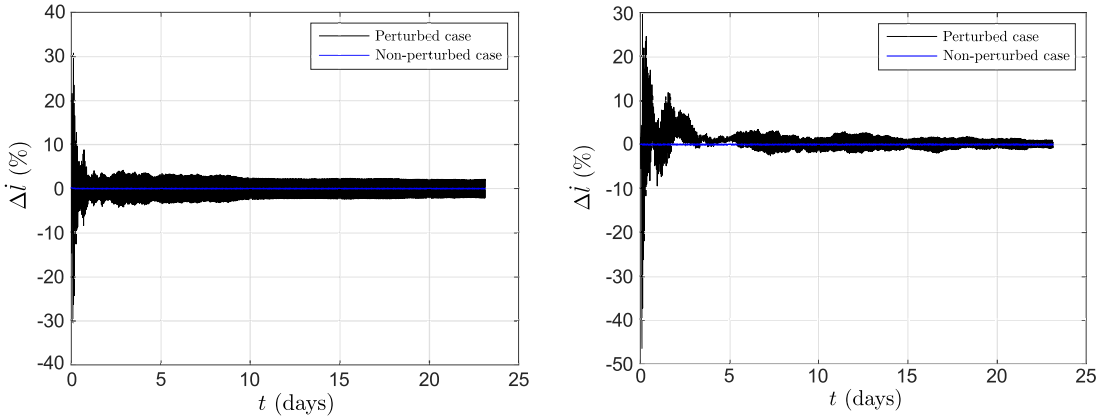

(a) Finite horizon LQR (b) Non-linear control law

Figure 6.4 Relative errors within the deployment rate ($\dot{l}$) within the usage of the proposed linear and non-linear control laws in perturbed and non-perturbed cases (unwrap dynamics).

Hence, there appears to be an analogous performance in terms of this magnitude with respect to the evolution of ω within Figure 6.3. Thus, for both linear and non-linear control laws, the implemented control algorithm allows the stabilization of this magnitude mitigating the initial perturbation introduced at the beginning of the manoeuvre, where again the non-linear control laws shows a more oscillating behaviour as a result of the topology of the control algorithm.

This statement can be further justified appealing to the evolution of the applied torque within the deployment in both perturbed and non-perturbed cases for the implemented control laws (Figure 6.5). Thus, for both linear and non-linear controllers, the perturbations produce oscillations of the applied torque with respect to their reference non-perturbed evolution, whereas these disturbances are magnified for the non-linear control law.

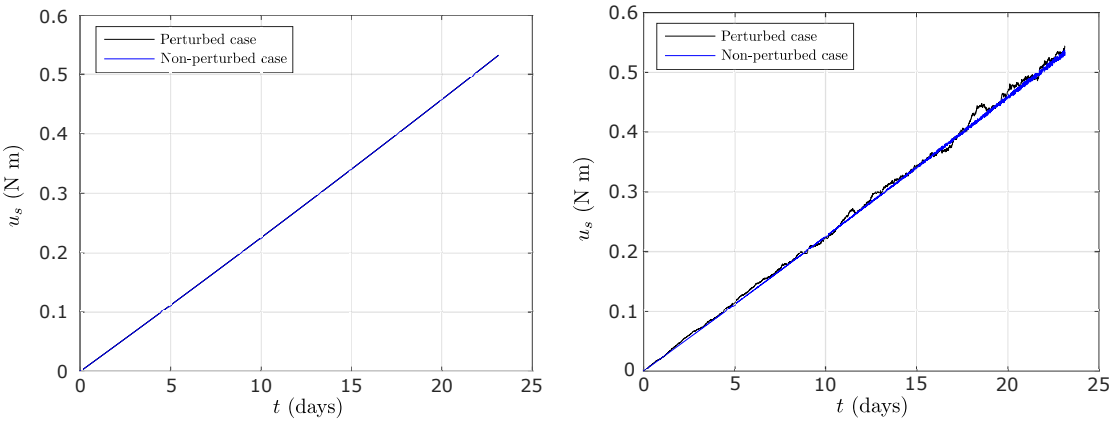

(a) Finite horizon LQR (b) Non-linear control law

Figure 6.5 Evolution of the applied torque (u_s) within the usage of the proposed linear and non-linear control laws in perturbed and non-perturbed cases (unwrap dynamics).

To finish with the analysis, Figure 6.6 represents the evolution of the tension of each individual tether through the deployment in both perturbed and non-perturbed simulations within the usage of both of the proposed control laws. Therefore, it can be stated that this magnitude is less sensitive to the perturbations introduced into the system, whereas the biggest disturbances with respect to the non-perturbed tension distribution are found within the evolution associated to the non-linear control algorithm.

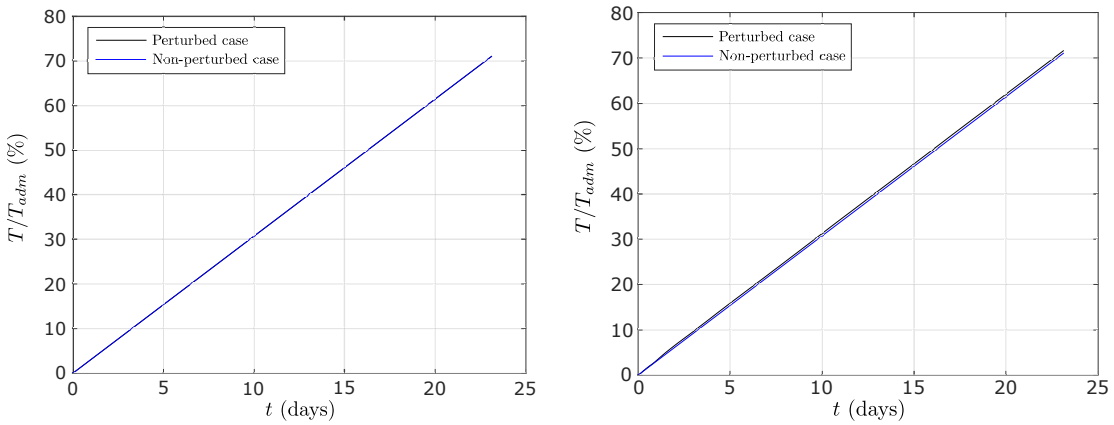

(a) Finite horizon LQR

(b) Non-linear control law

Figure 6.6 Evolution of the tether tension (T) within the usage of the proposed linear and non-linear control laws in perturbed and non-perturbed cases (unwrap dynamics).

6.1.2 Hinging dynamics

As in Subsection 6.1.1, the main target of the simulations to be analyzed is to compare the performance of the proposed control laws within this hinging phase (i.e., the finite horizon LQR and the non-linear control law) for perturbed and non-perturbed cases. For this purpose, the initial conditions that have been used for the simulations that have been carried out can be found in Table 6.4.

Table 6.3 Initial conditions (hinging phase).

Magnitude	Value	Units
Initial spacecraft angular velocity (ω_0)	$2 \cdot 10^{-3}$	rad/s
Initial spacecraft spin angle (θ_0)	0	rad
Initial β rate ($\dot{\beta}_0$)	0	rad/s
Initial tether angle (β_0)	0	rad

Similarly to the analysis performed for the unwrap phase of the deployment, the perturbations introduced into the system are the ones associated to the dynamics of the sensors involved within the estimation process, whose effects have been simulated through the topology of the system introduced in Chapter 5. To begin with this analysis, the evolution of both the spacecraft rate, and the angle of the tethers with respect to the tangential direction for both of the considered control laws in the non-perturbed case can be found in Figure 6.7.

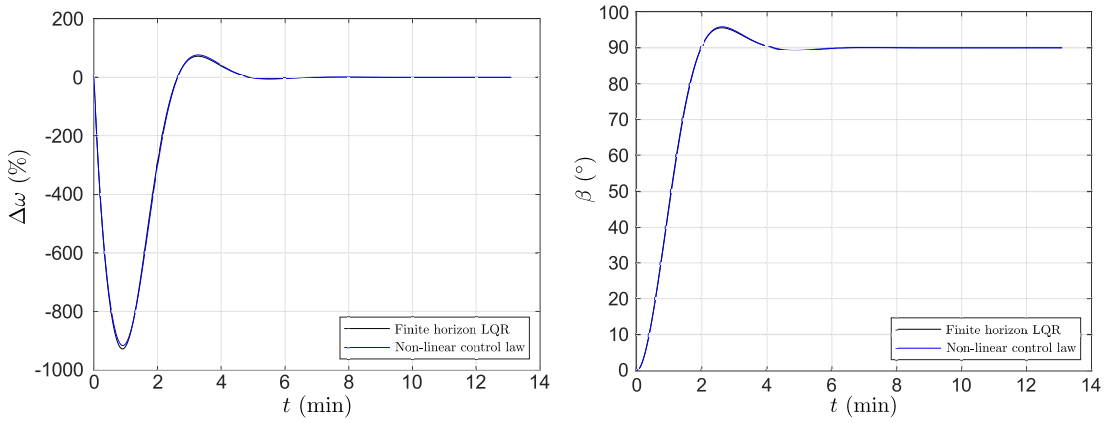

(a) Hub angular velocity errors ($\Delta\omega$)

(b) Angle of the tethers with respect to the tangential direction (β)

Figure 6.7 Evolution of the hub angular velocity and the angle of the tethers with respect to the tangential direction (hinging dynamics, non-perturbed case).

As it can be observed, both of the proposed control laws have been tuned in order to have a nearly identical response for this ideal case, so that the differences between them in terms of performance can be better accounted when perturbations are introduced into the dynamical system. Thus, the usage of both control laws lead to typical responses within second-order systems, where the steady-state value for both variables is reached after a single oscillation as a result of the tuning of the implemented control algorithms. Moreover, it should be noted that the time span of this hinging phase (i.e., on the order of minutes) is considerably smaller that the one associated to the unwrap phase (which was on the order of tens of days, see Figure 6.1).

To continue with the analysis, the evolution of both the tension of the tethers and the applied torque for this ideal hinging simulation can be found in Figure 6.8. Again, nearly identical responses on these two magnitudes are achieved for both of the proposed control algorithms as a result of the performed tuning. In particular, both magnitudes present their maximum values where the minimum value in terms of ω is obtained as a consequence of the coupling between the state variables within the dynamical system.

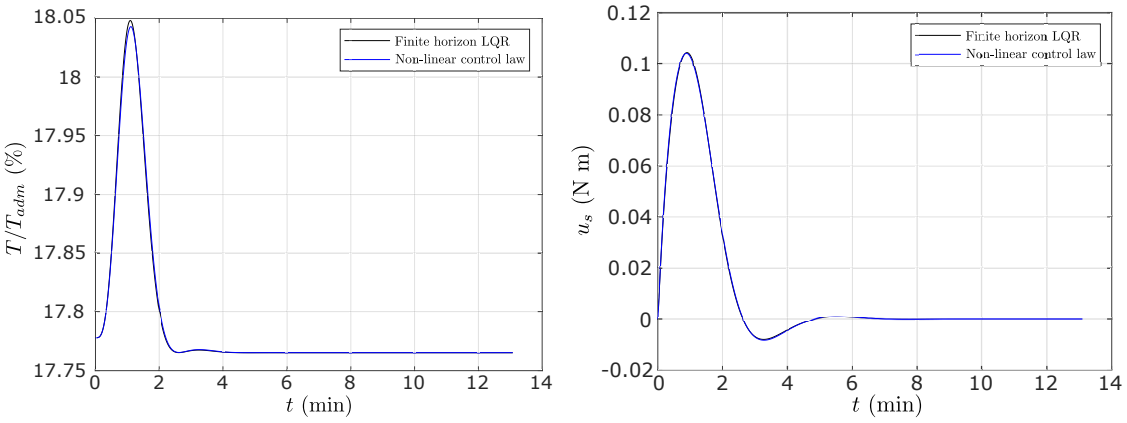

(a) Tether tension (T)

(b) Applied torque (u_s)

Figure 6.8 Evolution of the tension of each tether and the applied torque (hinging dynamics, non-perturbed case).

Additionally, it should be noted that the maximum torque that needs to be applied to the spacecraft hub in order to perform the control of this hinging phase is one order of magnitude smaller than the one associated to the unwrap phase of the deployment (Figure 6.2). Equivalently, the requirements in terms of tension have a minor relevance with respect to the overall deployment manoeuvre as a result of the tension distribution within the ideal unwrap simulation given by Figure 6.2.

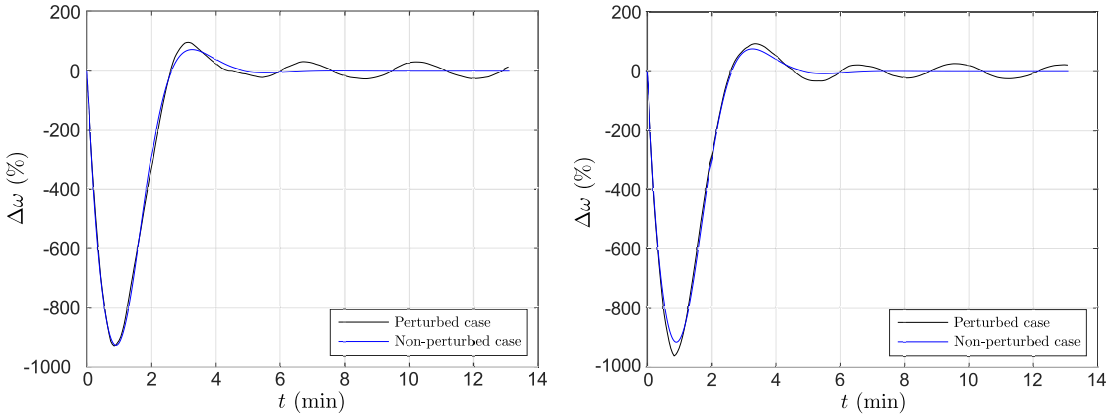

(a) Finite horizon LQR

(b) Non-linear control law

Figure 6.9 Relative errors within the angular hub velocity (ω) within the usage of the proposed linear and non-linear control laws in perturbed and non-perturbed cases (hinging dynamics).

Once the perturbations associated to the dynamics of the sensors involved within the manoeuvre have been introduced into the system, the evolution of the spacecraft rate for both linear and non-linear control laws can be found in Figure 6.9. Thus, the introduction of the described perturbations produces a degradation of the performance of the control algorithms for both of the studied cases (for instance, an increase in the overshoot appears within the nonstationary phase of the response, and oscillating behaviour is found in its steady state phase), whereas the effects are more pronounced on the finite horizon LQR.

This behaviour can be identically observed within the response in terms of β for both linear and non-linear control algorithms in this perturbed case (Figure 6.10). Nonetheless, it should be noted that the introduced perturbations produce a less pronounced effect with regard to this magnitude as a result of the standard deviations of the normal distributions that characterize the sensors involved in the estimation of this state.

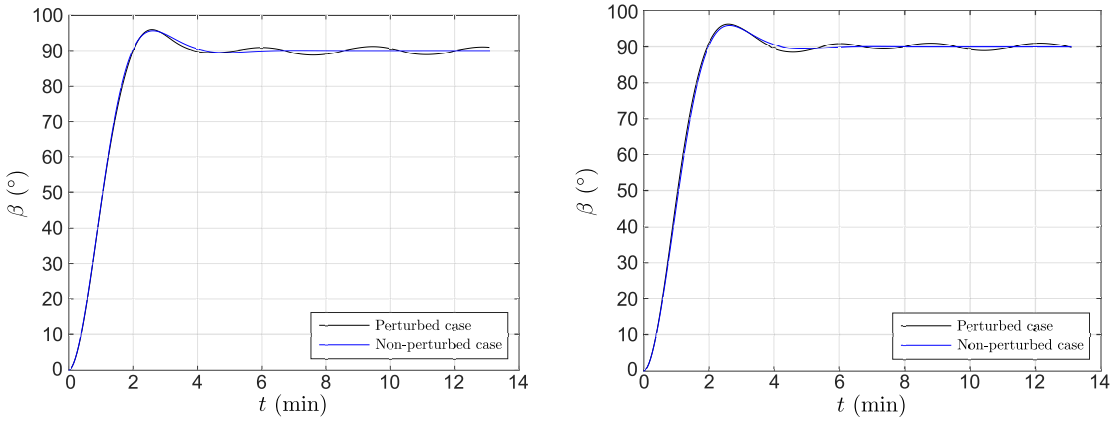

(a) Finite horizon LQR (b) Non-linear control law

Figure 6.10 Evolution of the angle of the tethers with respect to the tangential direction (β) within the usage of the proposed linear and non-linear control laws in perturbed and non-perturbed cases (hinging dynamics).

To follow with the analysis, the effect that the introduced perturbations produce on each of the proposed control laws can be clearly accounted by observing the applied torque distributions within Figure 6.11. Therefore, for both controllers (i.e., the finite horizon LQR and the non-linear control law), the perturbations deviate the torque profile with respect to their reference distributions (associated to the previously simulated ideal cases).

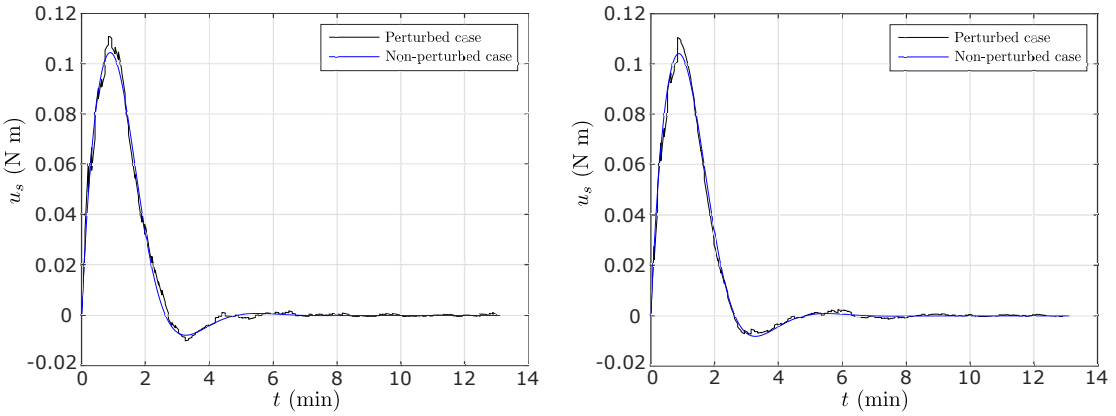

(a) Finite horizon LQR (b) Non-linear control law

Figure 6.11 Evolution of the applied torque (u_s) within the usage of the proposed linear and non-linear control laws in perturbed and non-perturbed cases (hinging dynamics).

Identically to Subsection 6.1.1, the tension of the tethers within these non-perturbed simulations (Figure 6.12) is less sensitive to the introduction of the perturbations into the system for both of the proposed control algorithms.

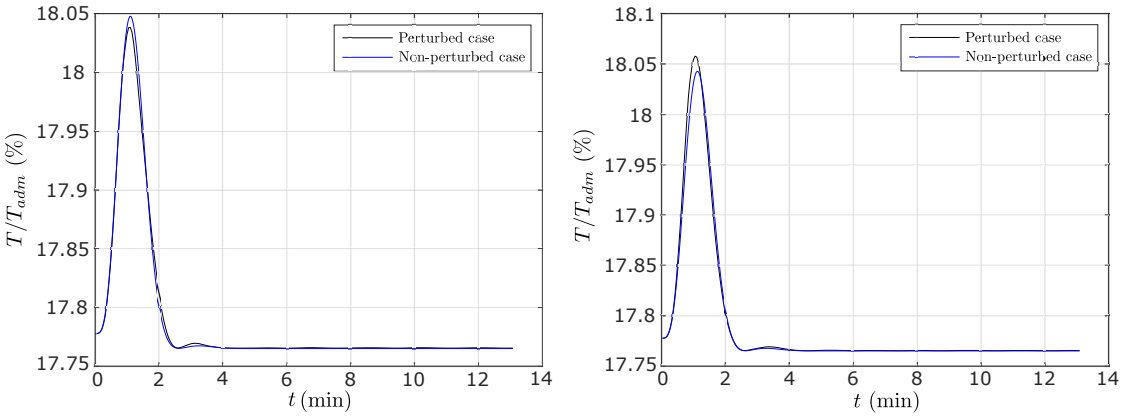

(a) Finite horizon LQR

(b) Non-linear control law

Figure 6.12 Evolution of the tether tension (T) within the usage of the proposed linear and non-linear control laws in perturbed and non-perturbed cases (hinging dynamics).

To finish with the analysis of this hinging phase, the performance of the infinite horizon LQR (with the aim of stabilizing the tethers into the radial direction once the deployment manoeuvre is finished) is aimed to be analyzed for both perturbed and non-perturbed cases. For this purpose, the dynamical system has been simulated using the initial conditions given by Table 6.4.

Table 6.4 Initial conditions (stabilization, hinging phase).

Magnitude	Value	Units
Initial spacecraft angular velocity (ω_0)	$2 \cdot 10^{-3}$	rad/s
Initial spacecraft spin angle (θ_0)	0	rad
Initial β rate ($\dot{\beta}_0$)	$\pi/2$	rad/s
Initial tether angle (β_0)	0	rad

For instance, Figure 6.13 represents the evolution of the spacecraft rate and the angle of the tethers with respect to the tangential direction for perturbed and non-perturbed cases within the usage of this control algorithm. Thus, the infinite horizon LQR allows the mitigation of the initial perturbations introduced into the system for both of the represented state variables.

Analogously, Figure 6.14 contains the evolutions of the tension and the applied torque for both perturbed and non-perturbed simulations. On one hand, the tension of each individual tethers for both perturbed and non-perturbed cases is nearly identical as a result of the less-sensitive nature of this magnitude, which has been identified through the development of the current Section.

On the other hand, the torque applied to the spacecraft spin axis is nearly negligible in comparison with the previously considered manoeuvres since the adjustments that needs to be made within this phase have a minor relevance with respect to the ones that have been previously analyzed.

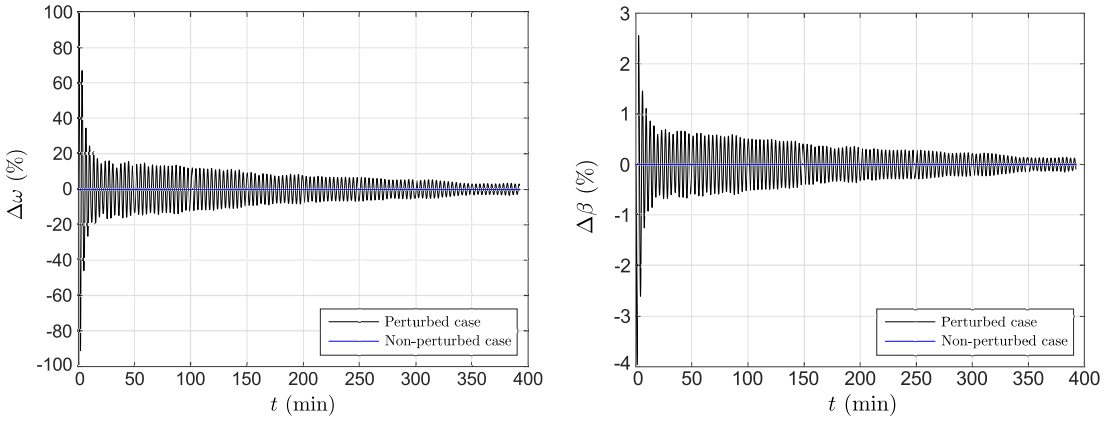

(a) Hub angular velocity errors ($\Delta\omega$) (b) Angle of the tethers with respect to the tangential direction (β)

Figure 6.13 Evolution of the hub angular velocity and the angle of the tethers with respect to the tangential direction within the usage of the proposed infinite horizon LQR (stabilization, hinging dynamics).

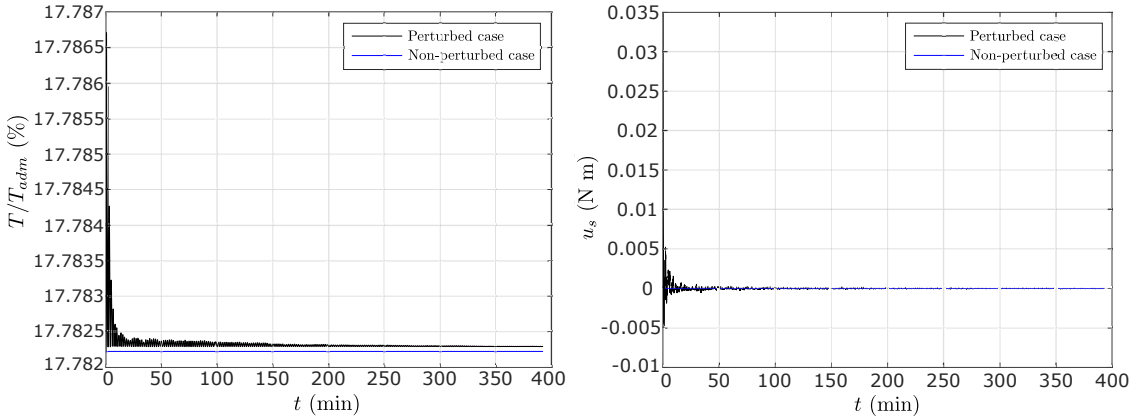

(a) Tether tension (T) (b) Applied torque (u_s)

Figure 6.14 Evolution of the tether tension and the applied torque within the usage of the proposed infinite horizon LQR (stabilization, hinging dynamics).

6.2 Radial deployment

Similarly to the review of the results of the tangential deployment strategy performed within Section 6.1, the simulations regarding the radial deployment strategy comprises the analysis of the deployment using the proposed finite and infinite horizon LQRs (i.e., with the aim of assuring the proper deployment and stabilization of the tethers, respectively), considering both perturbed and non-perturbed cases. With respect to the deployment of the tethers, the initial conditions given by Table 6.5 have been considered for the simulations, where again the initial tether length cannot be strictly equalled to zero as a result of the singularity that appears in the numerical integration of the system of differential equations.

Table 6.5 Initial conditions (radial deployment).

Magnitude	Value	Units
Initial angle with respect to the radial direction (β_0)	0	rad
Initial tether angular velocity ($\dot{\beta}_0$)	0	rad/s
Initial deployment rate ($\dot{l}_0$)	$2 \cdot 10^{-3}$	m/s
Initial tether length (l_0)	$1 \cdot 10^{-3}$	m
Initial spacecraft angular velocity (ω_0)	$2 \cdot 10^{-3}$	rad/s
Initial spacecraft spin angle (θ_0)	0	rad

To begin with the analysis, the evolution of the angle of the tethers with respect to the radial configuration (β), and the difference between the spacecraft spin rate with respect to its initial value ($\Delta\omega$) can be found in Figure 6.15. As stated in Section 4.2, the deployment aimed to be performed relies on the maintenance of both the deployment rate and the hub angular velocity through a purely radial manoeuvre (i.e., $\beta = 0$).

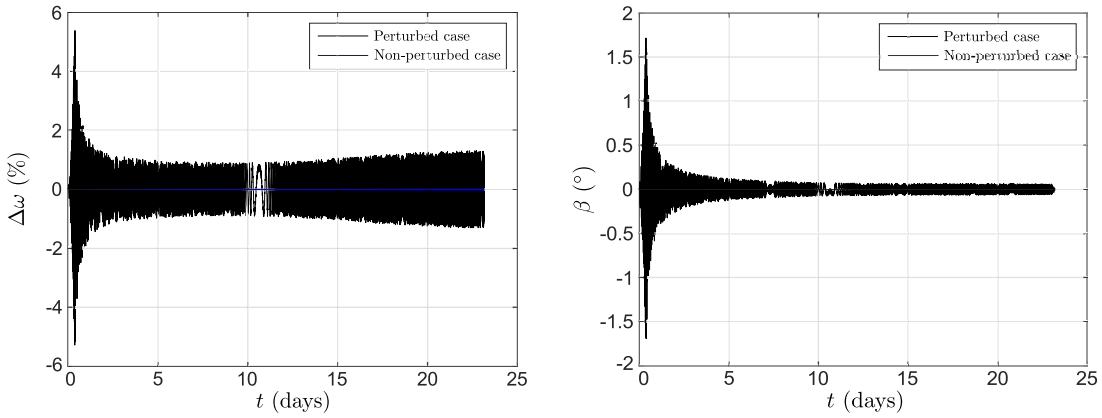

(a) Hub angular velocity errors ($\Delta\omega$)

(b) Angle of the tethers with respect to the radial direction (β)

Figure 6.15 Evolution of the hub angular velocity and the angle of the tethers with respect to the radial direction within the usage of the proposed finite horizon LQR control law in perturbed and non-perturbed cases (radial deployment).

As a result of the definition of this reference behaviour, the implemented control law allows to achieve a proper E-sail deployment in terms of ω and β in both perturbed and non perturbed cases taking into account the results within Figure 6.15. In particular, errors on the order of a 1 % and 0.25° are obtained for ω and β respectively, in the case where the perturbations introduced by the sensors are considered through the simulation of the deployment.

To continue with the analysis, Figure 6.16 represents the deployment rate variations, and the evolution of the tension of the tethers through the deployment manoeuvre for both perturbed and non perturbed simulations. Again and given that the target behaviour relies on the maintenance of the deployment rate within the manoeuvre, the introduced finite horizon LQR properly controls the dynamics of the system in terms of $\dot{l}$.

Nonetheless, it should be noted that the errors within this magnitude when perturbations are introduced into the system (being on the order of a 10 % of the reference deployment rate), point out the higher sensibility of $\dot{l}$ with regard to the introduced perturbations in comparison with ω and β. On the other hand, no significant differences appear on the evolution of the tension of the tether through the deployment with respect to its non-perturbed distribution, where this magnitude follows a linear profile having its maximum value at the end of the deployment, comprising a nearly 18 % of the overall admissible tension for the considered case.

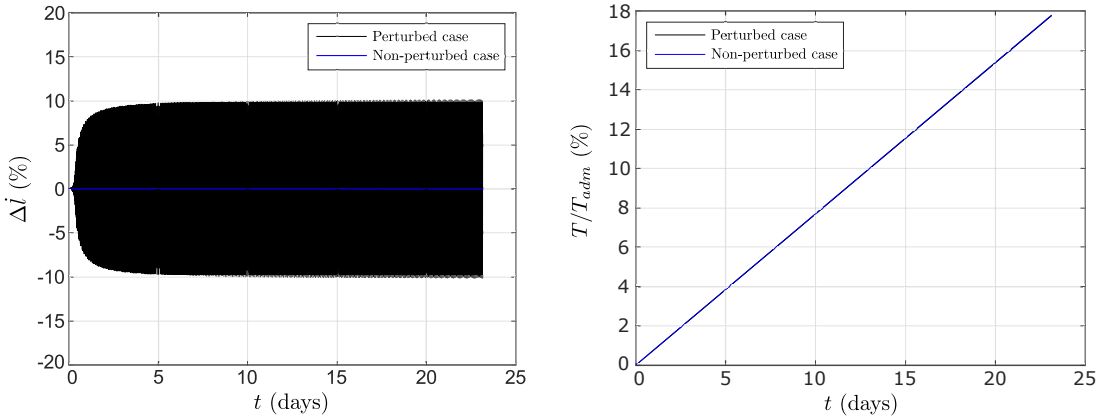

(a) Deployment rate errors ($\Delta\dot{l}$)

(b) Tether tension (T)

Figure 6.16 Evolution of the deployment rate and the tension of each tether within the usage of the proposed finite horizon LQR control law in perturbed and non-perturbed cases (radial deployment).

This low sensibility of the system in terms of T can be further justified appealing to the results obtained for the tangential deployment strategy within Section 6.1. In addition, it should be noted that the maximum tension obtained for this radial deployment strategy is considerably smaller than the one associated to the tangential deployment strategy, which can be justified by appealing to the radial alignment of this latter deployment procedure, representing a major advantage of this radial alternative in terms of the structural limitations of the tethered system.

To finish with the deployment simulations, the evolution of the imposed control magnitudes through the manoeuvre can be found in Figure 6.20. To begin with the torque applied to the hub spin axis (u_1, which comprises the only control variable in common with the tangential deployment strategy), this magnitude follows a linear profile, where its maximum vale is achieved at the end of the manoeuvre as a result of the increasing inertia of the ensemble of the tethers. Nonetheless and appealing to the non-perturbed simulation of the unwrap phase of the tangential deployment (Figure 6.2), the obtained maximum torque is nearly a half of the one associated to this latter case, in spite of using the same spacecraft spin and deployment rates.

This fact, which reinforces the analysis made for the evolution of the tension within the tethers, justifies the bigger flexibility that this deployment strategy allows in terms of both the hub angular velocity and deployment rate to be established as a target. To follow with the axial force to be applied to the tethers by their spooling drives (u_2), the magnitude follows again a linear profile (with negative slope in this case) aiming to balance the centrifugal acceleration experienced by the tethers in order not to accelerate the deployment.

Finally, the force applied by each of the remote units of the tethers (u_3) similarly follow a linear profile, where the maximum value of the magnitude is achieved at the end of the deployment manoeuvre. The control requirements of this magnitude (U_3) has to be compared within the specifications of the remote units given in Chapter 2 in order to justify the suitability of the deployment willing to be performed:

$$U_3 = \int_0^{t_{man,r}} u_3 \, dt = 1.3 \cdot 10^2 \text{ N s} \tag{6.1}$$

Thus, the control requirements allow in terms of u_3 the usage of an ionic liquid FEEP (with a total impulse capability of 2000 N s), but not the simpler cold gas thruster (with a total impulse capability of 40 N s) given the defined E-sail parameters. Nonetheless, this result validate the definition of the E-sail configuration in terms of the mass of the remote units.

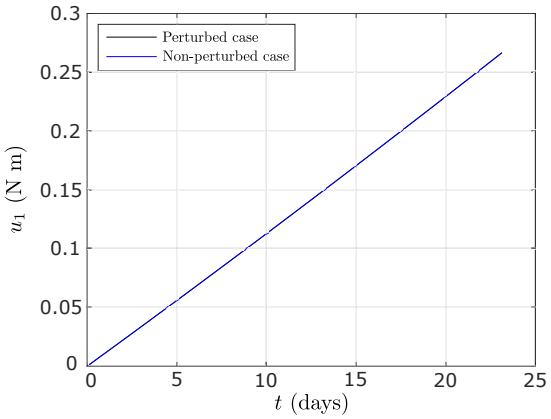

(a) Torque applied to the hub spin axis (u_1)

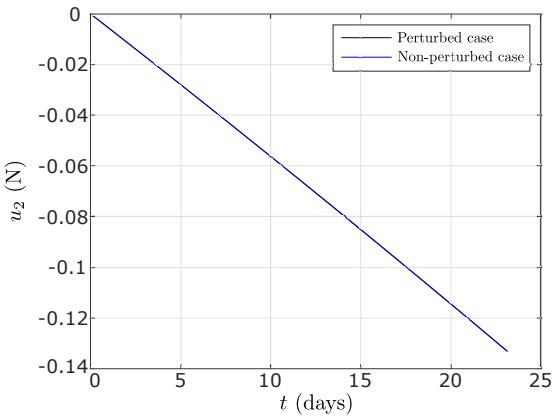

(b) Reaction of the force applied by the spooling drives of the tethers (u_2)

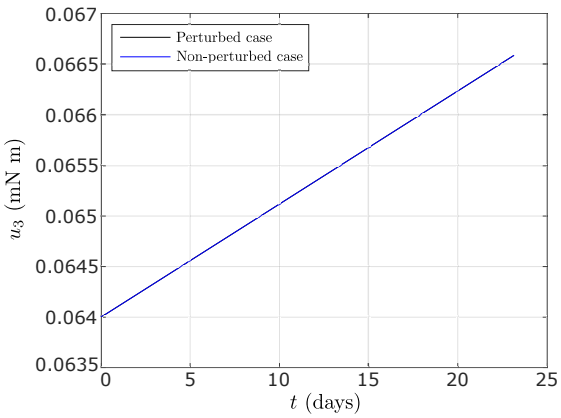

(c) Tangential force applied by the remote units (u_3)

Figure 6.17 Evolution of the control variables within the usage of the proposed finite horizon LQR control law in perturbed and non-perturbed cases (radial deployment).

This procedure can be identically performed for u_1 and u_2 in order to obtain the control requirements of the deployment, and their results will be compared with the ones associated to the tangential deployment strategy within Chapter 7.

Table 6.6 Initial conditions (stabilization, radial deployment).

Magnitude	Value	Units
Initial angle with respect to the radial direction (β_0)	0	rad
Initial tether angular velocity ($\dot{\beta}_0$)	0	rad/s
Initial deployment rate ($\dot{l}_0$)	0	m/s
Initial tether length (l_0)	$4 \cdot 10^3$	m
Initial spacecraft angular velocity (ω_0)	$2 \cdot 10^{-3}$	rad/s
Initial spacecraft spin angle (θ_0)	0	rad

For the sake of completing the analysis of this radial deployment strategy, simulations regarding the stabilization of the tethers once they have been deployed (within perturbed and non-perturbed cases) have been performed. These simulations have been carried out using the infinite horizon LQR control law introduced within Section 4.2 and the initial conditions given by Table 6.6. Hence, the tethers are assumed to be totally deployed with a purely radial configuration, where their deployment rates and angular velocities are imposed to be zero.

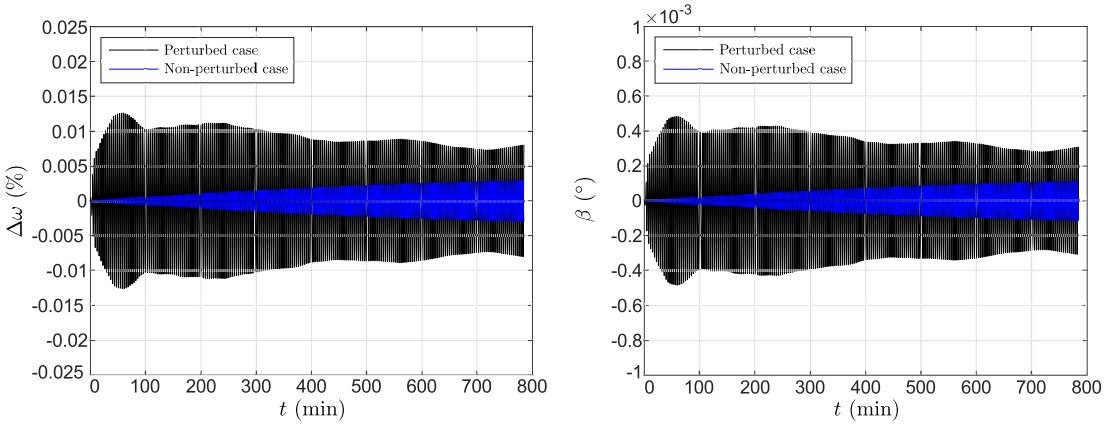

(a) Hub angular velocity errors ($\Delta\omega$)

(b) Angle of the tethers with respect to the radial direction (β)

Figure 6.18 Evolution of the hub angular velocity and the angle of the tethers with respect to the radial direction within the usage of the proposed infinite horizon LQR control law in perturbed and non-perturbed cases (stabilization, radial deployment).

Given the results obtained from both the perturbed and non-pertubed simulations, the evolution of the spacecraft rate and the angle of the tethers with respect to the radial direction on both cases can be found in Figure 6.18. Identically to the simulations carried out with regard to the deployment itself, the target behaviour of these simulations relies on the maintenance of the initial hub angular velocity with a purely radial configuration of the tethers (i.e., $\beta = 0$).

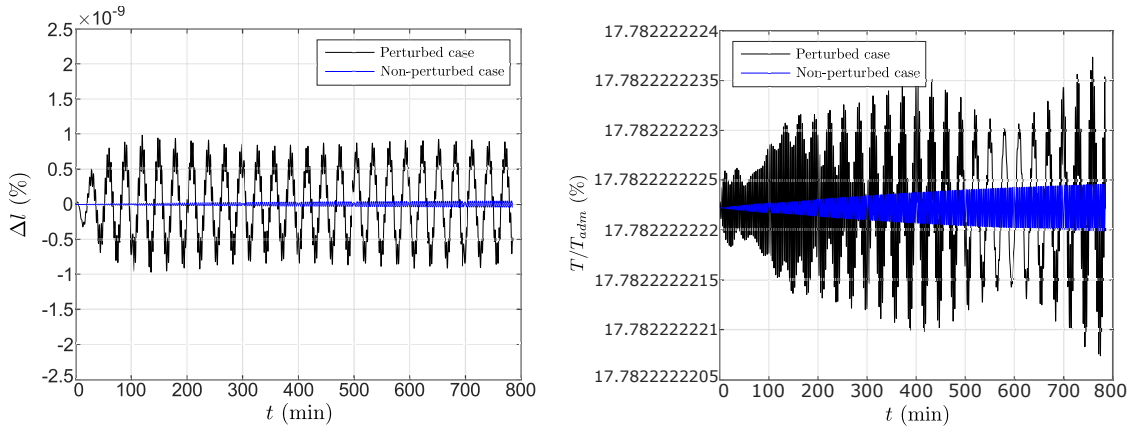

(a) Tether length errors (Δl)

(b) Tether tension (T)

Figure 6.19 Evolution of the tether length and the tension of each tether within the usage of the proposed infinite horizon LQR control law in perturbed and non-perturbed cases (stabilization, radial deployment).

Hence and given the results within Figure 6.18, the implemented infinite horizon LQR allows a proper stabilization of the tethers in terms of ω and β, whereas the differences of these magnitudes with respect to their reference values are nearly negligible in comparison with the results associated to the deployment manoeuvre (Figure 6.15). Identically, Figure 6.19 shows the evolution of the tether length (in terms of relative errors with respect to the initial length of the tethers, which is aimed to be maintained) and the tension of the tethers within the two considered cases.

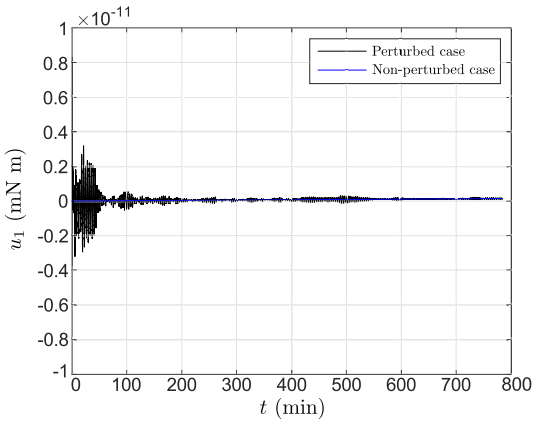

(a) Torque applied to the hub spin axis (u_1)

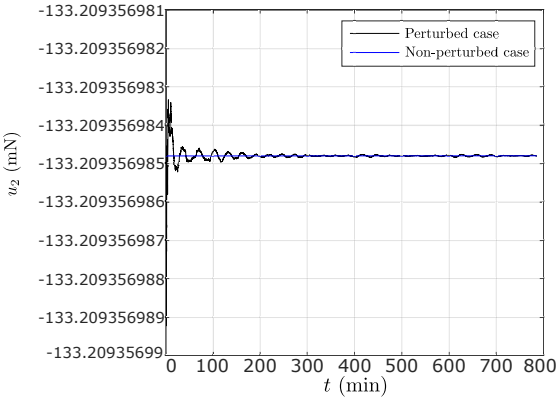

(b) Reaction of the force applied by the spooling drives of the tethers (u_2)

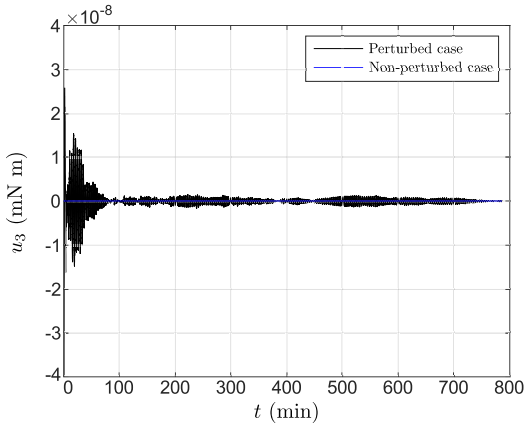

(c) Tangential force applied by the remote units (u_3)

Figure 6.20 Evolution of the control variables within the usage of the proposed infinite horizon LQR control law in perturbed and non-perturbed cases (stabilization, radial deployment).

Again, these two magnitudes show negligible differences with respect to their reference values in despite of having introduced perturbations into the system as a result of the dynamics involved in the state estimation process. Additionally, the tether tension does not comprise a significant fraction of the admissible value of this magnitude, fact that further justifies the lower requirements of this deployment strategy with respect to this magnitude.

To finish with the analysis, Figure 6.20 represents the evolution of the defined control variables within this stabilization phase of the deployment. Thus, the torque applied to the hub spin axis (u_1) is nearly negligible in comparison with the orders of magnitude involved within the deployment manoeuvre (Figure 6.20), whereas no significant differences are found between the evolution of this magnitude on both perturbed and non-perturbed cases.

Equivalently, the same behaviour is obtained regarding the force applied by the remote units (u_3), fact that could be justified appealing to the low tangential acceleration of the tether end masses as a result of the nearly negligible deployment rate (see Equation (3.97)). Finally, the reaction force applied to the ensemble of the tethers by their individual spooling drives (u_2) nearly experiences differences with respect to its reference value.

7 Conclusions and future work

In this project, the dynamical modelling and control of E-sail deployment strategies have been extensively explored. In particular, the non-dimensional bidimensional equations of motion for both tangential and radial deployment strategies were derived taking a Lagrangian-based approximation. Therefore, taking these models as a baseline, both linear and non-linear control laws were derived, as well as an Extended Kalman Filter (EKF). Thus, the performance of the output feedback control laws (i.e., where the state used for computing the control algorithm had been estimated by the EKF) was evaluated by taking into account a realistic level of noise within the available measurements.

On one hand, the tangential deployment strategy (similar to a yo-yo de-spinner mechanism) was analyzed dividing the manouvre into the so-called unwrap and hinging phases. For both cases, linear and non-linear control laws probed the controllability of the derived dynamical models for both and non-perturbed cases with reasonable errors on the state variables.

On the other hand, an analogous Lagrangian-based dynamical model was derived for the so-called radial deployment strategy, which is based on the usage of individual spooling drives for each of the tethers. As a result of the higher complexity of the model given the bigger amount of degrees of freedom and control variables, only linear control algorithms were proposed for assuring a proper E-sail behaviour through the deployment.

This latter statement was verified for both perturbed and non-perturbed cases, where the order of magnitude of the errors with respect to their defined references were reasonable given the perturbations introduced into the system. In order to compare both of the deployment strategies, the reference behaviour for both cases was based on a constant deployment rate, whereas the length of the tethers aimed to be deployed was identically defined.

Therefore, the control requirements for both strategies can be compared regarding their evolution within the simulated non-perturbed cases (Table 7.1). Therefore, in spite of its higher mechanical complexity, the radial deployment strategy requires nearly half of the torque applied to the hub spin axis within the tangential deployment case.

Table 7.1 Integral of the applied torque (U_1), the axial force applied to the tethers by their individual spooling drives (U_2) and the tangential force applied by the remote units (U_3) within both considered tangential and radial deployment manoeuvres.

Magnitude	Tangential deployment	Radial deployment
U_1 (N m s)	$5.3 \cdot 10^5$	$2.6 \cdot 10^5$
U_2 (N s)	-	$1.3 \cdot 10^5$
U_3 (N s)	-	$1.3 \cdot 10^2$

Nonetheless, it should be noted that this radial strategy requires the usage of both individual spooling drives and remote units, which nonetheless allows individual control of each tether reducing the risk of general deployment failure. On the other hand, despite its simplicity in terms of architecture of the control system, the tangential strategy requires a transition or hinge phase from the purely tangential to the radial operating configuration of the tethers, in contrast with the radial deployment where there is no need for a hinging phase.

On this matter, it should be noted that efforts have been made regarding the transition between the unwrap and the hinging phases of this tangential deployment strategy. For instance, a number of transition schemes were tried in order to accomplish the latter transition that led to non-minimum phases that resulted in non-physical results regarding the evolution of β, which can be justified by the major differences between the applied torque at the end of the unwrap phase, and at the beginning of the hinging phase.

As a result of the latter analysis, efforts were made in order to accomplish the transition by using the dynamics of the system, allowing its natural oscillation meanwhile the hub actuator could perform its transition by an on/off switch. The main drawbacks regarding this alternative were the big overshoots that appeared in all the state variables (i.e., the natural dynamics of the tethers comprise the oscillation of the tethers around the β spin axis), where the response in terms of ω was particularly problematic. Therefore, the transition between the tangential and the radial configuration of the tethers represents a major drawback worth to be considered at the time of dealing with this deployment strategy.

Therefore, the derived dynamical models and feedback control laws represent a baseline for the understanding of E-sail deployment operations, which can serve to perform first order estimation of the control requirements within these manoeuvres. Hence, as a result of the presented conclusions, it has been considered that the main objectives of the project has been achieved through the development of the current study.

Nonetheless, the author wants to emphasize at this point the major difficulties that were found during the development of the presented numerical study. For instance, the high complexity of the derived equations of motion have lead to major difficulties with regard to their linearization and the derivation of their associated control laws. Additionally, the influence of the parameters that define the E-sail configuration (e.g., the tether end masses, the hub angular velocity...) should be noted. Thus, despite having analyzed a single case comprising a typical E-sail configuration within the study, the definition of these magnitudes greatly influences the E-sail behaviour through the deployment manoeuvre, and should therefore be wisely selected as a result of the non-linear coupling between the state variables.

7.1 Future work

As future lines of research, one of the major assumptions that were made during the development of the dynamical models of the considered deployment strategies was to ignore the in-plane bending of the tethers in order to obtain an analytical model capturing the main physics governing the problem. Therefore, the bending flexibility of the tethers can be considered through the introduction of additional finite elements or lumped masses in order to account the effect of this contribution into the deployment.

On the other hand, only symmetrical deployment operations were considered through the development of the study. Therefore, non-symmetrical radial[1] deployment operations (e.g., where an individual tether is blocked for a period of time during the deployment) can be studied using the generalized dynamical model derived within Appendix B. Hence, this model relies on the same assumptions of the previously introduced symmetrical models, whereas the degrees of freedom and control variables associated to each of the tethers are treated independently.

Finally, the current study has been only focused on the rotational-plane dynamics of the E-sail system, where the out of plane dynamics have been ignored for the sake of simplifying the subsequent equations of motion. Therefore, the derivation of numerical models (e.g, using the finite element method) considering these contributions represents another future line of research worth to be analyzed.

[1] Since the tangential strategy does not allow an individual control of each tether and it is not feasible to perform such a manoeuvre.

Bibliography

[1] Pekka Janhunen, Alessandro Quarta, and Giovanni Mengali. Electric solar wind sail mass budget model. *Geoscientific Instrumentation, Methods and Data Systems*, 2:85–95, 02 2013.

[2] Joanna Fulton and Hanspeter Schaub. Dynamics and control of the flexible electrostatic sail deployment. *AAS/AIAA Space Flight Mechanics Meeting, Napa (CA), USA*, 2016.

[3] Joanna Fulton and Hanspeter Schaub. Fixed-axis electric sail deployment dynamics analysis using hub-mounted momentum control. *Acta Astronautica*, 144, 12 2018.

[4] Li Gangqiang, Zheng Zhu, and Chonggang Du. Stability and control of radial deployment of electric solar wind sail. *Nonlinear Dynamics*, 105:481, 01 2021.

[5] Ce Zhao, Mingying Huo, Ji Qi, Shilei Cao, et al. Coupled attitude-vibration analysis of an E-sail using absolute nodal coordinate formulation. *Astrodynamics*, 4, 08 2020.

[6] Henri Seppänen. Tether factory (1 km) design, implementation and production. *Deliverable D21.3. Electric sail propulsion technology EU-FP7 Project*, 2013.

[7] Pekka Janhunen. Electric Sail for Spacecraft Propulsion. *Journal of Propulsion and Power*, 20(4):763–764, 2004.

[8] Bo Fu, Evan Sperber, and Fidelis Eke. Solar sail technology—A state of the art review. *Progress in Aerospace Sciences*, 86, 08 2016.

[9] David Spencer, Bruce Betts, John Bellardo, Alex Diaz, et al. The LightSail 2 Solar Sailing Technology Demonstration. *Advances in Space Research*, 67, 06 2020.

[10] Pekka Janhunen, Pihla Toivanen, Juhani Polkko, Sini Merikallio, et al. Electric solar wind sail: Toward test missions. *Review of Scientific Instruments*, 81, 11 2010.

[11] Pekka Janhunen. Increased electric sail thrust through removal of trapped shielding electrons by orbit chaotisation due to spacecraft body. *Annales Geophysicae*, 27, 08 2009.

[12] Pekka Janhunen. Status report of the electric sail in 2009. *Acta Astronautica*, 68(5):567–570, 2011.

[13] Pihla Toivanen and Pekka Janhunen. Thrust vectoring of an electric solar wind sail with a realistic sail shape. *Acta Astronautica*, 131:145–151, 2017.

[14] Petri Toivanen and Pekka Janhunen. Spin Plane Control and Thrust Vectoring of Electric Solar Wind Sail. *Journal of Propulsion and Power*, 29(1):178–185, 2013.

[15] ESAIL (Electric sail propulsion technology) EU-FP7 Project. *https://cordis.europa.eu/project/id/262733/reporting/es*. Accessed: 15/6/2023.

[16] Heliopause Electrostatic Rapid Transit System (HERTS) Project. *https://www.nasa.gov/feature/heliopause-electrostatic-rapid-transit-system-herts/*. Accessed: 15/6/2023.

[17] Pekka Janhunen. Electrostatic Plasma Brake for Deorbiting a Satellite. *Journal of Propulsion and Power - J PROPUL POWER*, 26:370–372, 03 2010.

[18] Andris Slavinskis, Mihkel Pajusalu, Henri Kuuste, Erik Ilbis, et al. ESTCube-1 In-Orbit Experience and Lessons Learned. *IEEE Aerospace and Electronic Systems Magazine*, 30:12–22, 10 2015.

[19] Iaroslav Iakubivskyi, Hendrik Ehrpais, Janis Dalbins, Ervin Oro, et al. ESTCube-2 mission analysis: plasma brake experiment for deorbiting. 09 2016.

[20] Antti Kestilä, Tero Tikka, Pyry Peitso, Jorma Rantanen, et al. Aalto-1 nanosatellite – technical description and mission objectives. *Geoscientific Instrumentation, Methods and Data Systems*, 2:121–130, 02 2013.

[21] Muhammad Mughal, Jaan Praks, Rami Vainio, Pekka Janhunen, et al. Aalto-1, multi-payload CubeSat: In-orbit results and lessons learned. *Acta Astronautica*, 187, 01 2021.

[22] Les Johnson and Jurtz Polzin. Electric Sail Propulsion for Deep Space Missions. *70th International Astronautical Congress (IAC)*, 2019.

[23] Michael Tinker, Thomas Bryan, Jason Vaughn, Stephen Canfield, et al. Electric sail tether deployment system for Cubesats. *IEEE Aerospace Conference*, 2019.

[24] Benjamin Hargis, Benjamin Brandt, Stephen Canfield, and Michael Tinker. Modeling, Validation and Prototype Development of Electric Sail Tether Deployment Systems for CubeSats. Volume 5A: 43rd Mechanisms and Robotics Conference, 08 2019.

[25] Iaroslav Iakubivskyi, Pekka Janhunen, Jaan Praks, Viljo Allik, et al. Coulomb drag propulsion experiments of Estcube-2 and Foresail-1. *Acta Astronautica*, 177:771–783, 12 2020.

[26] Minna Palmroth, Jaan Praks, Rami Vainio, Pekka Janhunen, et al. FORESAIL-1 CubeSat Mission to Measure Radiation Belt Losses and Demonstrate Deorbiting. *Journal of Geophysical Research: Space Physics*, 124:5783–5799, 07 2019.

[27] Zheng Zhu and Gangqiang Li. *Dynamic Analysis of Deployment of Electric Solar Wind Sail*.

Appendix A
Jacobian matrices of the defined dynamical systems

In this appendix, the derivation of the Jacobian matrices of the defined deployment dynamics is assessed. Thus, this analysis has been divided into the two considered deployment strategies (i.e., tangential and radial deployment) in order to follow the same structure of the rest of the document.

A.1 Tangential deployment

To begin with the tangential deployment strategy, the derivation has been particularized for the unwrap and hinging phases.

A.1.1 Unwrap dynamics

Given the definition of the unwrap dynamical system by Equation (4.12), the Jacobian matrices associated to this set of differential equations can be expressed as:

$$A_u\left(x_u,\, u_u,\, \tau\right) = \begin{bmatrix} \frac{\partial f_{u1}}{\partial x_{u1}} & \frac{\partial f_{u1}}{\partial x_{u2}} & \frac{\partial f_{u1}}{\partial x_{u3}} & \frac{\partial f_{u1}}{\partial x_{u4}} \\ \frac{\partial f_{u2}}{\partial x_{u1}} & \frac{\partial f_{u2}}{\partial x_{u2}} & \frac{\partial f_{u2}}{\partial x_{u3}} & \frac{\partial f_{u2}}{\partial x_{u4}} \\ \frac{\partial f_{u3}}{\partial x_{u1}} & \frac{\partial f_{u3}}{\partial x_{u2}} & \frac{\partial f_{u3}}{\partial x_{u3}} & \frac{\partial f_{u3}}{\partial x_{u4}} \\ \frac{\partial f_{u4}}{\partial x_{u1}} & \frac{\partial f_{u4}}{\partial x_{u2}} & \frac{\partial f_{u4}}{\partial x_{u3}} & \frac{\partial f_{u4}}{\partial x_{u4}} \end{bmatrix} \tag{A.1}$$

And analogously, for the matrix associated to the control vector:

$$B_u\left(x_u,\, u_u,\, \tau\right) = \begin{bmatrix} \frac{\partial f_{u1}}{\partial u_u} \\ \frac{\partial f_{u2}}{\partial u_u} \\ \frac{\partial f_{u3}}{\partial u_u} \\ \frac{\partial f_{u4}}{\partial u_u} \end{bmatrix} \tag{A.2}$$

Therefore, each of the components of (A.1) and (A.2) are defined as:

$$\frac{\partial f_{u1}}{\partial x_{u1}} = 0, \qquad \frac{\partial f_{u1}}{\partial x_{u2}} = 1, \qquad \frac{\partial f_{u1}}{\partial x_{u3}} = 0, \qquad \frac{\partial f_{u1}}{\partial x_{u4}} = 0, \qquad \frac{\partial f_{u1}}{\partial u_u} = 0 \tag{A.3}$$

Similarly, for the terms associated to f_{u2}:

$$\begin{aligned}\frac{\partial f_{u2}}{\partial x_{u1}} =& \frac{1}{b_{u2} - b_{u1}\,\dfrac{a_{u2}}{a_{u1}}} \left[-f_{u2} \left(\frac{\partial b_{u2}}{\partial x_{u1}} - \frac{a_{u1}\left(\dfrac{\partial b_{u1}}{\partial x_{u1}}\,a_{u2} + b_{u1}\,\dfrac{\partial a_{u2}}{\partial x_{u1}}\right) - b_{u1}\,a_{u2}\,\dfrac{\partial a_{u1}}{\partial x_{u1}}}{{a_{u1}}^2} \right) \right. \\ &+ {x_{u2}}^2 \left(\frac{a_{u1}\left(\dfrac{\partial b_{u1}}{\partial x_{u1}}\,a_{u3} + b_{u1}\,\dfrac{\partial a_{u3}}{\partial x_{u1}}\right) - b_{u1}\,a_{u3}\,\dfrac{\partial a_{u1}}{\partial x_{u1}}}{{a_{u1}}^2} - \frac{\partial b_{u4}}{\partial x_{u1}} \right) - \frac{\partial b_{u3}}{\partial x_{u1}}\,x_{u2}\,x_{u4} \\ &\left. - \frac{a_{u1}\left(\dfrac{\partial b_{u1}}{\partial x_{u1}}\,a_{u4} + b_{u1}\,\dfrac{\partial a_{u4}}{\partial x_{u1}}\right) - b_{u1}\,a_{u4}\,\dfrac{\partial a_{u1}}{\partial x_{u1}}}{{a_{u1}}^2}\,{x_{u4}}^2 \right]\end{aligned} \tag{A.4}$$

$$\frac{\partial f_{u2}}{\partial x_{u2}} = \frac{1}{b_{u2} - b_{u1}\,\dfrac{a_{u2}}{a_{u1}}} \left[2\left(b_{u1}\,\frac{a_{u3}}{a_{u1}} - b_{u4} \right) {x_{u2}}^2 - b_{u3}\,x_{u4} \right] \tag{A.5}$$

$$\frac{\partial f_{u2}}{\partial x_{u3}} = 0 \tag{A.6}$$

$$\frac{\partial f_{u2}}{\partial x_{u4}} = \frac{1}{b_{u2} - b_{u1}\,\dfrac{a_{u2}}{a_{u1}}} \left[-2\,b_{u1}\,\frac{a_{u4}}{a_{u1}}\,x_{u4} - b_{u3}\,x_{u2} \right] \tag{A.7}$$

$$\frac{\partial f_{u2}}{\partial u_u} = \frac{1}{b_{u2} - b_{u1}\,\dfrac{a_{u2}}{a_{u1}}} \tag{A.8}$$

Analogously:

$$\frac{\partial f_{u3}}{\partial x_{u1}} = 0, \qquad \frac{\partial f_{u3}}{\partial x_{u2}} = 0, \qquad \frac{\partial f_{u3}}{\partial x_{u3}} = 0, \qquad \frac{\partial f_{u3}}{\partial x_{u4}} = 1, \qquad \frac{\partial f_{u3}}{\partial u_u} = 0 \tag{A.9}$$

And finally, for the terms associated to f_{u4}:

$$\frac{\partial f_{u4}}{\partial x_{u1}} = \frac{1}{a_{u1}} \left[-f_{u4}\,\frac{\partial a_{u1}}{\partial x_{u1}} - \frac{\partial a_{u2}}{\partial x_{u1}}\,f_{u2} - a_{u2}\,\frac{\partial f_{u2}}{\partial x_{u1}} - \frac{\partial a_{u3}}{\partial x_{u1}}\,{x_{u2}}^2 + \frac{\partial a_{u4}}{\partial x_{u1}}\,{x_{u4}}^2 \right] \tag{A.10}$$

$$\frac{\partial f_{u4}}{\partial x_{u2}} = \frac{1}{a_{u1}} \left[-a_{u2}\,\frac{\partial f_{u2}}{\partial x_{u2}} - 2\,a_{u3}\,x_{u2} \right] \tag{A.11}$$

$$\frac{\partial f_{u4}}{\partial x_{u3}} = 0 \tag{A.12}$$

$$\frac{\partial f_{u4}}{\partial x_{u4}} = \frac{1}{a_{u1}} \left[-a_{u2} \frac{\partial f_{u2}}{\partial x_{u4}} + 2\, a_{u4}\, x_{u4} \right] \tag{A.13}$$

$$\frac{\partial f_{u4}}{\partial u_u} = -\frac{a_{u2}}{a_{u1}} \frac{\partial f_{u2}}{\partial u_u} \tag{A.14}$$

Where the derivatives of each of the defined auxiliary functions (i.e., a_{u1}, b_{u2}...) are given by:

$$\frac{\partial a_{u1}}{\partial x_{u1}} = 72\pi + 84\pi\, {x_{u1}}^2 + 96\pi\, \overline{m_E}\, x_{u1} \tag{A.15}$$

$$\frac{\partial a_{u2}}{\partial x_{u1}} = 30 + 42\, {x_{u1}}^2 + 48\, \overline{m_E}\, x_{u1} \tag{A.16}$$

$$\frac{\partial a_{u3}}{\partial x_{u1}} = 42\, x_{u1} + 24\, \overline{m_E} \tag{A.17}$$

$$\frac{\partial a_{u4}}{\partial x_{u1}} = 168\pi^2\, x_{u1} + 96\pi^2\, \overline{m_E} \tag{A.18}$$

And for the derivatives of the b_{ux} terms:

$$\frac{\partial b_{u1}}{\partial x_{u1}} = 42\pi\, {x_{u1}}^2 + 24\pi + 48\pi\, \overline{m_E}\, x_{u1} \tag{A.19}$$

$$\frac{\partial b_{u2}}{\partial x_{u1}} = 21\, {x_{u1}}^2 + 18 + 24\, \overline{m_E}\, x_{u1} \tag{A.20}$$

$$\frac{\partial b_{u3}}{\partial x_{u1}} = 84\pi\, x_{u1} + 48\pi\, \overline{m_E} \tag{A.21}$$

$$\frac{\partial b_{u4}}{\partial x_{u1}} = 42\, x_{u1} + 24\, \overline{m_E} \tag{A.22}$$

A.1.2 Hinging dynamics

Given the derivation of the hinging dynamics by Equation (4.69), the Jacobian matrices associated to this system of differential equations are defined as:

$$A_h\,(x_h,\,u_h,\,\tau) = \begin{bmatrix} \frac{\partial f_{h1}}{\partial x_{h1}} & \frac{\partial f_{h1}}{\partial x_{h2}} & \frac{\partial f_{h1}}{\partial x_{h3}} & \frac{\partial f_{h1}}{\partial x_{h4}} \\ \frac{\partial f_{h2}}{\partial x_{h1}} & \frac{\partial f_{h2}}{\partial x_{h2}} & \frac{\partial f_{h2}}{\partial x_{h3}} & \frac{\partial f_{h2}}{\partial x_{h4}} \\ \frac{\partial f_{h3}}{\partial x_{h1}} & \frac{\partial f_{h3}}{\partial x_{h2}} & \frac{\partial f_{h3}}{\partial x_{h3}} & \frac{\partial f_{h3}}{\partial x_{h4}} \\ \frac{\partial f_{h4}}{\partial x_{h1}} & \frac{\partial f_{h4}}{\partial x_{h2}} & \frac{\partial f_{h4}}{\partial x_{h3}} & \frac{\partial f_{h4}}{\partial x_{h4}} \end{bmatrix} \tag{A.23}$$

And analogously, for the matrix associated to the derivatives associated to the control vector:

$$B_h\,(x_h,\,u_h,\,\tau) = \begin{bmatrix} \frac{\partial f_{h1}}{\partial u_h} \\ \frac{\partial f_{h2}}{\partial u_h} \\ \frac{\partial f_{h3}}{\partial u_h} \\ \frac{\partial f_{h4}}{\partial u_h} \end{bmatrix} \tag{A.24}$$

Therefore, each of the components of (A.23) and (A.24) are defined as:

$$\frac{\partial f_{h1}}{\partial x_{h1}} = 0, \qquad \frac{\partial f_{h1}}{\partial x_{h2}} = 1, \qquad \frac{\partial f_{h1}}{\partial x_{h3}} = 0, \qquad \frac{\partial f_{h1}}{\partial x_{h4}} = 0, \qquad \frac{\partial f_{h1}}{\partial u_h} = 0 \tag{A.25}$$

Similarly:

$$\frac{\partial f_{h2}}{\partial x_{h1}} = 0 \tag{A.26}$$

$$\frac{\partial f_{h2}}{\partial x_{h2}} = \frac{1}{b_{h1} - b_{h2}\,\frac{a_{h1}}{a_{h2}}}\,\left[-2\,b_{h2}\,\frac{a_{h4}}{a_{h2}}\,x_{h2} - b_{h3}\,x_{h4}\right] \tag{A.27}$$

$$\begin{aligned} \frac{\partial f_{h2}}{\partial x_{h3}} =& \frac{1}{b_{h1} - b_{h2}\,\frac{a_{h1}}{a_{h2}}}\,\left[- f_{h2}\,\left(\frac{\partial b_{h1}}{\partial x_{h3}} - \frac{a_{h2}\,\left(\frac{\partial b_{h2}}{\partial x_{h3}}\,a_{h1} + b_{h2}\,\frac{\partial a_{h1}}{\partial x_{h3}}\right) - b_{h2}\,a_{h1}\,\frac{\partial a_{h2}}{\partial x_{h3}}}{{a_{h2}}^2} \right) \right. \\ &+ \left(\frac{a_{h2}\,\left(\frac{\partial b_{h2}}{\partial x_{h3}}\,a_{h3} + b_{h2}\,\frac{\partial a_{h3}}{\partial x_{h3}}\right) - b_{h2}\,a_{h3}\,\frac{\partial a_{h2}}{\partial x_{h3}}}{{a_{h2}}^2} - \frac{\partial b_{h4}}{\partial x_{h3}} \right)\,{x_{h4}}^2 \\ &\left. - \frac{a_{h2}\,\left(\frac{\partial b_{h2}}{x_{h3}}\,a_{h4} + b_{h2}\,\frac{\partial a_{h4}}{x_{h3}}\right) - b_{h2}\,a_{h4}\,\frac{\partial a_{h2}}{\partial x_{h3}}}{{a_{h2}}^2}\,{x_{h2}}^2 - \frac{\partial b_{h3}}{\partial x_{h3}}\,x_{h2}\,x_{h4} \right] \end{aligned} \tag{A.28}$$

$$\frac{\partial f_{h2}}{\partial x_{h4}} = \frac{1}{b_{h1} - b_{h2}\,\dfrac{a_{h1}}{a_{h2}}}\,\left[2\,\left(b_{h2}\,\frac{a_{h3}}{a_{h2}} - b_{h4}\right)\,x_{h4} - b_{h3}\,x_{h2}\right] \tag{A.29}$$

$$\frac{\partial f_{h2}}{\partial u_h} = \frac{1}{b_{h1} - b_{h2}\,\dfrac{a_{h1}}{a_{h2}}} \tag{A.30}$$

For the terms associated to f_{h3}:

$$\frac{\partial f_{h3}}{\partial x_{h1}} = 0, \qquad \frac{\partial f_{h3}}{\partial x_{h2}} = 0, \qquad \frac{\partial f_{h3}}{\partial x_{h3}} = 0, \qquad \frac{\partial f_{h3}}{\partial x_{h4}} = 1, \qquad \frac{\partial f_{h3}}{\partial u_h} = 0 \tag{A.31}$$

And finally:

$$\frac{\partial f_{h4}}{\partial x_{h1}} = 0 \tag{A.32}$$

$$\frac{\partial f_{h4}}{\partial x_{h2}} = \frac{1}{a_{h2}}\,\left[2\,a_{h4}\,x_{h2} - a_{h1}\,\frac{\partial f_{h2}}{\partial x_{h2}}\right] \tag{A.33}$$

$$\frac{\partial f_{h4}}{\partial x_{h3}} = \frac{1}{a_{h2}}\,\left[-f_{h4}\,\frac{\partial a_{h2}}{\partial x_{h3}} + \frac{\partial a_{h4}}{\partial x_{h3}}\,{x_{h2}}^2 - \frac{\partial a_{h3}}{\partial x_{h3}}\,{x_{h4}}^2 - \frac{\partial a_{h1}}{\partial x_{h3}}\,f_{h2} - a_{h1}\,\frac{\partial f_{h2}}{\partial x_{h3}}\right] \tag{A.34}$$

$$\frac{\partial f_{h4}}{\partial x_{h4}} = \frac{1}{a_{h2}}\,\left[-2\,a_{h3}\,x_{h4} - a_{h1}\,\frac{\partial f_{h2}}{\partial x_{h4}}\right] \tag{A.35}$$

$$\frac{\partial f_{h4}}{\partial u_h} = -\frac{a_{h1}}{a_{h2}}\,\frac{\partial f_{h2}}{\partial u_h} \tag{A.36}$$

Where the terms associated to each of the defined auxiliary functions (i.e., a_{h3}, b_{h1}...) are given by:

$$\frac{\partial a_{h1}}{\partial x_{h3}} = \left(36\pi\,\bar{l}^2 + 24\pi\,\overline{m_E}\,\bar{l}\right)\,\cos x_{h3} \tag{A.37}$$

$$\frac{\partial a_{h2}}{\partial x_{h3}} = 12\,\bar{l}^2\,\cos x_{h3} \tag{A.38}$$

$$\frac{\partial a_{h3}}{\partial x_{h3}} = -6\,\bar{l}^2\,\sin x_{h3} \tag{A.39}$$

$$\frac{\partial a_{h4}}{\partial x_{h3}} = -4\pi^2\,\left(12\,\bar{l}^2 + 12\,\overline{m_E}\,\bar{l}\right)\,\sin x_{h3} \tag{A.40}$$

And for the derivatives of the b_{hx} terms:

$$\frac{\partial b_{h1}}{\partial x_{h3}} = \left(48\pi\,\bar{l}^2 + 48\pi\,\overline{m_E}\,\bar{l}\right)\,\cos x_{h3} \tag{A.41}$$

$$\frac{\partial b_{h2}}{\partial x_{h3}} = \left(18\,\bar{l}^2 + 12\,\overline{m_E}\,\bar{l}\right)\,\cos x_{h3} \tag{A.42}$$

$$\frac{\partial b_{h3}}{\partial x_{h3}} = -\left(48\pi\,\bar{l}^2 + 48\pi\,\overline{m_E}\,\bar{l}\right)\ \sin x_{h3} \tag{A.43}$$

$$\frac{\partial b_{h4}}{\partial x_{h3}} = -\left(18\,\bar{l}^2 + 12\overline{m_E}\,\bar{l}\right)\ \sin x_{h3} \tag{A.44}$$

A.2 Radial deployment

To finish with the so-called radial deployment strategy, the Jacobian matrices associated to this dynamical system of differential equations (Equation (4.117)) are defined as:

$$A_r\left(x_r,\, u_r,\, \tau\right) = \begin{bmatrix} \frac{\partial f_{r1}}{\partial x_{r1}} & \frac{\partial f_{r1}}{\partial x_{r2}} & \frac{\partial f_{r1}}{\partial x_{r3}} & \frac{\partial f_{r1}}{\partial x_{r4}} & \frac{\partial f_{r1}}{\partial x_{r5}} & \frac{\partial f_{r1}}{\partial x_{r6}} \\ \frac{\partial f_{r2}}{\partial x_{r1}} & \frac{\partial f_{r2}}{\partial x_{r2}} & \frac{\partial f_{r2}}{\partial x_{r3}} & \frac{\partial f_{r2}}{\partial x_{r4}} & \frac{\partial f_{r2}}{\partial x_{r5}} & \frac{\partial f_{r2}}{\partial x_{64}} \\ \frac{\partial f_{r3}}{\partial x_{r1}} & \frac{\partial f_{r3}}{\partial x_{r2}} & \frac{\partial f_{r3}}{\partial x_{r3}} & \frac{\partial f_{r3}}{\partial x_{r4}} & \frac{\partial f_{r3}}{\partial x_{r5}} & \frac{\partial f_{r3}}{\partial x_{r6}} \\ \frac{\partial f_{r4}}{\partial x_{r1}} & \frac{\partial f_{r4}}{\partial x_{r2}} & \frac{\partial f_{r4}}{\partial x_{r3}} & \frac{\partial f_{r4}}{\partial x_{r4}} & \frac{\partial f_{r4}}{\partial x_{r5}} & \frac{\partial f_{r4}}{\partial x_{r6}} \\ \frac{\partial f_{r5}}{\partial x_{r1}} & \frac{\partial f_{r5}}{\partial x_{r2}} & \frac{\partial f_{r5}}{\partial x_{r3}} & \frac{\partial f_{r5}}{\partial x_{r4}} & \frac{\partial f_{r5}}{\partial x_{r5}} & \frac{\partial f_{r5}}{\partial x_{r6}} \\ \frac{\partial f_{r6}}{\partial x_{r1}} & \frac{\partial f_{r6}}{\partial x_{r2}} & \frac{\partial f_{r6}}{\partial x_{r3}} & \frac{\partial f_{r6}}{\partial x_{r4}} & \frac{\partial f_{r6}}{\partial x_{r5}} & \frac{\partial f_{r6}}{\partial x_{r6}} \end{bmatrix} \tag{A.45}$$

And similarly, the B_r matrix is given by:

$$B_r\left(x_r,\, u_r,\, \tau\right) = \begin{bmatrix} \frac{\partial f_{r1}}{\partial u_{r1}} & \frac{\partial f_{r1}}{\partial u_{r2}} & \frac{\partial f_{r1}}{\partial u_{r3}} \\ \frac{\partial f_{r2}}{\partial u_{r1}} & \frac{\partial f_{r2}}{\partial u_{r2}} & \frac{\partial f_{r2}}{\partial u_{r3}} \\ \frac{\partial f_{r3}}{\partial u_{r1}} & \frac{\partial f_{r3}}{\partial u_{r2}} & \frac{\partial f_{r3}}{\partial u_{r3}} \\ \frac{\partial f_{r4}}{\partial u_{r1}} & \frac{\partial f_{r4}}{\partial u_{r2}} & \frac{\partial f_{r4}}{\partial u_{r3}} \\ \frac{\partial f_{r5}}{\partial u_{r1}} & \frac{\partial f_{r5}}{\partial u_{r2}} & \frac{\partial f_{r5}}{\partial u_{r3}} \\ \frac{\partial f_{r6}}{\partial u_{r1}} & \frac{\partial f_{r6}}{\partial u_{r2}} & \frac{\partial f_{r6}}{\partial u_{r3}} \end{bmatrix} \tag{A.46}$$

Hence, each of the components of (A.45) and (A.46) are defined as:

$$\frac{\partial f_{r1}}{\partial x_{r1}} = 0, \qquad \frac{\partial f_{r1}}{\partial x_{r2}} = 1, \qquad \frac{\partial f_{r1}}{\partial x_{r3}} = 0 \tag{A.47}$$

$$\frac{\partial f_{r1}}{\partial x_{r4}} = 0, \qquad \frac{\partial f_{r1}}{\partial x_{r5}} = 0, \qquad \frac{\partial f_{r1}}{\partial x_{r6}} = 0 \tag{A.48}$$

$$\frac{\partial f_{r1}}{\partial u_{r1}} = 0, \qquad \frac{\partial f_{r1}}{\partial u_{r2}} = 0, \qquad \frac{\partial f_{r1}}{\partial u_{r3}} = 0 \tag{A.49}$$

Analogously:

$$\begin{aligned}\frac{\partial f_{r2}}{\partial x_{r1}} =& \frac{1}{a_{r3}\,\frac{b_{r2}}{b_{r1}}\,\frac{c_{r2}}{c_{r1}} + a_{r2} - a_{r1}\,\frac{c_{r2}}{c_{r1}}} \left[- f_{r2}\, g_{r1} - \frac{b_{r1}\,\frac{\partial a_{r3}}{\partial x_{r1}} - a_{r3}\,\frac{\partial b_{r1}}{\partial x_{r1}}}{{b_{r1}}^2}\, u_{r2} + g_{r2}\, u_{r3}\, x_{r3} + g_{r3}\, {x_{r6}}^2 \right. \\ &+ g_{r4}\, x_{r4}\, x_{r6} - \frac{b_{r1}\left(\frac{\partial a_{r3}}{\partial x_{r1}}\, b_{r3} + a_{r3}\,\frac{\partial b_{r3}}{\partial x_{r1}}\right) - a_{r3}\, b_{r3}\,\frac{\partial b_{r1}}{\partial x_{r1}}}{{b_{r1}}^2}\, x_{r2}\, x_{r6} + g_{r5}\, x_{r2} + g_{r6}\, {x_{r4}}^2 \\ &\left. - \frac{b_{r1}\left(\frac{\partial a_{r3}}{\partial x_{r1}}\, b_{r5} + a_{r3}\,\frac{\partial b_{r5}}{\partial x_{r1}}\right) - a_{r3}\, b_{r5}\,\frac{\partial b_{r1}}{\partial x_{r1}}}{{b_{r1}}^2}\, {x_{r2}}^2 - \frac{\partial a_{r4}}{\partial x_{r1}}\, x_{r6} \right]\end{aligned} \tag{A.50}$$

Where g_{r1}, g_{r2}, g_{r3}, g_{r4}, g_{r5} and g_{r6} are auxiliary functions defined as:

$$\begin{aligned}g_{r1} =& \frac{b_{r1}\, c_{r1}\left(\frac{\partial a_{r3}}{\partial x_{r1}}\, b_{r2}\, c_{r2} + a_{r3}\,\frac{\partial b_{r2}}{\partial x_{r1}}\, c_{r2} + a_{r3}\, b_{r2}\,\frac{\partial c_{r2}}{\partial x_{r1}}\right) - a_{r3}\, b_{r2}\, c_{r2}\left(\frac{\partial b_{r1}}{\partial x_{r1}}\, c_{r1} + b_{r1}\,\frac{\partial c_{r1}}{\partial x_{r1}}\right)}{\left(b_{r1}\, c_{r1}\right)^2} \\ &+ \frac{\partial a_{r2}}{\partial x_{r1}} - \frac{c_{r1}\left(\frac{\partial a_{r1}}{\partial x_{r1}}\, c_{r2} + a_{r1}\,\frac{\partial c_{r2}}{\partial x_{r1}}\right) - a_{r1}\, c_{r2}\,\frac{\partial c_{r1}}{\partial x_{r1}}}{{c_{r1}}^2}\end{aligned} \tag{A.51}$$

$$g_{r2} = \frac{b_{r1}\, c_{r1}\left(\frac{\partial a_{r3}}{\partial x_{r1}}\, b_{r2} + a_{r3}\,\frac{\partial b_{r2}}{\partial x_{r1}}\right) - a_{r3}\, b_{r2}\left(\frac{\partial b_{r1}}{\partial x_{r1}}\, c_{r1} + b_{r1}\,\frac{\partial c_{r1}}{\partial x_{r1}}\right)}{\left(b_{r1}\, c_{r1}\right)^2} - \frac{c_{r1}\,\frac{\partial a_{r1}}{\partial x_{r1}} - a_{r1}\,\frac{\partial c_{r1}}{\partial x_{r1}}}{{c_{r1}}^2} \tag{A.52}$$

$$\begin{aligned}g_{r3} =& \frac{c_{r1}\left(\frac{\partial a_{r1}}{\partial x_{r1}}\, c_{r3} + a_{r1}\,\frac{\partial c_{r3}}{\partial x_{r1}}\right) - a_{r1}\, c_{r3}\,\frac{\partial c_{r1}}{\partial x_{r1}}}{{c_{r1}}^2} - \frac{b_{r1}\left(\frac{\partial a_{r3}}{\partial x_{r1}}\, b_{r4} + a_{r3}\,\frac{\partial b_{r4}}{\partial x_{r1}}\right) - a_{r3}\, b_{r4}\,\frac{\partial b_{r1}}{\partial x_{r1}}}{{b_{r1}}^2} \\ &- \frac{b_{r1}\, c_{r1}\left(\frac{\partial a_{r3}}{\partial x_{r1}}\, b_{r2}\, c_{r3} + a_{r3}\,\frac{\partial b_{r2}}{\partial x_{r1}}\, c_{r3} + a_{r3}\, b_{r2}\,\frac{\partial c_{r3}}{\partial x_{r1}}\right) - a_{r3}\, b_{r2}\, c_{r3}\left(\frac{\partial b_{r1}}{\partial x_{r1}}\, c_{r1} + b_{r1}\,\frac{\partial c_{r1}}{\partial x_{r1}}\right)}{\left(b_{r1}\, c_{r1}\right)^2}\end{aligned} \tag{A.53}$$

$$\begin{aligned}g_{r4} =& - \frac{b_{r1}\, c_{r1}\left(\frac{\partial a_{r3}}{\partial x_{r1}}\, b_{r2}\, c_{r4} + a_{r3}\,\frac{\partial b_{r2}}{\partial x_{r1}}\, c_{r4} + a_{r3}\, b_{r2}\,\frac{\partial c_{r4}}{\partial x_{r1}}\right) - a_{r3}\, b_{r2}\, c_{r4}\left(\frac{\partial b_{r1}}{\partial x_{r1}}\, c_{r1} + b_{r1}\,\frac{\partial c_{r1}}{\partial x_{r1}}\right)}{\left(b_{r1}\, c_{r1}\right)^2} \\ &+ \frac{c_{r1}\left(\frac{\partial a_{r1}}{\partial x_{r1}}\, c_{r4} + a_{r1}\,\frac{\partial c_{r4}}{\partial x_{r1}}\right) - a_{r1}\, c_{r4}\,\frac{\partial c_{r1}}{\partial x_{r1}}}{{c_{r1}}^2}\end{aligned} \tag{A.54}$$

$$\begin{aligned}g_{r5} =& - \frac{b_{r1}\, c_{r1}\left(\frac{\partial a_{r3}}{\partial x_{r1}}\, b_{r2}\, c_{r5} + a_{r3}\,\frac{\partial b_{r2}}{\partial x_{r1}}\, c_{r5} + a_{r3}\, b_{r2}\,\frac{\partial c_{r5}}{\partial x_{r1}}\right) - a_{r3}\, b_{r2}\, c_{r5}\left(\frac{\partial b_{r1}}{\partial x_{r1}}\, c_{r1} + b_{r1}\,\frac{\partial c_{r1}}{\partial x_{r1}}\right)}{\left(b_{r1}\, c_{r1}\right)^2} \\ &+ \frac{c_{r1}\left(\frac{\partial a_{r1}}{\partial x_{r1}}\, c_{r5} + a_{r1}\,\frac{\partial c_{r5}}{\partial x_{r1}}\right) - a_{r1}\, c_{r5}\,\frac{\partial c_{r1}}{\partial x_{r1}}}{{c_{r1}}^2} - \frac{\partial a_{r5}}{\partial x_{r1}}\end{aligned} \tag{A.55}$$

$$g_{r6} = \frac{b_{r1}\,\dfrac{\partial a_{r3}}{\partial x_{r1}} - a_{r3}\,\dfrac{\partial b_{r1}}{\partial x_{r1}}}{{b_{r1}}^2} - \frac{\partial a_{r6}}{\partial x_{r1}} \tag{A.56}$$

Following with the derivatives associated to f_{r2}:

$$\begin{aligned}\frac{\partial f_{r2}}{\partial x_{r2}} =& \frac{1}{a_{r3}\,\dfrac{b_{r2}}{b_{r1}}\,\dfrac{c_{r2}}{c_{r1}} + a_{r2} - a_{r1}\,\dfrac{c_{r2}}{c_{r1}}}\left[\left(a_{r1}\,\frac{c_{r5}}{c_{r1}} - a_{r5} - a_{r3}\,\frac{b_{r2}}{b_{r1}}\,\frac{c_{r5}}{c_{r1}}\right) - a_{r3}\,\frac{b_{r3}}{b_{r1}}\,x_{r6} - \frac{\partial a_{r4}}{\partial x_{r2}}\,x_{r6}\right.\\ &\left. + \left(\frac{a_{r1}}{c_{r1}}\,\frac{\partial c_{r5}}{\partial x_{r2}} - \frac{\partial a_{r5}}{\partial x_{r2}} - \frac{a_{r3}}{c_{r1}}\,\frac{b_{r2}}{b_{r1}}\,\frac{\partial c_{r5}}{\partial x_{r2}}\right)x_{r2} - 2\,a_{r3}\,\frac{b_{r5}}{b_{r1}}\,x_{r2}\right]\end{aligned} \tag{A.57}$$

$$\begin{aligned}\frac{\partial f_{r2}}{\partial x_{r3}} =& \frac{1}{a_{r3}\,\dfrac{b_{r2}}{b_{r1}}\,\dfrac{c_{r2}}{c_{r1}} + a_{r2} - a_{r1}\,\dfrac{c_{r2}}{c_{r1}}}\left[-f_{r2}\,g_{r7} - \frac{b_{r1}\,\dfrac{\partial a_{r3}}{\partial x_{r3}} - a_{r3}\,\dfrac{\partial b_{r1}}{\partial x_{r3}}}{{b_{r1}}^2}\,u_{r2}\right.\\ &+ \left(a_{r3}\,\frac{b_{r2}}{b_{r1}\,c_{r1}} - \frac{a_{r1}}{c_{r1}}\right)u_{r3} + g_{r8}\,u_{r3}\,x_{r3} + g_{r9}\,{x_{r6}}^2 + g_{r10}\,x_{r4}\,x_{r6}\\ &- \frac{b_{r1}\left(\dfrac{\partial a_{r3}}{\partial x_{r3}}\,b_{r3} + a_{r3}\,\dfrac{\partial b_{r3}}{\partial x_{r3}}\right) - a_{r3}\,b_{r3}\,\dfrac{\partial b_{r1}}{\partial x_{r3}}}{{b_{r1}}^2}\,x_{r2}\,x_{r6} + g_{r11}\,x_{r2} + g_{r12}\,{x_{r4}}^2\\ &\left.- \frac{b_{r1}\left(\dfrac{\partial a_{r3}}{\partial x_{r3}}\,b_{r5} + a_{r3}\,\dfrac{\partial b_{r5}}{\partial x_{r3}}\right) - a_{r3}\,b_{r5}\,\dfrac{\partial b_{r1}}{\partial x_{r3}}}{{b_{r1}}^2}\,{x_{r2}}^2 - \frac{\partial a_{r4}}{\partial x_{r3}}\,x_{r6}\right]\end{aligned} \tag{A.58}$$

Again, g_{r7}, g_{r8}, g_{r9}, g_{r10}, g_{r11} and g_{r12} represent auxiliary functions given by:

$$\begin{aligned}g_{r7} =& \frac{b_{r1}\,c_{r1}\left(\dfrac{\partial a_{r3}}{\partial x_{r3}}\,b_{r2}\,c_{r2} + a_{r3}\,\dfrac{\partial b_{r2}}{\partial x_{r3}}\,c_{r2} + a_{r3}\,b_{r2}\,\dfrac{\partial c_{r2}}{\partial x_{r3}}\right) - a_{r3}\,b_{r2}\,c_{r2}\left(\dfrac{\partial b_{r1}}{\partial x_{r3}}\,c_{r1} + b_{r1}\,\dfrac{\partial c_{r1}}{\partial x_{r3}}\right)}{\left(b_{r1}\,c_{r1}\right)^2}\\ &+ \frac{\partial a_{r2}}{\partial x_{r3}} - \frac{c_{r1}\left(\dfrac{\partial a_{r1}}{\partial x_{r3}}\,c_{r2} + a_{r1}\,\dfrac{\partial c_{r2}}{\partial x_{r3}}\right) - a_{r1}\,c_{r2}\,\dfrac{\partial c_{r1}}{\partial x_{r3}}}{{c_{r1}}^2}\end{aligned} \tag{A.59}$$

$$g_{r8} = \frac{b_{r1}\,c_{r1}\left(\dfrac{\partial a_{r3}}{\partial x_{r3}}\,b_{r2} + a_{r3}\,\dfrac{\partial b_{r2}}{\partial x_{r3}}\right) - a_{r3}\,b_{r2}\left(\dfrac{\partial b_{r1}}{\partial x_{r3}}\,c_{r1} + b_{r1}\,\dfrac{\partial c_{r1}}{\partial x_{r3}}\right)}{\left(b_{r1}\,c_{r1}\right)^2} - \frac{c_{r1}\,\dfrac{\partial a_{r1}}{\partial x_{r3}} - a_{r1}\,\dfrac{\partial c_{r1}}{\partial x_{r3}}}{{c_{r1}}^2} \tag{A.60}$$

$$\begin{aligned}g_{r9} =& -\frac{b_{r1}\,c_{r1}\left(\dfrac{\partial a_{r3}}{\partial x_{r3}}\,b_{r2}\,c_{r3} + a_{r3}\,\dfrac{\partial b_{r2}}{\partial x_{r3}}\,c_{r3} + a_{r3}\,b_{r2}\,\dfrac{\partial c_{r3}}{\partial x_{r3}}\right) - a_{r3}\,b_{r2}\,c_{r3}\left(\dfrac{\partial b_{r1}}{\partial x_{r3}}\,c_{r1} + b_{r1}\,\dfrac{\partial c_{r1}}{\partial x_{r3}}\right)}{\left(b_{r1}\,c_{r1}\right)^2}\\ &+ \frac{c_{r1}\left(\dfrac{\partial a_{r1}}{\partial x_{r3}}\,c_{r3} + a_{r1}\,\dfrac{\partial c_{r3}}{\partial x_{r3}}\right) - a_{r1}\,c_{r3}\,\dfrac{\partial c_{r1}}{\partial x_{r3}}}{{c_{r1}}^2} - \frac{b_{r1}\left(\dfrac{\partial a_{r3}}{\partial x_{r3}}\,b_{r4} + a_{r3}\,\dfrac{\partial b_{r4}}{\partial x_{r3}}\right) - a_{r3}\,b_{r4}\,\dfrac{\partial b_{r1}}{\partial x_{r3}}}{{b_{r1}}^2}\end{aligned} \tag{A.61}$$

$$g_{r10} = -\frac{b_{r1}\, c_{r1} \left(\frac{\partial a_{r3}}{\partial x_{r3}}\, b_{r2}\, c_{r4} + a_{r3}\, \frac{\partial b_{r2}}{\partial x_{r3}}\, c_{r4} + a_{r3}\, b_{r2}\, \frac{\partial c_{r4}}{\partial x_{r3}}\right) - a_{r3}\, b_{r2}\, c_{r4} \left(\frac{\partial b_{r1}}{\partial x_{r3}}\, c_{r1} + b_{r1}\, \frac{\partial c_{r1}}{\partial x_{r3}}\right)}{\left(b_{r1}\, c_{r1}\right)^2} + \frac{c_{r1} \left(\frac{\partial a_{r1}}{\partial x_{r3}}\, c_{r4} + a_{r1}\, \frac{\partial c_{r4}}{\partial x_{r3}}\right) - a_{r1}\, c_{r4}\, \frac{\partial c_{r1}}{\partial x_{r3}}}{{c_{r1}}^2} \tag{A.62}$$

$$g_{r11} = -\frac{b_{r1}\, c_{r1} \left(\frac{\partial a_{r3}}{\partial x_{r3}}\, b_{r2}\, c_{r5} + a_{r3}\, \frac{\partial b_{r2}}{\partial x_{r3}}\, c_{r5} + a_{r3}\, b_{r2}\, \frac{\partial c_{r5}}{\partial x_{r3}}\right) - a_{r3}\, b_{r2}\, c_{r5} \left(\frac{\partial b_{r1}}{\partial x_{r3}}\, c_{r1} + b_{r1}\, \frac{\partial c_{r1}}{\partial x_{r3}}\right)}{\left(b_{r1}\, c_{r1}\right)^2} + \frac{c_{r1} \left(\frac{\partial a_{r1}}{\partial x_{r3}}\, c_{r5} + a_{r1}\, \frac{\partial c_{r5}}{\partial x_{r3}}\right) - a_{r1}\, c_{r5}\, \frac{\partial c_{r1}}{\partial x_{r3}}}{{c_{r1}}^2} - \frac{\partial a_{r5}}{\partial x_{r3}} \tag{A.63}$$

$$g_{r12} = \frac{b_{r1}\, \frac{\partial a_{r3}}{\partial x_{r3}} - a_{r3}\, \frac{\partial b_{r1}}{\partial x_{r3}}}{{b_{r1}}^2} - \frac{\partial a_{r6}}{\partial x_{r3}} \tag{A.64}$$

Continuing with the f_{r2} derivatives:

$$\frac{\partial f_{r2}}{\partial x_{r4}} = \frac{1}{a_{r3}\, \frac{b_{r2}}{b_{r1}}\, \frac{c_{r2}}{c_{r1}} + a_{r2} - a_{r1}\, \frac{c_{r2}}{c_{r1}}} \left[\left(a_{r1}\, \frac{c_{r4}}{c_{r1}} - a_{r3}\, \frac{b_{r2}}{b_{r1}}\, \frac{c_{r4}}{c_{r1}}\right) x_{r6} + \left(\frac{a_{r1}}{c_{r1}}\, \frac{\partial c_{r5}}{\partial x_{r4}} - \frac{\partial a_{r5}}{\partial x_{r4}} - \frac{a_{r3}}{c_{r1}}\, \frac{b_{r2}}{b_{r1}}\, \frac{\partial c_{r5}}{\partial x_{r4}}\right) x_{r2} + 2 \left(\frac{a_{r3}}{b_{r1}} - a_{r6}\right) x_{r4} - \frac{\partial a_{r4}}{\partial x_{r4}}\, x_{r6}\right] \tag{A.65}$$

$$\frac{\partial f_{r2}}{\partial x_{r5}} = 0 \tag{A.66}$$

$$\frac{\partial f_{r2}}{\partial x_{r6}} = \frac{1}{a_{r3}\, \frac{b_{r2}}{b_{r1}}\, \frac{c_{r2}}{c_{r1}} + a_{r2} - a_{r1}\, \frac{c_{r2}}{c_{r1}}} \left[2 \left(a_{r1}\, \frac{c_{r3}}{c_{r1}} - a_{r3}\, \frac{b_{r2}}{b_{r1}}\, \frac{c_{r3}}{c_{r1}} - a_{r3}\, \frac{b_{r4}}{b_{r1}}\right) x_{r6} + \left(a_{r1}\, \frac{c_{r4}}{c_{r1}} - a_{r3}\, \frac{b_{r2}}{b_{r1}}\, \frac{c_{r4}}{c_{r1}}\right) x_{r4} - a_{r3}\, \frac{b_{r3}}{b_{r1}}\, x_{r2} - a_{r4}\right] \tag{A.67}$$

$$\frac{\partial f_{r2}}{\partial u_{r1}} = \frac{1}{a_{r3}\, \frac{b_{r2}}{b_{r1}}\, \frac{c_{r2}}{c_{r1}} + a_{r2} - a_{r1}\, \frac{c_{r2}}{c_{r1}}} \tag{A.68}$$

$$\frac{\partial f_{r2}}{\partial u_{r2}} = \frac{-a_{r3} \,/\, b_{r1}}{a_{r3}\, \frac{b_{r2}}{b_{r1}}\, \frac{c_{r2}}{c_{r1}} + a_{r2} - a_{r1}\, \frac{c_{r2}}{c_{r1}}} \tag{A.69}$$

$$\frac{\partial f_{r2}}{\partial u_{r3}} = \frac{\left(a_{r3} \, \dfrac{b_{r2}}{b_{r1} \, c_{r1}} - \dfrac{a_{r1}}{c_{r1}} \right) x_{r3}}{a_{r3} \, \dfrac{b_{r2}}{b_{r1}} \, \dfrac{c_{r2}}{c_{r1}} + a_{r2} - a_{r1} \, \dfrac{c_{r2}}{c_{r1}}} \tag{A.70}$$

Similarly, for the f_{r3} derivatives:

$$\frac{\partial f_{r3}}{\partial x_{r1}} = 0, \qquad \frac{\partial f_{r3}}{\partial x_{r2}} = 0, \qquad \frac{\partial f_{r3}}{\partial x_{r3}} = 0 \tag{A.71}$$

$$\frac{\partial f_{r3}}{\partial x_{r4}} = 1, \qquad \frac{\partial f_{r3}}{\partial x_{r5}} = 0, \qquad \frac{\partial f_{r3}}{\partial x_{r6}} = 0 \tag{A.72}$$

$$\frac{\partial f_{r3}}{\partial u_{r1}} = 0, \qquad \frac{\partial f_{r3}}{\partial u_{r2}} = 0, \qquad \frac{\partial f_{r3}}{\partial u_{r3}} = 0 \tag{A.73}$$

Analogously:

$$\begin{aligned} \frac{\partial f_{r4}}{\partial x_{r1}} = & \frac{1}{b_{r1}} \left[- f_{r4} \, \frac{\partial b_{r1}}{\partial x_{r1}} - \frac{c_{r1} \, \dfrac{\partial b_{r2}}{\partial x_{r1}} - b_{r2} \, \dfrac{\partial c_{r1}}{\partial x_{r1}}}{{c_{r1}}^2} \, u_{r3} \, x_{r3} + b_{r2} \, \frac{c_{r2}}{c_{r1}} \, \frac{\partial f_{r2}}{\partial x_{r1}} \right. \\ & + \frac{c_{r1} \left(\dfrac{\partial b_{r2}}{\partial x_{r1}} \, c_{r2} + b_{r2} \, \dfrac{\partial c_{r2}}{\partial x_{r1}} \right) - b_{r2} \, c_{r2} \, \dfrac{\partial c_{r1}}{\partial x_{r1}}}{{c_{r1}}^2} \, f_{r2} + g_{r13} \, {x_{r6}}^2 \\ & + \frac{c_{r1} \left(\dfrac{\partial b_{r2}}{\partial x_{r1}} \, c_{r4} + b_{r2} \, \dfrac{\partial c_{r4}}{\partial x_{r1}} \right) - b_{r2} \, c_{r4} \, \dfrac{\partial c_{r1}}{\partial x_{r1}}}{{c_{r1}}^2} \, x_{r4} \, x_{r6} + \frac{\partial b_{r5}}{\partial x_{r1}} \, {x_{r2}}^2 \\ & \left. + \frac{c_{r1} \left(\dfrac{\partial b_{r2}}{\partial x_{r1}} \, c_{r5} + b_{r2} \, \dfrac{\partial c_{r5}}{\partial x_{r1}} \right) - b_{r2} \, c_{r5} \, \dfrac{\partial c_{r1}}{\partial x_{r1}}}{{c_{r1}}^2} \, x_{r2} + \frac{\partial b_{r3}}{\partial x_{r1}} \, x_{r2} \, x_{r6} \right] \end{aligned} \tag{A.74}$$

Where g_{r13} represents another auxiliary function defined for the sake of simplifying (A.74):

$$g_{r13} = \frac{c_{r1} \left(\dfrac{\partial b_{r2}}{\partial x_{r1}} \, c_{r3} + b_{r2} \, \dfrac{\partial c_{r3}}{\partial x_{r1}} \right) - b_{r2} \, c_{r3} \, \dfrac{\partial c_{r1}}{\partial x_{r1}}}{{c_{r1}}^2} + \frac{\partial b_{r4}}{\partial x_{r1}} \tag{A.75}$$

Thus:

$$\frac{\partial f_{r4}}{\partial x_{r2}} = \frac{1}{b_{r1}} \left[b_{r2} \, \frac{c_{r2}}{c_{r1}} \, \frac{\partial f_{r2}}{\partial x_{r2}} + b_{r2} \, \frac{c_{r5}}{c_{r1}} + \frac{b_{r2}}{c_{r1}} \, \frac{\partial c_{r5}}{\partial x_{r2}} \, x_{r2} + 2 \, b_{r5} \, x_{r2} + b_{r3} \, x_{r6} \right] \tag{A.76}$$

$$\begin{aligned}\frac{\partial f_{r4}}{\partial x_{r3}} = & \frac{1}{b_{r1}} \left[-f_{r4} \frac{\partial b_{r1}}{\partial x_{r3}} - \frac{c_{r1} \frac{\partial b_{r2}}{\partial x_{r3}} - b_{r2} \frac{\partial c_{r1}}{\partial x_{r3}}}{{c_{r1}}^2} u_{r3}\, x_{r3} - \frac{b_{r2}}{c_{r1}} u_{r3} + b_{r2} \frac{c_{r2}}{c_{r1}} \frac{\partial f_{r2}}{\partial x_{r3}} \right. \\ & + \frac{c_{r1} \left(\frac{\partial b_{r2}}{\partial x_{r3}} c_{r2} + b_{r2} \frac{\partial c_{r2}}{\partial x_{r3}} \right) - b_{r2}\, c_{r2} \frac{\partial c_{r1}}{\partial x_{r3}}}{{c_{r1}}^2} f_{r2} + g_{r14}\, {x_{r6}}^2 \\ & + \frac{c_{r1} \left(\frac{\partial b_{r2}}{\partial x_{r3}} c_{r4} + b_{r2} \frac{\partial c_{r4}}{\partial x_{r3}} \right) - b_{r2}\, c_{r4} \frac{\partial c_{r1}}{\partial x_{r3}}}{{c_{r1}}^2} x_{r4}\, x_{r6} + \frac{\partial b_{r5}}{\partial x_{r3}} {x_{r2}}^2 \\ & \left. + \frac{c_{r1} \left(\frac{\partial b_{r2}}{\partial x_{r3}} c_{r5} + b_{r2} \frac{\partial c_{r5}}{\partial x_{r3}} \right) - b_{r2}\, c_{r5} \frac{\partial c_{r1}}{\partial x_{r3}}}{{c_{r1}}^2} x_{r2} + \frac{\partial b_{r3}}{\partial x_{r3}} x_{r2}\, x_{r6} \right] \end{aligned} \tag{A.77}$$

Where g_{r14} represents again another auxiliary function given by:

$$g_{r14} = \frac{c_{r1} \left(\frac{\partial b_{r2}}{\partial x_{r3}} c_{r3} + b_{r2} \frac{\partial c_{r3}}{\partial x_{r3}} \right) - b_{r2}\, c_{r3} \frac{\partial c_{r1}}{\partial x_{r3}}}{{c_{r1}}^2} + \frac{\partial b_{r4}}{\partial x_{r3}} \tag{A.78}$$

To finish with the f_{r4} derivatives:

$$\frac{\partial f_{r4}}{\partial x_{r4}} = \frac{1}{b_{r1}} \left[b_{r2} \frac{c_{r2}}{c_{r1}} \frac{\partial f_{r2}}{\partial x_{r4}} + b_{r2} \frac{c_{r4}}{c_{r1}} x_{r6} - 2\, x_{r4} + \frac{b_{r2}}{c_{r1}} \frac{\partial c_{r5}}{\partial x_{r4}} x_{r2} \right] \tag{A.79}$$

$$\frac{\partial f_{r4}}{\partial x_{r5}} = 0 \tag{A.80}$$

$$\frac{\partial f_{r4}}{\partial x_{r6}} = \frac{1}{b_{r1}} \left[b_{r2} \frac{c_{r2}}{c_{r1}} \frac{\partial f_{r2}}{\partial x_{r6}} + 2 \left(b_{r2} \frac{c_{r3}}{c_{r1}} + b_{r4} \right) x_{r6} + b_{r2} \frac{c_{r4}}{c_{r1}} x_{r4} + b_{r3}\, x_{r2} \right] \tag{A.81}$$

$$\frac{\partial f_{r4}}{\partial u_{r1}} = \frac{1}{b_{r1}} \left[b_{r2} \frac{c_{r2}}{c_{r1}} \frac{\partial f_{r2}}{\partial u_{r1}} \right] \tag{A.82}$$

$$\frac{\partial f_{r4}}{\partial u_{r2}} = \frac{1}{b_{r1}} \left[1 + b_{r2} \frac{c_{r2}}{c_{r1}} \frac{\partial f_{r2}}{\partial u_{r2}} \right] \tag{A.83}$$

$$\frac{\partial f_{r4}}{\partial u_{r3}} = \frac{1}{b_{r1}} \left[-\frac{b_{r2}}{c_{r1}} x_{r3} + b_{r2} \frac{c_{r2}}{c_{r1}} \frac{\partial f_{r2}}{\partial u_{r3}} \right] \tag{A.84}$$

Following with the terms associated to f_{r5}:

$$\frac{\partial f_{r5}}{\partial x_{r1}} = 0, \qquad \frac{\partial f_{r5}}{\partial x_{r2}} = 0, \qquad \frac{\partial f_{r5}}{\partial x_{r3}} = 0 \tag{A.85}$$

$$\frac{\partial f_{r5}}{\partial x_{r4}} = 0, \qquad \frac{\partial f_{r5}}{\partial x_{r5}} = 0, \qquad \frac{\partial f_{r5}}{\partial x_{r6}} = 1 \tag{A.86}$$

$$\frac{\partial f_{r5}}{\partial u_{r1}} = 0, \qquad \frac{\partial f_{r5}}{\partial u_{r2}} = 0, \qquad \frac{\partial f_{r5}}{\partial u_{r3}} = 0 \tag{A.87}$$

And finally, for f_{r6}:

$$\frac{\partial f_{r6}}{\partial x_{r1}} = \frac{1}{c_{r1}} \left[-f_{r6} \frac{\partial c_{r1}}{\partial x_{r1}} - f_{r2} \frac{\partial c_{r2}}{\partial x_{r1}} - c_{r2} \frac{\partial f_{r2}}{\partial x_{r1}} - \frac{\partial c_{r3}}{\partial x_{r1}} {x_{r6}}^2 - \frac{\partial c_{r4}}{\partial x_{r1}} x_{r4} x_{r6} - \frac{\partial c_{r5}}{\partial x_{r1}} x_{r2} \right] \tag{A.88}$$

$$\frac{\partial f_{r6}}{\partial x_{r2}} = \frac{1}{c_{r1}} \left[-c_{r2} \frac{\partial f_{r2}}{\partial x_{r2}} - \frac{\partial c_{r5}}{\partial x_{r2}} x_{r2} - c_{r5} \right] \tag{A.89}$$

$$\frac{\partial f_{r6}}{\partial x_{r3}} = \frac{1}{c_{r1}} \left[-f_{r6} \frac{\partial c_{r1}}{\partial x_{r3}} + u_{r3} - \frac{\partial c_{r2}}{\partial x_{r3}} f_{r2} - c_{r2} \frac{\partial f_{r2}}{\partial x_{r3}} - \frac{\partial c_{r3}}{\partial x_{r3}} {x_{r6}}^2 - \frac{\partial c_{r4}}{\partial x_{r3}} x_{r4} x_{r6} - \frac{\partial c_{r5}}{\partial x_{r3}} x_{r2} \right] \tag{A.90}$$

$$\frac{\partial f_{r6}}{\partial x_{r4}} = \frac{1}{c_{r1}} \left[-c_{r2} \frac{\partial f_{r2}}{\partial x_{r4}} - c_{r4} x_{r6} - \frac{\partial c_{r5}}{\partial x_{r4}} x_{r2} \right] \tag{A.91}$$

$$\frac{\partial f_{r6}}{\partial x_{r5}} = 0 \tag{A.92}$$

$$\frac{\partial f_{r6}}{\partial x_{r6}} = \frac{1}{c_{r1}} \left[-c_{r2} \frac{\partial f_{r2}}{\partial x_{r6}} - 2\, c_{r3}\, x_{r6} - c_{r4}\, x_{r4} \right] \tag{A.93}$$

$$\frac{\partial f_{r6}}{\partial u_{r1}} = -\frac{c_{r2}}{c_{r1}} \frac{\partial f_{r2}}{\partial u_{r1}} \tag{A.94}$$

$$\frac{\partial f_{r6}}{\partial u_{r2}} = -\frac{c_{r2}}{c_{r1}} \frac{\partial f_{r2}}{\partial u_{r2}} \tag{A.95}$$

$$\frac{\partial f_{r6}}{\partial u_{r3}} = \frac{x_{r3}}{c_{r1}} - \frac{c_{r2}}{c_{r1}} \frac{\partial f_{r2}}{\partial u_{r3}} \tag{A.96}$$

Where the terms associated to each of the defined auxiliary functions (i.e., a_{r1}, b_{r2}, c_{r4}...) are defined as:

$$\frac{\partial a_{r1}}{\partial x_{r1}} = -48\pi\, {x_{r3}}^2\, \sin x_{r1} - 48\pi\, \overline{m_E}\, x_{r3}\, \sin x_{r1} \tag{A.97}$$

$$\frac{\partial a_{r1}}{\partial x_{r3}} = 42\pi\, {x_{r3}}^2 + 24\pi + 96\pi\, x_{r3}\, \cos x_{r1} + 24\pi\, \overline{m_E}\, (2\, x_{r3} + 2\, \cos x_{r1}) \tag{A.98}$$

$$\frac{\partial a_{r2}}{\partial x_{r1}} = -18\, {x_{r3}}^2 \sin x_{r1} - 12\, \overline{m_E}\, x_{r3} \sin x_{r1} \tag{A.99}$$

$$\frac{\partial a_{r2}}{\partial x_{r3}} = 21\, {x_{r3}}^2 + 12 + 36\, x_{r3} \cos x_{r1} + 12\, \overline{m_E}\, (2\, x_{r3} + \cos x_{r1}) \tag{A.100}$$

$$\frac{\partial a_{r3}}{\partial x_{r1}} = (12\ \overline{m_E} + 6x_{r3})\ \cos x_{r1} \tag{A.101}$$

$$\frac{\partial a_{r3}}{\partial x_{r3}} = 6\ \sin x_{r1} \tag{A.102}$$

$$\frac{\partial a_{r4}}{\partial x_{r1}} = -96\pi\ x_{r3}\ x_{r4} \sin x_{r1} - 48\pi\ {x_{r3}}^2\ x_{r2} \cos x_{r1} + 48\pi\ \overline{m_E}\ (-x_{r4}\ \sin x_{r1} - x_{r3}\ x_{r2}\ \cos x_{r1}) \tag{A.103}$$

$$\frac{\partial a_{r4}}{\partial x_{r2}} = -48\pi\ {x_{r3}}^2\ \sin x_{r1} - 48\pi\ \overline{m_E}\ x_{r3}\ \sin x_{r1} \tag{A.104}$$

$$\frac{\partial a_{r4}}{\partial x_{r3}} = 96\pi\ x_{r4}\ \cos x_{r1} + 84\pi\ x_{r3}\ x_{r4} - 96\pi\ x_{r3}\ x_{r2}\ \sin x_{r1} + 48\pi\ \overline{m_E}\ (x_{r4} - x_{r2}\ \sin x_{r1}) \tag{A.105}$$

$$\frac{\partial a_{r4}}{\partial x_{r4}} = 24\pi + 96\pi\ x_{r3}\ \cos x_{r1} + 42\pi\ {x_{r3}}^2 + 48\pi\ \overline{m_E}\ (x_{r3} + \cos x_{r1}) \tag{A.106}$$

$$\frac{\partial a_{r5}}{\partial x_{r1}} = -18\ {x_{r3}}^2\ x_{r2}\ \cos x_{r1} + 12\ \overline{m_E}\ (-2\ x_{r4}\ \sin x_{r1} - x_{r3}\ x_{r2}\ \cos x_{r1}) - 42\ x_{r3}\ x_{r4}\ \sin x_{r1} \tag{A.107}$$

$$\frac{\partial a_{r5}}{\partial x_{r2}} = -18\ {x_{r3}}^2\ \sin x_{r1} - 12\ \overline{m_E}\ x_{r3}\ \sin x_{r1} \tag{A.108}$$

$$\frac{\partial a_{r5}}{\partial x_{r3}} = 42\ x_{r3}\ x_{r4} - 36\ x_{r3}\ x_{r2}\ \sin x_{r1} + 12\ \overline{m_E}\ (2\ x_{r4} - x_{r2}\ \sin x_{r1}) + 42\ x_{r4}\ \cos x_{r1} \tag{A.109}$$

$$\frac{\partial a_{r5}}{\partial x_{r4}} = 12 + 21\ {x_{r3}}^2 + 12\ \overline{m_E}\ (2\ x_{r3} + 2\ \cos x_{r1}) + 42\ x_{r3}\ \cos x_{r1} \tag{A.110}$$

$$\frac{\partial a_{r6}}{\partial x_{r1}} = 6\ \cos x_{r1} \tag{A.111}$$

Whereas the derivatives of the b_{rx} terms:

$$\frac{\partial b_{r1}}{\partial x_{r3}} = 2 \tag{A.112}$$

$$\frac{\partial b_{r2}}{\partial x_{r1}} = 8\pi\ (x_{r3} + 2\ \overline{m_E})\ \cos x_{r1} \tag{A.113}$$

$$\frac{\partial b_{r2}}{\partial x_{r3}} = 8\pi\ \sin x_{r1} \tag{A.114}$$

$$\frac{\partial b_{r3}}{\partial x_{r1}} = -40\pi\ x_{r3}\ \sin x_{r1} \tag{A.115}$$

$$\frac{\partial b_{r3}}{\partial x_{r3}} = 40\pi\ \cos x_{r1} + 56\pi\ x_{r3} + 32\pi\ \overline{m_E} \tag{A.116}$$

$$\frac{\partial b_{r4}}{\partial x_{r1}} = -64\pi^2\ x_{r3}\ \sin x_{r1} - 32\pi^2\ \overline{m_E}\ \sin x_{r1} \tag{A.117}$$

$$\frac{\partial b_{r4}}{\partial x_{r3}} = 64\pi^2\ \cos x_{r1} + 56\pi^2\ x_{r3} + 32\pi^2\ \overline{m_E} \tag{A.118}$$

$$\frac{\partial b_{r5}}{\partial x_{r1}} = -8\ x_{r3}\ \sin x_{r1} \tag{A.119}$$

$$\frac{\partial b_{r5}}{\partial x_{r3}} = 8\ \cos x_{r1} + 14\ x_{r3} + 8\ \overline{m_E} \tag{A.120}$$

And finally, for the terms associated to c_{rx}:

$$\frac{\partial c_{r1}}{\partial x_{r1}} = -36\pi\ {x_{r3}}^2\ \sin x_{r1} - 24\pi\ \overline{m_E}\ x_{r3}\ \sin x_{r1} \tag{A.121}$$

$$\frac{\partial c_{r1}}{\partial x_{r3}} = 42\pi\ {x_{r3}}^2 + 72\pi\ x_{r3}\ \cos x_{r1} + 24\pi + 24\pi\ \overline{m_E}\ (2\ x_{r3} + \cos x_{r1}) \tag{A.122}$$

$$\frac{\partial c_{r2}}{\partial x_{r1}} = -12\ {x_{r3}}^2\ \sin x_{r1} \tag{A.123}$$

$$\frac{\partial c_{r2}}{\partial x_{r3}} = 21\ {x_{r3}}^2 + 24\ x_{r3}\ \cos x_{r1} + 12 + 24\ \overline{m_E}\ x_{r3} \tag{A.124}$$

$$\frac{\partial c_{r3}}{\partial x_{r1}} = 48\pi^2\ \left({x_{r3}}^2 + \overline{m_E}\ x_{r3}\right)\ \cos x_{r1} \tag{A.125}$$

$$\frac{\partial c_{r3}}{\partial x_{r3}} = \left(96\pi^2\ x_{r3} + 48\pi^2\ \overline{m_E}\right)\ \sin x_{r1} \tag{A.126}$$

$$\frac{\partial c_{r4}}{\partial x_{r1}} = -60\pi\ x_{r3}\ \sin x_{r1} \tag{A.127}$$

$$\frac{\partial c_{r4}}{\partial x_{r3}} = 84\pi\ x_{r3} + 48\pi\ \overline{m_E} + 60\pi\ \cos x_{r1} \tag{A.128}$$

$$\frac{\partial c_{r5}}{\partial x_{r1}} = -24\ x_{r3}\ x_{r4}\ \sin x_{r1} - 6\ {x_{r3}}^2\ x_{r2}\ \cos x_{r1} \tag{A.129}$$

$$\frac{\partial c_{r5}}{\partial x_{r2}} = -6\ {x_{r3}}^2\ \sin x_{r1} \tag{A.130}$$

$$\frac{\partial c_{r5}}{\partial x_{r3}} = 24\, x_{r4}\, \cos x_{r1} + 42\, x_{r3}\, x_{r4} + 24\, \overline{m_E}\, x_{r4} - 12\, x_{r3}\, x_{r2}\, \sin x_{r1} \tag{A.131}$$

$$\frac{\partial c_{r5}}{\partial x_{r4}} = 12 + 24\, x_{r3}\, \cos x_{r1} + 21\, {x_{r3}}^2 + 24\, \overline{m_E}\, x_{r3} \tag{A.132}$$

Appendix B
Non-symmetrical radial deployment model

In this appendix, a non-dimensional Lagrangian-based dynamical model is aimed to be derived in order to capture the physics within non-symmetrical radial deployment operations. Thus, the following assumptions are made for the sake of developing such a dynamical model:

- Bidimensional deployment, where the out of plane dynamics are ignored
- The tethers are modelled as length-varying slender rods with mass equal to the current tether mass
- End masses are assumed to be placed at the end of each tether (modelling the remote units to be mounted in a real configuration)
- The spacecraft has reached deep space conditions before initiating deployment (i.e., the gravity effects are not considered as a result of their minor importance in comparison with the kinetic energy terms governing the system's dynamics) and the sail is not charged during the deployment
- The flexibility of the tethers is not considered during the deployment

Taking into account these statements, the reference frames, degrees of freedom and control variables to be used for the description of the manoeuvre are defined within Figure B.1. Hence, $\mathcal{S}^{r,i}$ represents the "moving" reference frame associated to each of the i tethers, where $\mathcal{S}_1^{r,i}$ remains with the same direction as the tether through the deployment, and $\mathcal{S}_2^{r,i}$ encloses the reference system by assuring that $\mathcal{S}_3^{r,i}$ points outwards the rotational plane.

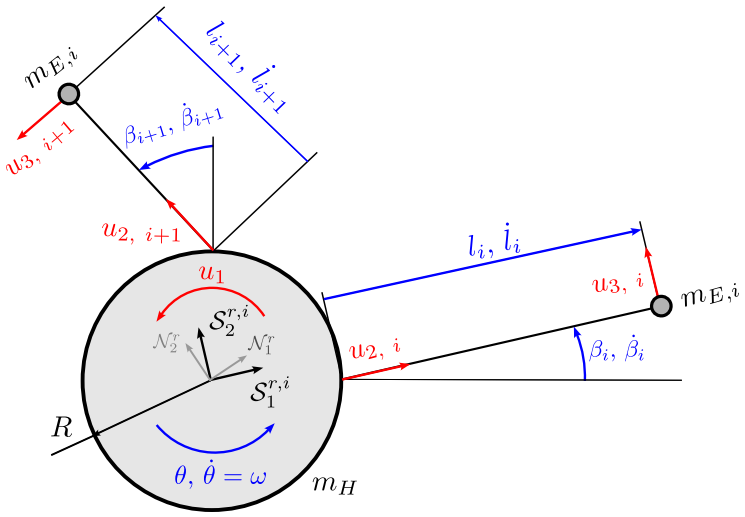

Figure B.1 Reference frames and degrees of freedom (non-symmetrical radial deployment dynamics).

On the other hand, $\mathcal{N}^r$ represents the inertial reference system to be used for the definition of the dynamic model. Continuing with the degrees of freedom to be used for the derivation of the Lagrangian model, 2+4N degrees of freedom are considered for the sake of deriving the introduced model (where N represents the total amount of tethers to be deployed):

- As in the previously described symmetrical deployment operations, both the hub rotational angle and spin velocity (θ and ω) are considered as degrees of freedom during the development
- The tether length and deployment rate of each i tether (l_i and $\dot{l}_i$, respectively) are also considered as degrees of freedom
- The angle and the angular velocity of each i tether with respect to the purely radial direction (β_i and $\dot{\beta}_i$) encloses the ensemble of degrees of freedom introduced within the development

With respect of the control variables to be used for the derivation of the dynamical model, 1+2N control variables are considered through the development:

- As in the previously described symmetrical deployment operations, the torque applied to the hub axis (u_1) is one of the major control variables of the dynamical model
- The reactions applied to each i tether by its associated reeling mechanism ($u_{2,\,i}$) comprise the following N control variables
- Additionally, the tangential forces applied by each of the remote units of the i tethers ($u_{3,\,i}$) are considered as well as control variables within the model

Given the described degrees of freedom and control variables, and taking into account the reference frames given by Figure B.1, the position of each i tether tip is expressed in the $\mathcal{S}^{r,i}$ frame as:

$$R_{E,\,i} = (R\,\cos\beta_i + l_i)\,\hat{s}_{r_i,\,1} - R\,\sin\beta_i\,\hat{s}_{r_i,\,2} \tag{B.1}$$

Similarly, the mid point of each i tether is expressed in this reference frame as:

$$R_{TC,\,i} = (R\,\cos\beta_i + l_i/2)\,\hat{s}_{r_i,\,1} - R\,\sin\beta_i\,\hat{s}_{r_i,\,2} \tag{B.2}$$

Since the $\mathcal{S}^{r,i}$ reference frame is not an inertial reference system, the tip velocity of each i tether is obtained as:

$$\dot{R}_{E,\,i} = \left.\frac{d(R_{E,\,i})}{dt}\right|_{\mathcal{S}^{r,i}} + \omega_{\mathcal{S}^{r,i}/\mathcal{N}^r} \times R_{E,\,i} \tag{B.3}$$

where:

$$\omega_{\mathcal{S}^{r,i}/\mathcal{N}^r} = (\omega + \dot{\beta}_i)\,\hat{s}_{r_i,\,3} \tag{B.4}$$

Operating with (B.3) and (B.4), the tip velocity of each tether remains:

$$\dot{R}_{E,\,i} = \left(\dot{l}_i + R\,\omega\,\sin\beta_i\right)\,\hat{s}_{r_i,\,1} + \left(R\,\omega\,\cos\beta_i + l_i\,\left(\omega + \dot{\beta}_i\right)\right)\,\hat{s}_{r_i,\,2} \tag{B.5}$$

Analogously, the obtention of the mid-point velocity of each i tether remains as:

$$\dot{R}_{TC,\,i} = \left.\frac{d(R_{TC,\,i})}{dt}\right|_{\mathcal{S}^{r,i}} + \omega_{\mathcal{S}^{r,i}/\mathcal{N}^r} \times R_{TC,\,i} \tag{B.6}$$

And operating with (B.4) and (B.6), this magnitude is expressed as:

$$\dot{R}_{TC,\,i} = \left(\dot{l}_i/2 + R\,\omega\,\sin\beta_i\right)\,\hat{s}_{r_i,\,1} + \left(R\,\omega\,\cos\beta_i + l_i/2\,\left(\omega + \dot{\beta}_i\right)\right)\,\hat{s}_{r_i,\,2} \tag{B.7}$$

Using (B.5) and (B.7), the kinetic energy of the system is expressed as:

$$E_c = E_{c,\,H} + E_{c,\,T} + E_{c,\,E} \tag{B.8}$$

where the terms in (B.8) represent:

- The kinetic energy associated to the hub ($E_{c,\,H}$), which experiences a rotational movement, that is:

$$E_{c,\,H} = \frac{1}{2}\,\omega_{\mathcal{N}^r}{}^T\, I_H\, \omega_{\mathcal{N}^r} \tag{B.9}$$

  where $\omega_{\mathcal{N}^r} = \omega\, \hat{s}_{r_i,\,3}$ is the hub rotational velocity, and I_H represents the hub inertia:

$$I_H = \frac{1}{2}\, m_H\, R^2 + R^2\, \left(m_T - \lambda \sum_{i=1}^{N} l_i\right) \tag{B.10}$$

  where m_H is the hub mass, m_T is the mass associated to the totally deployed tethers, R is the hub radius, and λ is the mass per unit length of each of the individual tethers.

- The kinetic energy associated to the tethers ($E_{c,\,T}$), which experience a combination of rotational and translational movements, that is:

$$E_{c,\,T} = \frac{1}{2} \sum_{i=1}^{N} \left[\omega_{S^{r,i}/N^r}{}^T\, I_{T,\,i}\, \omega_{S^{r,i}/N^r} + \lambda\, l_i\, \dot{R}_{TC,\,i} \cdot \dot{R}_{TC,\,i}\right] \tag{B.11}$$

  where $I_{T,\,i}$ is the inertia associated to the deployed portion of each i tether:

$$I_{T,\,i} = \lambda \left[\frac{1}{3}\, l_i{}^3 + R l_i{}^2 \cos\beta_i + l_i R^2\right] \tag{B.12}$$

- The kinetic energy associated to the remote units ($E_{c,\,E}$), which in this case experience a translational movement, that is:

$$E_{c,\,T} = \frac{1}{2}\, m_{E,\,i} \sum_{i=1}^{N} \dot{R}_{E,\,i} \cdot \dot{R}_{E,\,i} \tag{B.13}$$

  where $m_{E,\,i}$ represents the end-mass of each of the individual tethers.

Therefore, operating with (B.9), (B.11) and (B.13), the kinetic energy of the whole system is expressed as:

$$\begin{aligned} E_c =& \frac{1}{2}\, \omega^2\, \left(\frac{1}{2}\, m_H R^2 + R^2\, \left(m_T - \lambda \sum_{i=1}^{N} l_i\right)\right) + \frac{1}{2}\, \lambda \sum_{i=1}^{N} \left(\omega + \dot{\beta}_i\right)^2\, \left(\frac{1}{3}\, l_i{}^3 + l_i R^2 + R l_i{}^2 \cos\beta_i\right) \\ &+ \frac{1}{2}\, \lambda \sum_{i=1}^{N} l_i\, \left(\frac{1}{4}\, \left(\dot{l}_i\right)^2 + \omega^2 R^2 + \omega \dot{l}_i R \sin\beta_i + \frac{1}{4}\, l_i{}^2\, \left(\omega + \dot{\beta}_i\right)^2 + \omega R l_i\, \left(\omega + \dot{\beta}_i\right) \cos\beta_i\right) \\ &+ \frac{1}{2}\, m_{E,\,i} \sum_{i=1}^{N} \left(\left(\dot{l}_i\right)^2 + R^2\omega^2 + l_i^2\, \left(\omega + \dot{\beta}_i\right)^2 + 2\omega \dot{l}_i R \sin\beta_i + 2 R l_i \omega\, \left(\omega + \dot{\beta}_i\right) \cos\beta_i\right) \end{aligned} \tag{B.14}$$

Assuming Lagrange's approximation, the equations of motion the system are given by:

$$\frac{d}{dt}\left(\frac{\partial \mathcal{L}}{\partial \dot{q}_j}\right) - \left(\frac{\partial \mathcal{L}}{\partial q_j}\right) = Q_j \tag{B.15}$$

where $\mathcal{L} = E_c - E_p$, and Q_j is the generalized force term associated to each j Lagrangian equation. Since there are no potential energy sources, Lagrange's equations can be simplified into:

$$\frac{d}{dt}\left(\frac{\partial E_c}{\partial \dot{q}_j}\right) - \left(\frac{\partial E_c}{\partial q_j}\right) = Q_j \tag{B.16}$$

Therefore and defining $q_1 = \theta$, the first equation of motion is given by:

$$\begin{aligned}
u_1 =& \dot{\omega} \left(\frac{1}{2} m_H R^2 + m_T R^2 + \lambda \sum_{i=1}^{N} \left[\frac{7}{12} {l_i}^3 + 2R{l_i}^2 \cos\beta_i + l_i R^2 \right] + m_{E,i} \sum_{i=1}^{N} \left[{l_i}^2 + 2Rl_i \cos\beta_i + R^2 \right] \right) \\
&+ \sum_{i=1}^{N} \ddot{\beta}_i \left[\lambda \left(\frac{7}{12} {l_i}^3 + l_i R^2 + \frac{3}{2} R{l_i}^2 \cos\beta_i \right) + m_{E,i} \left({l_i}^2 + Rl_i \cos\beta_i \right) \right] + \sum_{i=1}^{N} \ddot{l}_i \left(m_{E,i} R + \frac{1}{2} \lambda l_i R \right) \sin\beta_i \\
&+ \omega \left[\lambda \sum_{i=1}^{N} \left(\dot{l}_i R^2 + 4Rl_i \dot{l}_i \cos\beta_i + \frac{7}{4} {l_i}^2 \dot{l}_i - 2R{l_i}^2 \dot{\beta}_i \sin\beta_i \right) + m_{E,i} \sum_{i=1}^{N} \left(2l_i \dot{l}_i + 2R\dot{l}_i \cos\beta_i - 2Rl_i \dot{\beta}_i \sin\beta_i \right) \right] \\
&+ \sum_{i=1}^{N} \dot{\beta}_i \left[\lambda \left(\frac{7}{2} l_i \dot{l}_i R \cos\beta_i + \dot{l}_i R^2 + \frac{7}{4} {l_i}^2 \dot{l}_i - \frac{3}{2} R{l_i}^2 \dot{\beta}_i \sin\beta_i \right) + m_{E,i} \left(2l_i \dot{l}_i + 2R\dot{l}_i \cos\beta_i - Rl_i \dot{\beta}_i \sin\beta_i \right) \right] \\
&+ \frac{1}{2} \lambda R \sum_{i=1}^{N} \left(\dot{l}_i \right)^2 \sin\beta_i
\end{aligned} \tag{B.17}$$

where, as introduced in Figure B.1, u_1 represents the torque to be applied in the hub spin axis. Defining the following non-dimensional variables:

$$\bar{l} = \frac{l}{R}, \qquad \overline{m_{E,i}} = \frac{m_{E,i}}{\lambda R}, \qquad \overline{m_H} = \frac{m_H}{\lambda R}, \qquad \overline{m_T} = \frac{m_T}{\lambda R}, \qquad \overline{\omega} = \frac{\omega}{\omega_0}, \qquad \tau = \frac{t\omega_0}{2\pi} \tag{B.18}$$

where ω_0 represents a reference spacecraft spin rate (that can be equalled to the initial spacecraft angular velocity for the sake of simplicity). Introducing (B.18) into (B.17), the $\overline{\omega}$ differential equation can be simplified into:

$$\begin{aligned}
\overline{u_1} =& \overline{\omega}' \left[12\pi\overline{m_H} + 24\pi\overline{m_T} + \sum_{i=1}^{N} \left(14\pi {\bar{l}_i}^3 + 24\pi\bar{l}_i + 48\pi {\bar{l}_i}^2 \cos\beta_i \right) + 24\pi\overline{m_{E,i}} \sum_{i=1}^{N} \left({\bar{l}_i}^2 + 2\bar{l}_i \cos\beta_i + 1 \right) \right] \\
&+ \sum_{i=1}^{N} \beta_i'' \left[7{\bar{l}_i}^3 + 12\bar{l}_i + 18{\bar{l}_i}^2 \cos\beta_i + 12\overline{m_{E,i}} \left({\bar{l}_i}^2 + \bar{l}_i \cos\beta_i \right) \right] + 6 \sum_{i=1}^{N} \bar{l}_i'' \left(2\overline{m_{E,i}} + \bar{l}_i \right) \sin\beta_i \\
&+ \overline{\omega} \left[\sum_{i=1}^{N} \left(24\pi\bar{l}_i' + 96\pi\bar{l}_i\bar{l}_i' \cos\beta_i + 42\pi {\bar{l}_i}^2 \bar{l}_i' - 48\pi {\bar{l}_i}^2 \beta_i' \sin\beta_i \right) + 48\pi\overline{m_{E,i}} \sum_{i=1}^{N} \left(\bar{l}_i\bar{l}_i' + \bar{l}_i' \cos\beta_i - \bar{l}_i\beta_i' \sin\beta_i \right) \right] \\
&+ \sum_{i=1}^{N} \beta_i' \left[12\bar{l}_i' + 21{\bar{l}_i}^2\bar{l}_i' - 18{\bar{l}_i}^2\beta_i' \sin\beta_i + 42\bar{l}_i\bar{l}_i' \cos\beta_i + 12\overline{m_{E,i}} \left(2\bar{l}_i\bar{l}_i' + 2\bar{l}_i' \cos\beta_i - \bar{l}_i\beta_i' \sin\beta_i \right) \right] \\
&+ 6 \sum_{i=1}^{N} \left(\bar{l}_i' \right)^2 \sin\beta_i \\
=& \frac{48\pi^2 u_1}{\lambda R^3 {\omega_0}^2}
\end{aligned} \tag{B.19}$$

where $\overline{u_1}$ is one of the control parameter to be used for the exploration of the control within the deployment procedure. Analogously, the equation associated to $q_{i+1} = l_i$ is given by:

$$\begin{aligned}
u_{2,i} =& \ddot{l}_i \left(\frac{1}{4} \lambda l_i + m_{E,i} \right) + \dot{\omega} \left(\frac{1}{2} \lambda R l_i \sin\beta_i + m_{E,i} R \sin\beta_i \right) \\
&+ \omega \left(-\lambda R^2 \dot{\beta}_i - \frac{5}{2} \lambda R l_i \dot{\beta}_i \cos\beta_i - \frac{7}{4} \lambda {l_i}^2 \dot{\beta}_i - 2m_{E,i} l_i \dot{\beta}_i \right) \\
&+ \omega^2 \left(-2\lambda R l_i \cos\beta_i - \frac{1}{2} \lambda R^2 - \frac{7}{8} \lambda {l_i}^2 - m_{E,i} l_i - m_{E,i} R \cos\beta_i \right) \\
&+ \left(\dot{\beta}_i \right)^2 \left(-\frac{1}{2} \lambda R^2 - \lambda R l_i \cos\beta_i - \frac{7}{8} \lambda {l_i}^2 - m_{E,i} l_i \right) + \frac{1}{8} \lambda \left(\dot{l}_i \right)^2
\end{aligned} \tag{B.20}$$

where $u_{2,\,i}$ represents the reaction applied to each i tether by its individual spooling drive. Simplifying (B.20) using the variables defined in (B.18), the $\bar{l}_i^{\,I}$ differential equation is given by:

$$\begin{aligned}\overline{u_{2,\,i}} =& \bar{l}_i''\ \left(2\bar{l}_i + 8\overline{m_{E,\,i}}\right) + \left(\bar{l}_i'\right)^2 + \overline{\omega}'\ \left(8\pi\bar{l}_i \sin\beta_i + 16\pi\overline{m_{E,\,i}}\ \sin\beta_i\right) \\ & - \overline{\omega}\beta_i'\ \left(16\pi + 40\pi\bar{l}_i\cos\beta_i + 28\pi\bar{l}_i^{\,2} + 32\pi\overline{m_{E,\,i}}\bar{l}_i\right) \\ & - \overline{\omega}^2\ \left(64\pi^2\bar{l}_i\cos\beta_i + 16\pi^2 + 28\pi^2\bar{l}_i^{\,2} + 32\pi^2\overline{m_{E,\,i}}\left(\bar{l}_i + \cos\beta_i\right)\right) \\ & - \left(\beta_i'\right)^2\ \left(4 + 8\bar{l}_i\cos\beta_i + 7\bar{l}_i^{\,2} + 8\overline{m_{E,\,i}}\bar{l}_i\right) \\ =& \frac{32\pi^2 u_{2,\,i}}{\lambda R^2 {\omega_0}^2}\end{aligned} \tag{B.21}$$

where $\overline{u_{2,\,i}}$ is part of the control parameters to be used for the sake of controlling of the dynamical system. For completing the definition of the dynamics of this deployment strategy, the equation associated to $q_{i+2} = \beta_i$ is given by:

$$\begin{aligned}u_{3,\,i}\, l_i =& \dot{\omega}\ \left(\frac{7}{12}\ \lambda {l_i}^3 + \lambda l_i R^2 + m_{E,\,i}{l_i}^2 + \frac{3}{2}\ \lambda R {l_i}^2\cos\beta_i + m_{E,\,i}Rl_i\cos\beta_i\right) \\ & + \ddot{\beta}_i\ \left(\frac{7}{12}\ \lambda {l_i}^3 + \lambda l_i R^2 + \lambda R {l_i}^2\cos\beta_i + m_{E,\,i}{l_i}^2\right) + \omega^2\ \left(\lambda R {l_i}^2 + m_{E,\,i}Rl_i\right)\sin\beta_i \\ & + \omega\dot{l}_i\ \left(\lambda R^2 + \frac{7}{4}\ \lambda {l_i}^2 + 2m_{E,\,i}l_i + \frac{5}{2}\ \lambda R l_i\cos\beta_i\right) \\ & + \dot{\beta}_i\ \left(\lambda\dot{l}_i R^2 + 2\lambda R l_i\dot{l}_i\cos\beta_i + \frac{7}{4}\lambda {l_i}^2\dot{l}_i + 2m_{E,\,i}l_i\dot{l}_i - \frac{1}{2}\ \lambda R {l_i}^2\dot{\beta}_i\sin\beta_i\right)\end{aligned} \tag{B.22}$$

where $u_{3,\,i}$ represents the tangential force applied by each of the i remote units of the tethers. Simplifying (B.22) and using (B.18), the $\beta_i^{\,I}$ differential equation is given by:

$$\begin{aligned}\overline{u_{3,\,i}}\,\bar{l}_i =& \overline{\omega}'\ \left(14\pi\bar{l}_i^{\,3} + 36\pi\bar{l}_i^{\,2}\cos\beta_i + 24\pi\bar{l}_i + 24\pi\overline{m_{E,\,i}}\ \left(\bar{l}_i^{\,2} + \bar{l}_i\cos\beta_i\right)\right) \\ & + \beta_i''\ \left(7\bar{l}_i^{\,3} + 12\bar{l}_i^{\,2}\cos\beta_i + 12\bar{l}_i + 12\overline{m_{E,\,i}}\bar{l}_i^{\,2}\right) + \overline{\omega}^2\ \left(48\pi^2\bar{l}_i^{\,2} + 48\pi^2\overline{m_{E,\,i}}\bar{l}_i\right)\sin\beta_i \\ & + \overline{\omega}\ \bar{l}_i'\ \left(24\pi + 42\pi\bar{l}_i^{\,2} + 48\pi\overline{m_{E,\,i}}\bar{l}_i + 60\pi\bar{l}_i\cos\beta_i\right) \\ & + \beta_i'\ (12\bar{l}_i' + 24\bar{l}_i\bar{l}_i'\cos\beta_i + 21\bar{l}_i^{\,2}\bar{l}_i' + 24\overline{m_{E,\,i}}\bar{l}_i\bar{l}_i' - 6\bar{l}_i^{\,2}\beta_i'\sin\beta_i) \\ =& \frac{48\pi^2 u_{3,\,i}}{\lambda R^2 {\omega_0}^2}\ \bar{l}_i\end{aligned} \tag{B.23}$$

where $\overline{u_{3,\,i}}$ is part of the control parameters to be used for the control of the dynamics within the deployment. Defining the state vector associated to the derived dynamical model (x_r) as:

$$x_r = \left[\theta,\ \overline{\omega},\ \bar{l}_i,\ \bar{l}_i'\,,\ \beta_i,\ \beta_i',\ldots\right]^T = \left[x_{r,\,1},\ x_{r,\,2},\ x_{r,\,4i-1},\ x_{r,\,4i},\ x_{r,\,4i+1},\ x_{r,\,4i+2},\ldots\right]^T \tag{B.24}$$

and, equivalently, defining the control vector (u_r) as:

$$u_r = \left[\overline{u_1},\ \overline{u_{2,\,i}},\ \overline{u_{3,\,i}},\ldots\right]^T = \left[u_{r,\,1},\ u_{r,\,2i},\ u_{r,\,2i+1},\ldots\right]^T \tag{B.25}$$

equations (B.19), (B.21) and (B.23) can be expressed as:

$$\begin{aligned} a_{r1}\,\dot{x}_{r,\,2}+\sum_{i=1}^{N}a_{r2,\,i}\,\dot{x}_{r,\,4i+2}+\sum_{i=1}^{N}a_{r3,\,i}\,\dot{x}_{r,\,4i}+a_{r4}\,x_{r2}+\sum_{i=1}^{N}a_{r5,\,i}\,x_{r,\,4i+2}+\sum_{i=1}^{N}a_{r6,\,i}\,{x_{r,\,4i}}^{2}&=u_{r,\,1}\\ b_{r1,\,i}\,\dot{x}_{r,\,4i}+{x_{r,\,4i}}^{2}+b_{r2,\,i}\,\dot{x}_{r2}-b_{r3,\,i}\,x_{r2}\,x_{r,\,4i+2}-b_{r4,\,i}\,{x_{r2}}^{2}-b_{r5,\,i}\,{x_{r,\,4i+2}}^{2}&=u_{r,\,2i}\\ c_{r1,\,i}\,\dot{x}_{r2}+c_{r2,\,i}\,\dot{x}_{r,\,4i+2}+c_{r3,\,i}\,{x_{r2}}^{2}+c_{r4,\,i}\,x_{r2}\,x_{r,\,4i}+c_{r5,\,i}\,x_{r,\,4i+2}&=u_{r,\,2i+1}\,x_{r,\,4i-1}\end{aligned} \tag{B.26}$$

where a series of auxiliary functions (e.g., a_{r1}, $b_{r2,\,i}$, $c_{r3,\,i}$) have been defined in order to simplify the original set of differential equations. In particular, these expressions are given by:

$$\begin{aligned} a_{r1}=&\sum_{i=1}^{N}\left(14\pi\left(x_{r,\,4i-1}\right)^{3}+24\pi\,x_{r,\,4i-1}+48\pi\left(x_{r,\,4i-1}\right)^{2}\cos x_{r,\,4i+1}\right)\\ &+24\pi\overline{m_{E,\,i}}\sum_{i=1}^{N}\left(\left(x_{r,\,4i-1}\right)^{2}+2\,x_{r,\,4i-1}\cos x_{r,\,4i+1}+1\right)+12\pi\overline{m_{H}}+24\pi\overline{m_{T}}\end{aligned} \tag{B.27}$$

$$\begin{aligned} a_{r2,\,i}=&7\left(x_{r,\,4i-1}\right)^{3}+12\,x_{r,\,4i-1}+18\left(x_{r,\,4i-1}\right)^{2}\cos x_{r,\,4i+1}\\ &+12\overline{m_{E,\,i}}\left(\left(x_{r,\,4i-1}\right)^{2}+x_{r,\,4i-1}\cos x_{r,\,4i+1}\right)\end{aligned} \tag{B.28}$$

$$a_{r3,\,i}=6\,\left(2\overline{m_{E,\,i}}+x_{r,\,4i-1}\right)\sin x_{r,\,4i+1} \tag{B.29}$$

$$\begin{aligned} a_{r4}=&\sum_{i=1}^{N}\left(24\pi\,x_{r,\,4i}+96\pi\,x_{r,\,4i-1}\,x_{r,\,4i}\cos x_{r,\,4i+1}+42\pi\,\left(x_{r,\,4i-1}\right)^{2}x_{r,\,4i}-48\pi\left(x_{r,\,4i-1}\right)^{2}x_{r,\,4i+2}\sin x_{r,\,4i+1}\right)\\ &+48\pi\overline{m_{E,\,i}}\sum_{i=1}^{N}\left(x_{r,\,4i-1}\,x_{r,\,4i}+x_{r,\,4i}\cos x_{r,\,4i+1}-x_{r,\,4i-1}\,x_{r,\,4i+2}\sin x_{r,\,4i+1}\right)\end{aligned} \tag{B.30}$$

$$\begin{aligned} a_{r5,\,i}=&12\,x_{r,\,4i}+21\left(x_{r,\,4i-1}\right)^{2}x_{r,\,4i}-18\left(x_{r,\,4i-1}\right)^{2}x_{r,\,4i+2}\sin x_{r,\,4i+1}\\ &+12\overline{m_{E,\,i}}\left(2\,x_{r,\,4i-1}\,x_{r,\,4i}+2\,x_{r,\,4i}\cos x_{r,\,4i+1}-x_{r,\,4i-1}\,x_{r,\,4i+2}\sin x_{r,\,4i+1}\right)\end{aligned} \tag{B.31}$$

$$a_{r6}=6\sin x_{r,\,4i+1} \tag{B.32}$$

Analogously, for $b_{r1,\,i}$, $b_{r2,\,i}$, $b_{r3,\,i}$, $b_{r4,\,i}$ and $b_{r5,\,i}$:

$$b_{r1,\,i}=2\,x_{r,\,4i-1}+8\overline{m_{E,\,i}} \tag{B.33}$$

$$b_{r2,\,i}=\left(8\pi\,x_{r,\,4i-1}+16\pi\overline{m_{E,\,i}}\right)\sin x_{r,\,4i+1} \tag{B.34}$$

$$b_{r3,\,i}=16\pi+40\pi\,x_{r,\,4i-1}\cos x_{r,\,4i+1}+28\pi\left(x_{r,\,4i-1}\right)^{2}+32\pi\overline{m_{E,\,i}}x_{r,\,4i-1} \tag{B.35}$$

$$b_{r4,\,i}=64\pi^{2}\,x_{r,\,4i-1}\cos x_{r,\,4i+1}+16\pi^{2}+28\pi^{2}\left(x_{r,\,4i-1}\right)^{2}+32\pi^{2}\overline{m_{E,\,i}}\left(x_{r,\,4i-1}+\cos x_{r,\,4i+1}\right) \tag{B.36}$$

$$b_{r5,\,i}=4+8\,x_{r,\,4i-1}\cos x_{r,\,4i+1}+7\left(x_{r,\,4i-1}\right)^{2}+8\overline{m_{E,\,i}}\,x_{r,\,4i-1} \tag{B.37}$$

And finally, for $c_{r1,\,i}$, $c_{r2,\,i}$, $c_{r3,\,i}$, $c_{r4,\,i}$ and $c_{r5,\,i}$:

$$\begin{aligned} c_{r1,\,i} =& 14\pi \left(x_{r,\,4i-1}\right)^3 + 36\pi \left(x_{r,\,4i-1}\right)^2 \cos x_{r,\,4i+1} + 24\pi\, x_{r,\,4i-1} \\ &+ 24\pi \overline{m_{E,\,i}} \left(\left(x_{r,\,4i-1}\right)^2 + x_{r,\,4i-1} \cos x_{r,\,4i+1}\right) \end{aligned} \tag{B.38}$$

$$c_{r2,\,i} = 7\left(x_{r,\,4i-1}\right)^3 + 12\left(x_{r,\,4i-1}\right)^2 \cos x_{r,\,4i+1} + 12 x_{r,\,4i-1} + 12\overline{m_{E,\,i}} \left(x_{r,\,4i-1}\right)^2 \tag{B.39}$$

$$c_{r3,\,i} = \left(48\pi^2 \left(x_{r,\,4i-1}\right)^2 + 48\pi^2 \overline{m_{E,\,i}}\, x_{r,\,4i-1}\right) \sin x_{r,\,4i+1} \tag{B.40}$$

$$c_{r4,\,i} = 24\pi + 42\pi \left(x_{r,\,4i-1}\right)^2 + 48\pi \overline{m_{E,\,i}}\, x_{r,\,4i-1} + 60\pi\, x_{r,\,4i-1} \cos x_{r,\,4i+1} \tag{B.41}$$

$$\begin{aligned} c_{r5,\,i} =& 12\, x_{r,\,4i} + 24\, x_{r,\,4i-1}\, x_{r,\,4i1} \cos x_{r,\,4i+1} + 21 \left(x_{r,\,4i-1}\right)^2 x_{r,\,4i} \\ &+ 24\overline{m_{E,\,i}}\, x_{r,\,4i-1}\, x_{r,\,4i} - 6\left(x_{r,\,4i-1}\right)^2 x_{r,\,4i+2} \sin x_{r,\,4i+1} \end{aligned} \tag{B.42}$$

Moreover, the system of differential equations in (B.26) can be generally expressed as:

$$\dot{x}_r = f_r\left(x_r, u_r, \tau\right) = \left[f_{r,\,1},\, f_{r,\,2},\, f_{r,\,4i-1},\, f_{r,\,4i},\, f_{r,\,4i+1},\, f_{r,\,4i+2}, \ldots\right]^T \tag{B.43}$$

Thus, f_r is comprised by 2+4N components ($f_{r,\,1}$, $f_{r,\,2}$, $f_{r,\,4i-1}$, $f_{r,\,4i}$, $f_{r,\,4i+1}$, $f_{r,\,4i+2}$...) defined as:

- $f_{r,\,1}$

$$f_{r,\,1} = x_{r,\,2} \tag{B.44}$$

- $f_{r,\,2}$

$$\begin{aligned} f_{r,\,2} =& \frac{1}{a_{r1} - \sum_{i=1}^{N}\left[a_{r2,\,i}\dfrac{c_{r1,\,i}}{c_{r2,\,i}} + a_{r3,\,i}\dfrac{b_{r2,\,i}}{b_{r1,\,i}}\right]} \left[u_{r,\,1} - \sum_{i=1}^{N}\left[\frac{a_{r2,\,i}}{c_{r2,\,i}}\, u_{r,\,2i+1}\, x_{r,\,4i-1} + \frac{a_{r3,\,i}}{b_{r1,\,i}}\, u_{r,\,2i}\right]\right. \\ &+ {x_{r,\,2}}^2 \sum_{i=1}^{N}\left[c_{r3,\,i} - a_{r3,\,i}\frac{b_{r4,\,i}}{b_{r1,\,i}}\right] + x_{r,\,2}\sum_{i=1}^{N}\left[a_{r2,\,i}\frac{c_{r4,\,i}}{c_{r2,\,i}} - a_{r4}\right] + \sum_{i=1}^{N}\left(1 - a_{r6,\,i}\right){x_{r,\,4i}}^2 \\ &\left. + \sum_{i=1}^{N}\left[a_{r2,\,i}\frac{c_{r5,\,i}}{c_{r2,\,i}} - a_{r5,\,i}\right] x_{r,\,4i+2} - x_{r,\,2}\sum_{i=1}^{N} a_{r3,\,i}\frac{b_{r3,\,i}}{b_{r1,\,i}} x_{r,\,4i+2} - \sum_{i=1}^{N} a_{r3,\,i}\frac{b_{r5,\,i}}{b_{r1,\,i}}\, {x_{r,\,4i+2}}^2\right] \end{aligned} \tag{B.45}$$

- $f_{r,\,4i-1}$

$$f_{r,\,4i-1} = x_{r,\,4i} \tag{B.46}$$

- $f_{r,\,4i}$

$$f_{r,\,4i} = \frac{1}{b_{r1,\,i}}\left[u_{r,\,2i} + b_{r3,\,i}\, x_{r,\,2}\, x_{r,\,4i+2} + b_{r4,\,i}\, {x_{r,\,2}}^2 + b_{r5,\,i}\, {x_{r,\,4i+2}}^2 - {x_{r,\,4i}}^2 - b_{r2,\,i}\, f_{r,\,2}\right] \tag{B.47}$$

- $f_{r,\,4i+1}$

$$f_{r,\,4i+1} = x_{r,\,4i+2} \tag{B.48}$$

- $f_{r,\,4i+2}$

$$f_{r,\,4i+2} = \frac{1}{c_{r2,\,i}} \left[u_{r,\,2i+1}\, x_{r,\,4i-1} - c_{r1,\,i}\, f_{r,\,2} - c_{r3,\,i}\, {x_{r,\,2}}^2 - c_{r4,\,i}\, x_{r,\,2} - c_{r5,\,i}\, x_{r,\,4i+2} \right] \tag{B.49}$$

Using this formulation, an exploration of the control of non-symmetrical deployment could be performed in order to assess whether this strategy represents a feasible alternative for the sake of solving partial failures during the normal performance of E-sail deployment operations.